

Cost effective FTire parameterisation methods for ride simulations with large off-the-road tyres

by

Martin Joachim Stallmann

A dissertation submitted in partial fulfilment

of the requirements for the degree of

Doctor of Philosophy

(Mechanical Engineering)

at the University of Pretoria

2018

Abstract

Title: Cost effective FTire parameterisation methods for ride simulations with large off-the-road tyres
Author: Martin Joachim Stallmann
Study Leader: Prof. P.S. Els
Department: Mechanical and Aeronautical Engineering, University of Pretoria
Degree: Doctor of Philosophy in Mechanical Engineering

All forces acting on a road vehicle are either generated in the tyre-road interface or are due to aerodynamic effects, where at low speeds the latter can be ignored. The accuracy of the tyre model, describing the forces at the tyre-road interface, is thus of utmost importance in vehicle dynamics simulations. Accurate tyre models are essential to ensure that vehicle dynamics models are an accurate representation of the actual vehicle so that it can be used with confidence to study and improve the vehicle's safety, durability, ride comfort and handling capabilities.

Various tyre models have been developed to describe the forces and moments that are generated in the tyre contact patch. FTire is one of the well-known and widely used nonlinear physics-based models that has been developed for vehicle comfort and handling simulations and the prediction of road loads due to short wave-lengths obstacles. The parameterisation of the FTire model is done by extracting model parameters from experimental results that cover the operational conditions of the tyre. Acquiring these parameterisation datasets, with an acceptable accuracy, is however a challenge. This is especially true for large off-the-road (OTR) tyres. Expensive test equipment is typically required to conduct these tests for passenger car tyres but virtually no test equipment is available to test OTR tyres. Due to a lack of standardisation, the test equipment is often custom built and adapted to the required test conditions. The situation is further complicated due to the large range of possible tyre operating and loading conditions of OTR tyres, as well as the differences in tyre and rim sizes, that the test equipment should be able to accommodate. Alternative methods of obtaining parameterisation data for large OTR tyres thus need to be investigated. This thesis describes two alternative methods that can be used to parameterise an FTire model of a large OTR tyre. Parameterisation methods were investigated that can be applied irrespective of the tyre size and operating load.

A baseline parameterisation process, using an experimental data set, was performed. The obtained FTire model was validated against experimental results. The validation process showed that the parameterised model can be used to accurately predict the tyre forces and moments, of large OTR tyres, while driving over uneven terrain. This method can thus successfully be used if the tyre forces and moments, and the applied boundary, as well as environmental conditions, can accurately be measured. Conducting these measurements was however found to be challenging, limited by the available test equipment and problematic to expand to higher loads and larger tyres.

One alternative, to experimentally obtained data for the parameterisation process, is to use finite element models to generate the relevant parameterisation data. The required input data of a finite element tyre model can be obtained with the same effort irrespective of the tyre size or operating condition. Geometric and material tests were conducted, and a nonlinear finite element model was created and validated against experimental test. The finite element tyre model was used to replicate the parameterisation tests that are required to parameterise a FTire model without tuning any model parameters. A FTire parameterisation was conducted using FEA data and the model was validated.

A second alternative is the use of carcass deformation results to parameterise FTire models. The carcass deformation data can be obtained from experimental testing or from FE simulation results. To obtain the measured carcass deformation data, a set of cameras were mounted to the inside of the test tyre. The stereo vision principle is applied to determine the deformation of the tyre during static tyre tests. Initial results of using the carcass deformation data to parameterise a FTire model is also presented. Carcass deformation measurements can further be used to validate FE tyre models if force and moment measurements are limited or non-existent to improve the confidence in the model.

The proposed methods create new possibilities to parameterise FTire models of large off-the-road tyres. These methods are especially useful if experimental results of the tyre are limited or non-existent. This thesis presents results that show that these methods can be used successfully to extract model parameters. More research is however required to extend these capabilities and to standardize these parameterisation methods.

Acknowledgements

I would like to my gratitude to:

- My wife, Bianca, for her constant support in all my endeavours.
- My parents Walter and Christine, for their support and aid in my work.
- Prof. Dr. Schalk Els, for this mentorship through my postgraduate studies.
- Prof. Dr Michael Gipser and Gerald Hofmann from cosin scientific software, for their help and licensing support with FTire.
- Carl Becker, and all technical staff at the University of Pretoria, for their help during testing.
- My fellow postgraduate students Anria, Theunis and Herman, for their advice, support during testing and the everyday conversations that made the project so much more interesting.
- The financial assistance of the National Research Foundation (DAAD-NRF) towards this research is hereby acknowledged. Opinions expressed, and conclusions arrived at, are those of the author and are not necessarily to be attributed to the DAAD-NRF.

"If you cannot measure it, you cannot improve it."

- *Lord Kelvin, 1885*

Index

Abstract	I
Acknowledgements	III
Index	V
List of Figures	VIII
List of Tables	XI
Notation	XII
1. Introduction	2
1.1. Motivation and problem statement.....	2
1.2. Objective and scope	4
1.3. Thesis Outline.....	5
2. Literature review of tyre models	7
2.1. Introduction to mathematical tyre modelling	7
2.2. Recent advances in parameterising large OTR tyre models	15
2.3. FE tyre modelling.....	16
2.4. Tyre deformation measurement.....	19
2.5. Tyre model used in this study	20
2.6. Chapter summary	22
3. Investigated tyre	26
4. Established FTire parameterisation method	30
4.1. Introduction to the established FTire parameterisation method.....	30
4.2. Experimental test setup	32
4.3. Parameterisation Procedure	36
4.4. FTire Validation.....	43
4.4.1. Discrete obstacles.....	45
4.4.2. Uneven road	46
4.5. Chapter Summary.....	52
5. Finite element tyre model parameterisation	56
5.1. Material testing for FE analysis.....	56
5.2. Material models	56

5.3.	Experimental testing and results.....	59
5.3.1.	Tyre geometric properties	60
5.3.2.	Tyre material properties	62
5.3.3.	Reinforcing material	69
5.4.	MARC finite element tyre model	70
5.4.1.	Material model fit.....	70
5.5.	FE tyre model	75
5.6.	FE tyre model validation	82
5.7.	FTire parameterisation using FE simulation results.....	89
5.8.	FTire validation	93
5.8.1.	Discrete obstacle	93
5.8.2.	Uneven road	94
5.9.	Chapter Summary.....	96
6.	Carcass deformation for tyre model parameterisation	99
6.1.	Introduction to carcass deformation tyre model parameterisation.....	99
6.2.	Tyre deformation measurements.....	99
6.2.1.	Introduction to computer stereographic vision	99
6.2.2.	Tyre sidewall measurements	100
6.2.3.	“Inside tyre camera” test rig validation	104
6.2.4.	Tyre deformation test setup	105
6.2.5.	Tracking algorithm	107
6.2.6.	Tyre deformation test results	110
6.3.	Tyre deformation for FEM validation.....	114
6.3.1.	FEM validation metric	114
6.3.2.	FE validation results.....	116
6.4.	FTire parameterisation using carcass deformation data.....	118
6.5.	Chapter Summary.....	125
7.	Comparison of parameterisation methods	128
7.1.	FTire parameterisation using experimentally obtained test data	128
7.2.	FTire parameterisation using FE tyre models.....	131
7.3.	FTire parameterisation using carcass deformation information.....	133
8.	Conclusions and Recommendations.....	136
8.1.	Conclusions	136

8.2. Recommendations on future research.....	139
9. Bibliography.....	141
10. Appendix A.....	150

List of Figures

Figure 2-1 First production vehicle [Daimler, 2015].....	7
Figure 2-2 Frequency range requirements for vehicle-system analyses [Figure adapted by author from Antoine et al., 2005]	10
Figure 2-3 Commercial tyre model classification [Figure adapted by author from Gipser, 2016].....	13
Figure 2-4 FTire belt elements degree of freedom [cosin scientific software, 2017e]	21
Figure 3-1 Left: Michelin 16.00R20 XZL. Right: thread pattern [Michelin, n.d.].....	26
Figure 3-2 Tyre construction	27
Figure 3-3 CAD representation of the tyre construction	28
Figure 4-1 FTire/fit workflow [cosin scientific software, 2017d]	31
Figure 4-2 Static tyre test setup	33
Figure 4-3 Longitudinal cleat test setup	34
Figure 4-4 Load cell location of the tyre test trailer	34
Figure 4-5 Tyre test trailer during a 50x50 mm dynamic cleat test	35
Figure 4-6 Experimental results of a 50 mm lateral cleat test	35
Figure 4-7 Footprint measurement, 3.0 Bar, 56.3 kN	37
Figure 4-8 1.0 Bar footprint validation. Left: 19.2 kN. Right: 7.3 kN -4.0 deg camber	37
Figure 4-9 3.0 Bar footprint validation. Left: 56.3 kN. Right: 30.9 kN -4.0 deg camber	38
Figure 4-10 Radial stiffness validation. Left: 1.0 Bar. Right: 3.0 Bar	38
Figure 4-11 Radial stiffness -4.0 deg camber validation. Left: 1.0 Bar. Right: 3.0 Bar	39
Figure 4-12 50mm transversal cleat validation, 1.0 Bar	39
Figure 4-13 50mm longitudinal cleat validation, 3.0 Bar	40
Figure 4-14 Left: Longitudinal tyre stiffness. Right: Lateral tyre stiffness 1.0 Bar	40
Figure 4-15 Tyre handling characteristics, 3.0 Bar	41
Figure 4-16 Radial hysteresis characteristics.....	41
Figure 4-17 Tyre damping parameterisation	42
Figure 4-18 Trailer yaw, pitch and roll velocities during validation test.	44
Figure 4-19 Discrete obstacle validation, 50mm transversal cleat. 18 km/h, 3.0 Bar.....	46
Figure 4-20 Can-Can road profiling machine	47
Figure 4-21 Increasing frequency cleat test track CRG road representation	47
Figure 4-22 Belgian paving validation test	48
Figure 4-23 Displacement Spectral Density of the Belgian block road [Becker, 2008]	49
Figure 4-24 Validation results of the increasing frequency cleat test.	50
Figure 4-25 Force Histogram, Belgian paving	51
Figure 4-26 Force PSD validation, Belgian Paving	52
Figure 5-1 Outer contour test results.....	60
Figure 5-2 Michelin 16.00R20 CAD model.....	61
Figure 5-3 Tyre rubber layers, Left: tread block, Right: carcass section near tyre sidewall	61
Figure 5-4 Uniaxial tension test.....	64
Figure 5-5 Uniaxial tension test results	65
Figure 5-6 Equibiaxial tension test setup	66
Figure 5-7 Equibiaxial tension test results.....	67

Figure 5-8 Planar shear stretch diagram	68
Figure 5-9 Comparison of principal stretch ratios λ_1 and λ_2	68
Figure 5-10 Planar shear test results	69
Figure 5-11 Finite element model of the lateral four-point bending test	74
Figure 5-12 Lateral four-point bending results	74
Figure 5-13 Longitudinal four-point bending results	75
Figure 5-14 Tyre axisymmetric FE model	77
Figure 5-15 Glued tread elements	78
Figure 5-16 Left: Equal mesh spacing. Right: Variable mesh spacing	79
Figure 5-17 FE result comparison between the simplified model and the complete model	81
Figure 5-18 FE tyre model boundary conditions	82
Figure 5-19 Vertical tyre stiffness on a flat surface at 0.1Bar	84
Figure 5-20 0.1Bar footprint validation	85
Figure 5-21 Vertical tyre stiffness at 1.0Bar, Left: 0deg camber, Right: 4deg camber	86
Figure 5-22 Node displacement during a lateral cleat test	86
Figure 5-23 Vertical tyre stiffness at 3.0Bar, flat surface and 50mm lateral cleat	87
Figure 5-24 Validation of 3.0Bar footprints. Left: 0degree camber, Right: 4degree camber	88
Figure 5-25 Validation of the tyre longitudinal stiffness	88
Figure 5-26 Vertical tyre stiffness, Left: 1.0Bar, Right: 3.0Bar	90
Figure 5-27 Tyre stiffness on cleat, Left: 1.0 Bar transversal, Right: 3.0Bar longitudinal	90
Figure 5-28 3.0Bar footprint. Left: 56.3kN 0deg camber. Right: 41.7kN 8.0deg camber	91
Figure 5-29 Radial stiffness validation: -8.0deg camber, 3.0Bar	91
Figure 5-30 50mm transversal cleat validation: -8.0deg camber, 3.0Bar	92
Figure 5-31 Parking torque validation, 29.4kN tyre load	92
Figure 5-32 Discrete obstacle validation, 50mm transversal cleat. 18km/h, 3Bar	93
Figure 5-33 Validation results of the increasing frequency cleat test	94
Figure 5-34 Force Histogram, Belgian paving	95
Figure 5-35 Force PSD validation, Belgian Paving	96
Figure 6-1 Stereovision working principal [Botha, 2015]	100
Figure 6-2 Initial experimental setup	101
Figure 6-3 Left: Test tyre as viewed from camera, Right: marker close-up (red dot results from post-processing)	102
Figure 6-4 Left: Test Result, 100mm displacement, 100kPa, Right: Manipulated image	102
Figure 6-5 Tracked point positions and velocity vectors, 100 kPa	103
Figure 6-6 Validation test setup	104
Figure 6-7 Camera setup accuracy	105
Figure 6-8 Camera test setup mounted on the inside of the tyre	106
Figure 6-9 Marker position on tyre carcass (50mm cleat)	106
Figure 6-10 Camera view of markers	107
Figure 6-11 Corresponding markers used during post-processing	107
Figure 6-12 Test procedure	108
Figure 6-13 Sub-Pixel edge detection algorithm	109
Figure 6-14 Carcass markers in global coordinate system	110
Figure 6-15 Observed tyre carcass area	111

Figure 6-16 Lateral cleat test result, 50mm, 1bar.....	112
Figure 6-17 Local carcass deformation during lateral cleat test.....	112
Figure 6-18 Marker movement during 50 mm cleat test.....	113
Figure 6-19 Precision of measurement	113
Figure 6-20 Tyre carcass deformation on a flat surface, 1Bar. Left: Unladen. Right: Laden ...	115
Figure 6-21 Projected node location	115
Figure 6-22 Tyre carcass deformation deviation, flat surface, 1Bar. Left: Unladen. Right: Laden	117
Figure 6-23 Tyre carcass deformation deviation, 50mm lateral cleat, 3Bar. Left: Unladen. Right: Laden	118
Figure 6-24 Tyre tread orientation. Left: Experiment. Right: Model	118
Figure 6-25 Nodes selected for FTire parameterisation file	119
Figure 6-26 FTire FER-file format	120
Figure 6-27 FTire FEM validation, flat surface, 3Bar, deflection 50mm	121
Figure 6-28 FTire FEM validation, flat surface, 1Bar, deflection 50mm camber -6deg	121
Figure 6-29 Tyre carcass deformation deviation, flat surface, 3Bar. Left: Unladen. Right: Laden	122
Figure 6-30 Cross-section of the carcass deformation. Left: Unladen. Right: Laden.....	123
Figure 6-31 Simulated tyre carcass deformation, 50mm lateral cleat, 3Bar.....	124
Figure 6-32 Tyre carcass deformation deviation, 50mm lateral cleat, 3Bar. Left: Unladen. Right: Laden	124

List of Tables

Table 2-1 Tyre development milestones [Mullineux, 2011; Rill, 2006] 8

Table 3-1 Michelin XZL specification (Michelin, n.d.) 26

Table 3-2 Tyre section description 27

Table 5-1 ShoreA test results 63

Table 5-2 Reinforcing material test results 70

Table 5-3 Tread outer material properties 71

Table 5-4 Sidewall inner material properties 72

Table 5-5 Inner liner material properties 73

Table 5-6 FE tyre model number of elements 79

Notation

Symbol	Unit	Description
A	m^2	deformed area
A_0	m^2	original area
A_x	$m^2/cycles/m$	roughness coefficient
B		left Cauchy-Green deformation tensor
C_{ijk}		material constant
D	m	diameter
E	N/m^2	Young's modulus
F_{ij}		deformation gradient tensor
I_1		first strain invariant of the green deformation tensor
I_2		second strain invariant of the green deformation tensor
I_3		third strain invariant of the green deformation tensor
J		elastic volume ratio
K_i		material constant
L	m	Deformed length
L_0	m	original length
n		road exponent
n_p		number of periods
P	N	load
S		ShoreA hardness
S_z	$m^2/cycle/m$	vertical displacement spectral density
t	sec	time
t_0	m	original tickness
t_t	m	deformed thickness
T		transpose of a matrix
T_s	sec	period of oscillation
u		displacement field

U	J/m^3	strain energy density
U_d	J/m^3	deviatoric strain energy density
U_h	J/m^3	hydrostatic strain energy density
x	m	displacement amplitude
$x_{i,m}$	m	measured x coordiante of the the i th marker during unladen condition
$x'_{i,m}$	m	measured x coordiante of the the i th marker during laden condition
$x_{i,p}$	m	simulated x coordiante of the the i th marker during the unladen condition
$x'_{i,p}$	m	simulated x coordiante of the the i th marker during the laden condition
$y_{i,m}$	m	measured y coordiante of the the i th marker during the unladen condition
$y'_{i,m}$	m	measured y coordiante of the the i th marker during the laden condition
$y_{i,p}$	m	simulated y coordiante of the the i th marker during the unladen condition
$y'_{i,p}$	m	simulated y coordiante of the the i th marker during the laden condition
$z_{i,m}$	m	measured z coordiante of the the i th marker during the unladen condition
$z'_{i,m}$	m	measured z coordiante of the the i th marker during the laden condition
$z_{i,p}$	m	simulated z coordiante of the the i th marker during the unladen condition
$z'_{i,p}$	m	simulated z coordiante of the the i th marker during the laden condition

Greek letters	Unit	Description
α_i		Ogden material property constants
δ		logarithmic decrement
δ_{ij}		Kronecker delta
μ_i		Ogden material property constants
σ_{ij}	N/m^2	stress tensor
σ_1	N/m^2	first principal Stress
σ_2	N/m^2	second principal Stress
σ_3	N/m^2	third principal Stress

λ		stretch ratio
λ_1		first principal stretch ratio
λ_2		second principal stretch ratio
λ_3		third principal stretch ratio
φ	<i>cycles/m</i>	spatial frequency

Abbreviations	Description
3D	three dimensional
CAD	computer-aided design
DIC	digital image correlation
DMA	dynamic mechanical analysis
DOT	Department of Transport
DSD	Displacement Spectral Density
FE	finite element
FEA	finite element analyses
FEM	Finite element method
LI	load index
MF	magic formula tyre model
NVH	Noise, vibration and hardness
OTR	off the road
PSD	Power Spectral Density
TYDEX	tyre data exchange

Chapter 1

Introduction

1. Introduction

This chapter introduces the research that was conducted and discussed in this thesis. The motivation and background as well as objective and scope of the study are presented. The outline of the thesis content is also presented in this chapter.

1.1. Motivation and problem statement

The tyre plays an important role in the performance, handling, and ride-comfort of a vehicle. Researchers have developed numerous tyre models in an ongoing effort to improve our understanding of the tyre and to predict the forces and moments that are generated in the tyre contact patch. These models vary in complexity, ranging from simple empirical formulations to three-dimensional nonlinear finite element tyre models. The parameterisation process of these models in many cases requires some sort of experimentally obtained test data of the tyre. This data is used to extract the necessary information about the underlying tyre behaviour.

Parameterisation of any tyre model is always a delicate task and depends not only on the availability of parameterisation data and the accuracy of the data but also on the user. The user is required to select and prepare the appropriate measurements to be used for the parameter identification.

The extend of the required test data is generally dependent on the complexity of the tyre model. Simple empirical tyre models, with only a few parameters, usually only require a few parameterisation tests. These parameterisation tests can be conducted relatively easily and cost effectively, but the models tend to have limitations in the range of valid operating conditions and accuracy. Complex physics-based tyre models on the other hand require a comprehensive set of experimental parameterisation data to identify all the required model parameters. These tests include static tyre stiffness tests as well as dynamic tests on a rolling tyre. The advantage of these models is that they tend to be highly accurate for a wide range of operating conditions [Stallmann and Els, 2014; Babulal et al., 2015]. Tyre models that are developed based on a mechanical or a physical approach, rather than empirical or semi empirical approach, have the added advantage that they inherently predict physically meaningful results. This characteristic is extremely important if the model is used for simulations that differ from the test conditions that were investigated during the parameterisation process of the tyre model.

Obtaining the required experimental results poses a major challenge. Expensive test equipment is typically required to conduct these tests. The situation is further complicated due to the large range of possible tyre operating and loading conditions, as well as the difference in tyre size, that the test equipment should be able to accommodate. Tyre models are required for small tyres with a low load index, used for recreational vehicles, up to large tyres with a high load index, used for earth moving equipment. In recent years', researchers have mainly focused on improving and extending the measurement capabilities of passenger car and light truck tyres. Researchers developed drum and flat track test rigs to perform accurately controlled tyre parameterisation tests [fka, 2017; Sovamotion, 2017; Stackpole Engineering Services, 2017]. These test rigs are very popular and widely used to conduct tyre model parameterisation tests. The parameterisation methods, of not only physical based tyre models but also some of the empirical or semi-empirical models, were adapted and specifically developed for these test conditions and experimental data sets.

Large off-highway truck tyres can however not be tested on standard drum and flat track test rigs due to their large size and high operating load conditions. The current design of this test equipment cannot be scaled efficiently to accommodate these tyres. The reaction forces, that are applied to the test rig during cleat tests for instance, or the power required, to drive the drum during traction and braking tests, would simply be too large. To obtain the required parameterisation data, researchers have successfully developed various alternative methods to perform these tests [Stallmann and Els, 2014; Stallmann et al., 2014]. The test setups include static as well as dynamic tests conducted on a trailer or are obtained during in-situ tyre testing. Challenges of these test methods include the accurate control of the test conditions and the compatibility of the test data with the parameterisation software. Due to a lack of standardisation, the test equipment is often custom built and adapted to the required test conditions. Expert knowledge is also needed to interpret the test data to isolate the tyre behaviour from the noise, effects of the test equipment and external disturbances. These limitations of the available test equipment make it difficult to parameterise tyre models of large off-road tyres. It furthermore increases the cost of testing and parameterising tyre models of these large tyres.

1.2. Objective and scope

The objective of this thesis is to investigate methods that can be used to parameterise a highly accurate physical tyre model of a large off-the-road (OTR) truck tyre where limited or no parameterisation test data is available. For this thesis, a large OTR tyre is defined as a tyre that is used on heavy machinery operating primarily on off-road conditions in the agricultural, mining, construction or industrial environment. These tyres usually have a 20" or larger rim diameter, a overall diameter larger than one meter and a load index (LI) of at least 145. Any off-the-road passenger car or light truck tyres are thus excluded.

The model must be capable of accurately predicting the tyre behaviour for a wide range of operating conditions. The operating conditions must reflect the general operating conditions of the off-road tyres. The presented method or methods must be easily scalable to the wide range of OTR truck tyres that are currently available on the market. The methods should thus be independent on the size and load rating of the tyres. The research is further aimed at reducing the effort and cost of the parameterisation procedure.

A physics-based tyre model is required for this investigation as only a limited subset of the parameterisation data can be expected to be available for parameter identification process. A physics-based tyre model would ensure that the outputs of the tyre model are still physically meaningful and thus useful to predict the tyre behaviour for a wide range of operating conditions.

The following aspects are included in the scope of this research:

- Identification of the limitations of the established parameterisation methods when applied to large OTR tyres;
- Detailed parameterisation and validation of a physics-based tyre model with the established methods;
- Investigation of alternative methods that may be used to identify the required tyre model parameters;
- Performing a tyre model parameterisation process with the proposed alternative methods;
- Comparing the tyre models obtained with the established and alternative parameterisation methods to determine the expected accuracy of the models;
- Investigation into the advantages and shortcomings of the proposed methods;
- Investigating the cost of performing a tyre model parameterisation for the different methods;

1.3. Thesis Outline

This chapter discussed the motivation and problem statement of this thesis. The objectives and the scope of the research were also presented.

Chapter 2 is a literature review on tyre models and their applications in the vehicle research and development environment. A short discussion on the difficulties that are faced by researchers and engineers when validating tyre models is also presented in this chapter.

Chapter 3 describes the test tyre that was used for this investigation.

In Chapter 4 the established FTire parameterisation method is presented. Parameterisation tests of a large off-the-road tyre are discussed, and the experimental results are presented. The parameterisation and validation process of a FTire model is described.

Chapter 5 presents a method to develop a finite element model of a large OTR tyre. Geometric and material properties tests are conducted, and the results are presented. The finite element model is validated with parameterisation test results from Chapter 4. Simulations with the finite element tyre model are conducted and used to parameterise a FTire model. The model is validated against experimentally obtained test data and the accuracy is discussed.

Chapter 6 describes a method of measuring the carcass deformation. The results obtained are compared to the simulation results of the finite element model. The chapter also presents a method to use the data to validate FE tyre models. Initial results of using the carcass deformation data to parameterise a FTire model is presented in this chapter.

Chapter 7 compares the FTire tyre models that were parameterised with the proposed methods. Advantages and short comings of the methods are discussed. A discussion on the expected cost implications is also included.

Chapter 8 presents the conclusion and findings of this research. Recommendations are made to future studies to further improve the presented parameterisation methods.

Chapter 2

Literature review of tyre models

2. Literature review of tyre models

This chapter presents a review of the pneumatic tyre and the mathematical modelling approaches for tyres. The literature review includes a summary on the parameterisation procedures and data requirements of tyre models. Finite element tyre modelling techniques are introduced and recent advances in tyre deformation measurement techniques are discussed.

2.1. Introduction to mathematical tyre modelling

One of mankind's greatest inventions is the automobile. The first automobile, capable of human transport was developed in 1769 [Eckermann, 2001]. The steam powered automobile was built by Nicolas-Joseph Cugnot. The first automobile with an internal combustion engine was developed in 1807 and was fuelled by hydrogen. Karl Benz developed the first production gasoline powered vehicle. The corresponding patent, DRP Nr. 37435, for the vehicle was granted to Benz in 1886. The three-wheeled vehicle was the first vehicle that was suitable for practical use and thus marks the birth of the modern automobile.



Figure 2-1 First production vehicle [Daimler, 2015]

The wheels used for the first automobiles were spoked wheels, like those found on horse drawn carriages. To improve the traction of the wheels the outer ring, made from wood or steel, was later coated with a rubber liner. The pneumatic tyre, as we know today, was first developed by Andre and Edouard Michelin in 1891 [Mullineux, 2011].

The modern pneumatic tyre is a complex structure that comprises of dozens of components that are pressed, assembled, and cured together. Modern tyres are a combination of materials, such as steel, fabric, and rubber. Tyre development is a continuous and ongoing process. A few milestones in the development of the automobile tyre thus far are listed in Table 2-1.

Table 2-1 Tyre development milestones [Mullineux, 2011; Rill, 2006]

Year	Milestone
1839	Vulcanization; Charles Goodyear
1845	First pneumatic tyre - Several thin inflated tubes inside a leather cover; Robert William Thompson
1846	First solid rubber tyre; Thomas Hancock
1888	Patent for pneumatic bicycle tyres; John Boyd Dunlop
1891	Patent for a removable pneumatic tyre; Andre and Edouard Michelin
1895	Michelin pneumatic tyres are used during the Paris–Bordeaux–Paris race; 760km: 50 tyre deflations, 22 complete inner tube changes
1899	“Long-lived” tyres, approx. 500 Kilometres; Continental
1904	First grooved tread tyre; Continental A.G.
1908	Grooved tyres to improve road friction; Frank Seiberling
1922	Steel cord tread in tyre bead; Dunlop
1943	Patent for tubeless tyres; Continental
1948	Steel-belted radial tyre; Michelin
1983	Radial tyres are standard in America, more than two decades after Europe
2005	Michelin develops a non-pneumatic tyre called the Tweel

For the development of new vehicle concepts and improvements of the dynamic vehicle behaviour simulations play an important role. Traditionally vehicle manufactures mainly used vehicle dynamic simulations in the concept and prototype development phase. Today however vehicle dynamics simulations play an important role in the entire product development phase of a vehicle [Benz, 2008]. The use of virtual vehicle models allows the manufacturers to reduce both the development time and cost by eliminating costly prototype development iterations. This development is further aided by the ever-increasing computational performance of computers [Hennessy and Patterson, 2011]. Software tools, used to model vehicles and vehicle components, are also constantly developed and improved to enable the developer to use these tools for a wide

range of applications [Schiehlen, 2013]. These factors permitted the developers to increase the model complexity and thus enabled them to investigate complex engineering problems.

The tyres are often the only link between the vehicle chassis and the environment. This is especially true when the aerodynamic forces, acting on the vehicle, are ignored. The tyre must thus transmit the vertical, lateral, and longitudinal forces, as well as moments, acting on the vehicle. The tyres play an important role in the performance, handling, and ride-comfort of a vehicle. The tyre-road interaction presents one of the biggest challenges in creating an accurate vehicle dynamics simulation model. To accurately describe a vehicle's behaviour, it is necessary to understand the tyre characteristics and their effect on the vehicle behaviour. The resulting tyre forces and moments are nonlinear and depend on the operating environments, such as road surface, inflation pressure, etc., and imposed states, such as slip angle, magnitude of loading, and others. Research has focused on accurately describing the forces generated in the tyre-road contact area for many years.

Pacejka and Sharp [1991] developed a list of features that mathematical tyre models should have to be relevant and useful in vehicle dynamical simulations. These features include:

- i. Accuracy;
- ii. Range of behaviour encompassed;
- iii. Number of parameters;
- iv. Physical significance of the parameters;
- v. The means by which the parameters may be obtained and the data that is required;
- vi. The capability and simplicity of extension to cover behaviour outside the range used for parameter evaluation and;
- vii. Computational load.

Researchers have developed numerous tyre models to improve our understanding of tyre behaviour and to accurately predict the tyre behaviour [Lugner et al., 2005]. These models vary in complexity, ranging from simple empirical formulations to three-dimensional nonlinear finite element tyre models. The complexity and modelling approach is dependent on the intended use and the required accuracy of the model. Antoine et al. [2005] presented the tyre model detail requirements, including the required excitation frequency, for various vehicle dynamic simulation scenarios. An overview of the model applications is shown in Figure 2-2.

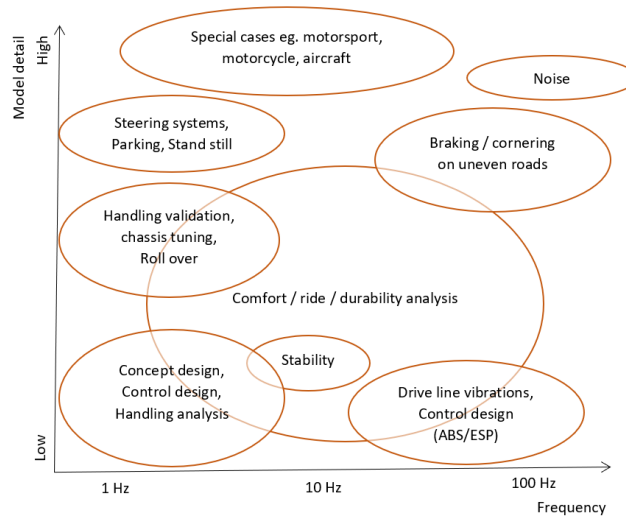


Figure 2-2 Frequency range requirements for vehicle-system analyses [Figure adapted by author from Antoine et al., 2005]

Several tyre modelling approaches have been developed to describe the physics of the tyre so that they can be analysed and evaluated mathematically [Schmid, 2011]. Most of the early models were used to describe the lateral tyre forces and accompanying moments for handling analyses. These models are mostly used in simulations which investigate the vehicle behaviour during handling manoeuvres on smooth road surfaces. Schlippe and Dietrich [1942] investigated the tyre side force slip characteristics to better understand tyre shimmy. They developed a tyre model that is based on the working principle of a string. The tyre belt is modelled as a massless, infinitely long string. The model generates the tyre forces due to the stretching and deformation of the string. A similar approach was followed by Fiala a few years later [Fiala, 1954; MSC Software, 2015]. The Fiala tyre model is a physical tyre model where the tyre carcass is modelled as a beam on an elastic foundation in the lateral direction. The contact between the tyre and the road is modelled with elastic brush elements. These assumptions form the basis on which an analytical expression for the steady-state slip characteristics can be derived. The brush model is commonly encountered in the tyre modelling literature [Pacejka, 2005]. In this modelling approach the tyre is approximated by elastic bristles that are attached to a elastic or rigid carcass. These bristles, or tread elements, make contact with the road surface. The brush model relies on the assumption that the tyre slip is caused due to the compliance of the carcass and tread elements.

One of the most important, and certainly one of the best known, handling tyre models is the Magic formula tyre model of Pacejka [Pacejka et al., 1987]. Pacejka presented the semi-empirical tyre model in 1987 and since then Pacejka and others have published several versions and

improvements of this tyre model. The latest developments from Pacejka himself have been published in a book, Tyre and vehicle dynamics [Pacejka, 2005]. The Magic Formula is a mathematical formula that can describe the basic tyre characteristics for the interaction forces between the tyre and the road under several steady-state operating conditions. The Pacejka semi-empirical model was not derived from the physical background of the tyre structure but consists of a set of approximation curves.

The first investigations of the tyre behaviour on road irregularities were conducted in the 1960's [Benz, 2008]. Initially only experimental tests were conducted to investigate the enveloping behaviour of the tyre while rolling over an obstacle or over roads with short wavelength unevenness. Models describing the dynamic response of tyres to short wavelength road irregularities were only developed in the 1980s [Schmeitz, 2004]. Since then many tyre models were developed due to the growing interest in the simulation of vehicle models and the demand to accurately model the tyre behaviour to investigate the ride comfort and durability of the vehicles driving over uneven terrain [Els et al., 2007; Cao et al., 2011] and deformable terrain [Taheri et al., 2015].

Commercially available tyre models are generally used for vehicle dynamics simulations. The tyre models developed in the university environment can in many cases not supply the constant and professional model support and development that is required. Secondly, the integration of the tyre models into various commercially available simulation software requires constant development and modification [Benz, 2008]. Commercially developed and supported tyre models on the other hand have the capacity to supply the required model support and constant model development. In general, commercial tyre models however don't allow the user a detailed insight into the model construction and the underlying model equations. These models can thus be considered as a grey box as some of the information about the modelling approach is available, but the specific construction is unknown to the user. Some of the most commonly used tyre models that are commercially available are MF-Swift [TNO, 2013], TameTire [IPG-Automotive, 2017], TMeasy [TMeasy, 2017], FTire [cosin scientific software, 2017b], CDTire [CDTire, 2017] and RMOD-K [RMOD-K, 2017a]. FE tyre models can also be added to the group as many commercial FE codes include tools to support the user with the modelling of tyres [MSC Software Corporation, 2016].

In literature, several authors including Zegelaar [1998] and Schmeitz [2004] present a comprehensive overview of various tyre models that were developed to accurately simulate the tyre behaviour. Both authors sort various modelling approaches into categories. Some of the

discussed modelling approaches are single point contact, roller contact, footprint, radial spring, flexible-ring, and finite element models. Many tyre models can however not be clearly associated to a specific group as many models comprise of a combination of these modelling approaches. An example of this is the SWIFT tyre model. Although the dynamic properties of the SWIFT model are based on a physical modelling approach, a semi-empirical magic formula is used to describe the contact forces [TNO, 2013]. Einsle [2010] furthermore poses the question whether a tyre model, based on a physical modelling approach, can still be classified as a physical tyre model when the model uses empirical tuning parameters to improve the accuracy of the model. It is thus difficult to discuss the modelling approach of these tyre models in groups but should rather be discussed based on the individual modelling approach. A summary of the different modelling and parameterisation approaches of the most common and commercially available tyre models is presented in Appendix A.

These tyre models can be subdivided into three groups depending on the modelling approach and modelling complexity. A tyre model classification, as summarized by Gipser [2016], is shown in Figure 2-3. To accurately model a system in the simulation environment, suitable parameters for the model need to be available. The usual procedure to parameterise multi-body-dynamic tyre models is measurement based. Many tyre models thus depend heavily on experimentally obtained parameterisation data to ensure an accurate model representation. These tyre models vary in complexity and have different applications, and thus the requirements of the essential parameterisation data vary greatly. The cost and effort to obtain the parameters are thus an important consideration for model selection.

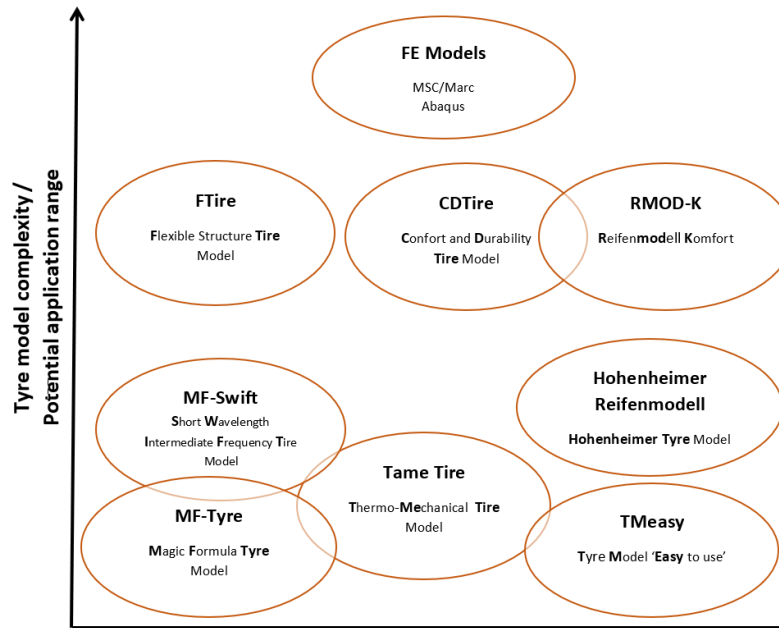


Figure 2-3 Commercial tyre model classification [Figure adapted by author from Gipser, 2016]

The first modelling approach of the first group is characterized by the focus on modelling the effects of the tyre to certain conditions rather than the underlying cause of the tyre behaviour [Gipser, 2016]. Examples of this approach are MF-Swift [TNO, 2013], TameTire [IPG-Automotive, 2017], and TMeasy [TMeasy, 2017]. The predicted tyre behaviour of these models is computed using a combination of nonlinear tyre properties that are superimposed on to each other to predict the tyre behaviour. Since these models are based on an empirical or semi-physical modelling approach the application range is limited as the models don't inherently guarantee physical meaningful results. A simplified approach is used in these models to model the tyre contact patch. These models are thus suited for vehicle handling analysis on a smooth road. For ride comfort and durability simulations the MF-Swift model incorporates an enveloping model with elliptical cams [Schmeitz, 2004]. The cams move over the road surface and generate an effective road surface. The effective road surface is then used as an input to the dynamic tyre model. Advantages of this modelling approach include the accessibility of scaling factors for parametric studies. The tyre models of this group are primarily focused in describing the handling characteristics of a tyre. As such the parameterisation is also focused on this area and thus requires experimental test data that describe pure and combined steady state slip characteristics.

The MF-Swift parameter identification process requires pure and combined steady state slip characteristic tests, basic tyre properties such as the tyre stiffness, rolling radius, contact patch

dimensions, and rolling resistance, as well as cleat test data is to determine the enveloping and in- and out-of-plane tyre dynamics [Schmeitz and Verstedden, 2009].

The TameTire model is parameterised from test data that is obtained from a flat track tyre test machine. The machine is used to simulate track conditions of a standard reference test track. In addition to these tests additional tests are conducted at various loads, velocities, and inflation pressures. During the measurements, the thermal state of the tyre is recorded [Pearson et al., 2016].

The parameterisation of TMeasy requires tests to be conducted to determine the vertical, lateral, longitudinal and torsional stiffness and damping parameters of the tyre. The lateral and longitudinal force characteristics are defined by an initial slope, maximum force, slip where the maximum force occurs, sliding force, and the slip where sliding occurs. A set of aligning parameters are used to determine the self-aligning torque. Tests need to be conducted to determine the normalized pneumatic trail, lateral slip where the pneumatic trail changes sign, the slip where the trail tends to be zero, rolling resistance coefficient and the dynamic rolling radius [TMeasy, 2017].

The second group of tyre models is developed to describe physical behaviour of the tyre [Gipser, 2016]. This modelling approach inherently captures the underlying tyre behaviour allowing the model to be used for a wide range of applications. Physics based tyre models often include inflation pressure dependencies, temperature and tyre footprint pressure distribution effects on the tyre behaviour. These models are suited for ride comfort and durability simulations, on road irregularities even with extremely short wave-lengths, as well as handling simulations. FTire [cosin scientific software, 2017b], CDTire [CDTire, 2017] and RMOD-K [RMOD-K, 2017a] models fall in this category. The Hohenheim Tyre Model [Universität Hohenheim, 2017] also falls into a sub-category of this modelling approach as it is based on a physical approach. The tyre is modelled in a two-dimensional plane whereas all other models of this category are modelled in three dimensions. The parameterisation of this group of tyre models is heavily dependent on an extensive set of experimental test data and requires an experienced user [Stallmann and Els, 2014].

The seventeen Hohenheimer Reifenmodell model parameters can be extracted from test data from a flat track and single wheel tyre tester found at the University of Hohenheim [Hohenheimer Reifenmodell, 2017b]. Data that is required to parameterise the tyre model includes the tyre

radius, roll radius, radial runout and tests that can be used to extract the radial, tangential, axial-spring and damper coefficients as well as the inter-radial spring coefficients.

The parameterisation of physically based tyre models is challenging and clearly needs some experience [cosin scientific software, 2017c]. Due to the complexity of the parameterisation process of FTire [cosin scientific software, 2017d], RMOD-K and CDTire [CDTire, 2014b] tyre model specific software tools have been developed to support the user with the parameterisation of these tyre models. The codes provide several optimization routines to minimize the error between measured results and the corresponding model behaviour. A wide range of experimental test data, including quasi-static vertical, lateral, longitudinal, and torsional tyre stiffness, modal data, footprint, handling and dynamic cleat test results can be used to parameterise these models. The outcome of the model parameterisation is largely dependent on the availability and quality of the available test data.

The third and final group is the finite element (FE) modelling approach. This numerical technique finds the approximate solution to a boundary value problem for a set of partial differential equations. The tyre is discretized into elements to accurately describe the tyre geometry. Different material properties can be assigned to these elements to accurately represent the local and global tyre behaviour. These tyre models can provide the user with a powerful tool to study the tyre behaviour due to the tyre construction [Schmeitz, 2004]. Compared to the previous modelling approaches this method is more computationally intensive. This computational expense is considered a major limitation of FE tyre models [Zhang, 2001]. One of the biggest challenges of modelling the tyre in a FE environment is to obtain the necessary geometry and material properties. These properties are not readily available, and manufacturers tend not to share this proprietary information.

2.2. Recent advances in parameterising large OTR tyre models

To accurately capture the road input, during rough terrain vehicle simulation, a physical tyre modelling approach is required. The physical tyre description furthermore inherently captures the relevant tyre mechanics and is thus capable to predict the tyre forces and moments during off-road simulations. The biggest challenge to use these models however is to obtain the extensive experimental test data sets that are required for the parameter identification processes. Acquiring the necessary test data for such large off-the-road (OTR) tyres remains a challenge due to their size and high operating load conditions.

Most tyre models are developed for passenger car tyres; however, research has shown that these models can also be used for large off-road truck tyres [Stallmann and Els, 2014; Babulal et al., 2015]. Various test rigs have been developed by research institutes and Universities [Stallmann and Els, 2014, Witzel, 2016] to obtain test data from these tyres. The Vehicle Dynamics Group at the University of Pretoria has specialized in the developed various test rigs to perform tests on large tyres. A static test rig has been developed that can perform quasi static tests on non-rolling tyres. The test rig can be used to determine the lateral, longitudinal and torsional tyre stiffness's at a vertical load of up to 250kN. The test rig can also be used to perform tyre contact area tests as well as modal analyses tests. If required, the camber of the tyre can be adjusted from -5 to 5 in 1-degree increments. A tyre test trailer is available to obtain tyre test results on a rolling tyre. The test trailer can be used to conduct dynamic handling tests as well as tests over uneven terrain. Vertical tyre loads of up to 52kN can be tested with the trailer [Stallmann et al., 2014].

These test rigs have been successfully used to conduct tyre model parameterisation tests. Challenges however still exist and need to be addressed. Test rigs are often specifically designed and built to perform these tests. The high operating loads and the large tyre size also make it difficult to accurately control the tests conditions and to isolate the tyre behaviour, from the overall system response, during the tyre tests. The standardisation of testing procedures, and exchange of test data, is challenging due to the individual design and construction of the test rigs. Measurement trailers, used to conduct parameterisation tests on a rolling tyre, reveal challenges concerning the reproducibility of the tests due to the changing environmental conditions such as temperature and road friction values [Schmid and Förschl, 2009], as well as difficulties in controlling the test conditions, such as wheel loading conditions.

The test equipment is often custom built and adapted to the test tyre and required test conditions. Expert knowledge is also needed to interpret the test data to isolate the tyre behaviour from the noise, effects of the test equipment and external disturbances. These limitations, and the available test equipment make it difficult to parameterise tyre models of large off-road tyres.

2.3. FE tyre modelling

FE methods are well established in the automotive industry [Abbey, 2014]. These methods are often used in the structural analyses of vehicle components or assemblies. In recent years, the mechanical analysis using finite element models has increased. This can be attributed to the improved accuracy; increased model fidelity requirements and the ever-increasing computational performance of computers.

FE models are often used by tyre manufactures to aid in the development and construction of new tyres because analytical models are insufficient to explain many problems related to tyre dynamics [Nakajima, 2011]. FE models are also used to visualize the stress and strain behaviour of a tyre. Modern finite element analysis (FEA) tyre models can vary in complexity but allows for a wide range of analysis ranging from:

- 1) Dynamic Mechanical Analyses (DMA) to improve the vehicle performance for traction, braking and handling manoeuvres [Olatunbosun and Bolarinwa, 2004; Tönük and Ünlüsoy, 2001; Koishi et al., 1998; Kabe and Koishi, 2000]
- 2) Noise, vibration, and harshness analyses (NVH) to improve vehicle comfort and reduce noise in and around the vehicle [Zheng, 2006; Jeong et al., 2007]
- 3) Durability analyses to ensure that the tyre will not fail prematurely [Jeong, 2016; Behroozi, et al., 2012]
- 4) Tread design analyses to improve braking, traction and wet tyre performance [Abbey, 2014]
- 5) Nonuniformity of tyres [Jeong et al., 2007]
- 6) Environmental analyses to reduce the rolling resistance of the tyre [Hoever, 2014; Behroozi, et al., 2012; Wei et al., 2016; Ghosh et al., 2003]
- 7) Coupled tyre–terrain interaction [Shoop, 2001]

FE tyre models are also used to overcome limitations of laboratory test equipment or as a viable alternative for destructive tests such as burst tests [Behroozi et al., 2012]. Researchers have also successfully shown that FE tyre models can be used to parameterise passenger car tyre models [Balaramakrishna and Kumar, 2009; Wei, 2015]. FE tyre models thus have a wide range of applications and provide the researcher or engineer with important information about the behaviour of a pneumatic tyre.

One of the biggest challenges of modelling the tyre in a FE environment is to obtain the necessary geometry and material properties. These properties are not readily available, and manufacturers tend not to share this proprietary information. Hyper-elastic and viscoelastic material properties can be obtained from physical material tests. The experimental results are used to fit various material models. To successfully extract the required material model parameters from the test data, tests must be conducted for multiple states of strain under carefully considered loading conditions [Miller, 2000]. Miller notes that the required experiments, for defining material models, are not yet clearly defined by international standard organisations. Miller proposes that tests

should be conducted to test the simple tension, equal biaxial, and planar shear strain state of the material.

Researchers have used different approaches to acquire the necessary material properties. Olatunbosun and Bolarinwa [2004] used a FE tyre model to investigate the effect of tyre design parameters on lateral forces and moments. The authors acquired the material properties by cutting samples from the tyre and conducting tensile tests. The samples were cut from different sections of the tyre and at different orientations. The samples were modelled in the FE environment consisting of solid rubber elements and rebar elements representing the reinforcing material. The material properties were tuned until optimal correlation between the measured and simulated tensile test results were found. The authors presented the Mooney-Rivlin coefficients and the Young's modulus of the reinforcing material. A similar approach to obtain the material properties was followed by Conradie et al. [2015] to determine the material properties of an off-road passenger car tyre, and by Song et al. [2008] to determine the material properties of agricultural tyres.

Researchers also fit hyperplastic material models using experimental results from a simple uniaxial tension test [Jeong, 2016; Behroozi et al., 2012; Wei et al., 2016; Ghosh et al., 2003; Yang et al., 2010]. Some of the models, fitted to uni-axial test results, also included higher order models. It has been shown that fitting models to uniaxial tests may result in extremely poor material behaviour for operational modes other than uniaxial tension such as planar shear or biaxial tension [Ali et al., 2010; MSC Software Corporation, 2016]. It was thus recommended to force the material constants to improve the behaviour to more realistic stress strain behaviour or to use the Yeoh model. If no test data is however available, no ruling can be made about the accuracy of the model for the other operating modes.

Researchers also use material properties that were published. The published test results may however not correspond to the same tyre or even type of tyre [Hölscher et al., 2004; Zhang, 2001; Tönük, and Ünlüsoy, 2001; Mohsenimanesh et al, 2009; Korunović, et al.,2011].

Researchers are using a wide range of experiments to validate finite element tyre models. Hölscher et al. [2014] and Barbani et al. [2012] developed FE tyre models and validated the models by comparing the predicted tyre vertical force deflection characteristics to experimental results. The same approach was followed by Zhang [2001] to validate a composite FE truck tyre model. Zhang noted a considerable deviation at high deflection values. Zhang concluded that these deviations are most likely due to a lack of precise material properties and errors in the

geometric measurements. Wang [2012] also validated a FE tyre model by comparing simulation results to measurements. To improve the accuracy of the model Wang, adjusted the material and model properties.

2.4. Tyre deformation measurement

To provide information about the tire state, such as tire deformation or tire-road contact information, a new approach, called tire sensing, has emerged [Xiong et al.,2015]. Researchers have developed various methods, and measurement systems, to obtain tire deflection information on non-rolling as well as on non-rolling tires. A ultrasonic sensor for vertical tyre deflection measurements was proposed by Magori et al. [1998] Tuonen [2009] placed light emitting diodes (LEDs) on the tyre surface of a truck tyre to measure tyre carcass movement. These measurements were then used to estimate the tyre forces during heavy braking manoeuvres. Xiong and Tounonen [2015] used a two-dimensional line scan laser measurement system to examine the tire deformation over a wider area. The system was successfully used to measure the inner profile of the sidewall and part of the tread. These methods have a limitation that only a single point or only a small area is measured.

Digital Image Correlation (DIC) is an image analysis method, based on tracking features in recorded digital images [Grimson, 1981]. DIC is used to perform full field surface measurements using sub-pixel registration between the left and right images of a stereo camera setup. Using triangulation techniques, the 3D locations and deformation of features in the image can be determined.

According to Botha [2015] digital image correlation techniques reached maturity and the algorithms are robust and relatively easy to implement. The cost and size of the digital cameras has also significantly decreased in recent years. These factors lead to a surge in the use of these measurement techniques. These techniques are now often used in conjunction with optimisation and machine learning techniques. Very little work has however been published where this technique has been used for tyre testing.

Moser et al. [2010] used the digital image correlation technique to perform a variety of tyre tests. The technique was successfully used to measure the full field tyre surface deformation and strain state of the tyre sidewall during laboratory tests. Moser further proposes that this technique could be used during the validation process of finite element tyre models. The technique is also used to obtain material properties of rubber [Seibert et al., 2014].

Botha [2015] also used digital image correlation techniques to determine the side slip angle, as well as longitudinal slip ratio, during vehicle tests. Botha further showed that the technique could be successfully employed for rough terrain profiling.

Guthrie et al. [2016] expanded the work of Botha et al. [2012] to measure the three-dimensional contact patch inside rolling tyres. A set of digital cameras were mounted on the inside of a tyre. A stabilisation mechanism was used to position the cameras near the bottom of the tyre and facing towards the tyre contact patch while the wheel was rotating.

The parameter identification tool, CDTire/PI [CDTire, 2014b], supports the use of local tyre deformation information, from the sidewall and belt, to identify model parameters. The tyre deformation information that is currently supported with the CDTire/PI are local tyre shape measurements of the belt and sidewall. The CDTire/PI documentation showed that outer contour measurements, of the sidewall, during loading for a big agricultural tyre can be used to extract model parameters.

From the 2016-4 release of FTire, FTire/fit can extract model parameters from tyre carcass deformation results [Gipser M. 2016, personal communication, 27 April]. A new data category, FE results, was created for this purpose. This new development allows the user to identify model parameters from finite element tests and thus expands the list of tests that can be used to identify FTire parameters.

2.5. Tyre model used in this study

FTire [cosin scientific software. 2017b] is a full 3D nonlinear in-plane and out-of-plane tyre model. The Model was developed by Gipser [1999; 2002] over the past 20 years. FTire was developed for vehicle comfort simulations and the prediction of road loads with extremely short wave-lengths obstacles but can also be used for handling simulations.

FTire is based on a structural dynamics approach [cosin scientific software, 2017e]. The tyre model describes the tyre belt as a flexible ring that can flex and extend in the radial, tangential, and lateral directions. The belt is approximated by a finite number of rigid belt elements that are connected to each other in such a way that in-plane as well as out-of-plane movement of the elements is possible. The “belt elements” and their associated degrees of freedom are shown in Figure 2-4. In general, 100 to 200 of these belt elements are used to represent the tyre.

Every belt element is again associated with a finite number, between 10 and 100, of mass less “tread blocks”. Tread blocks are connected to their neighbours with nonlinear stiffness and damping properties in the radial, tangential, and lateral directions. These tread blocks are located along parallel lines. The user can prescribe the tread pattern geometry. The tread blocks height will then be defined according to the prescribed tread pattern. All 6 tyre forces and torque components, acting on the rim, are calculated by integrating the forces in the elastic foundation of the belt.

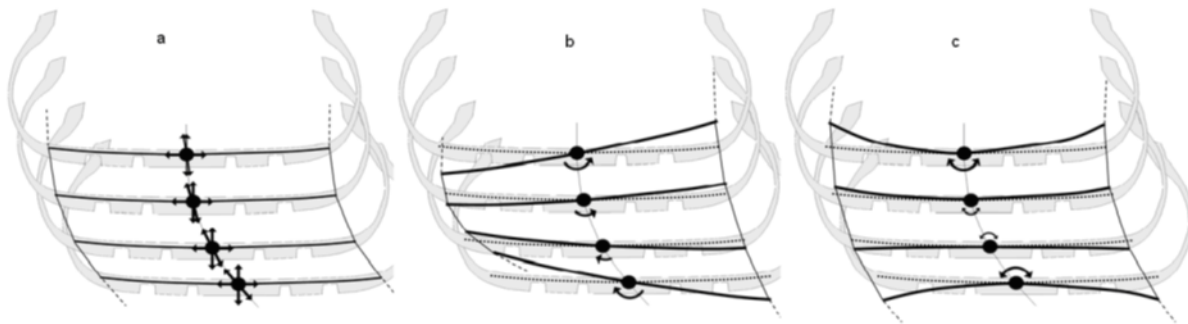


Figure 2-4 FTire belt elements degree of freedom [cosin scientific software, 2017e]

Due to the structural dynamics approach, there are very few restrictions to the simulated operating conditions of the model. FTire can deal with large or short-wave obstacles. It works for out of, and up to, complete stand still. FTire is also capable of running in strict real-time without any model switch or reduction of model accuracy.

An optional tyre thermal model is also provided with FTire. The model can be used to compute the actual inflation pressure as a function of the filling gas mass, cold tyre inflation pressure, tyre temperature, and actual interior volume. A heat generation and transfer model is introduced to determine the temperature of the tyre structure, the filling gas, and the temperature of each individual tread contact element. The rubber temperature of the tread, in addition to the ground pressure and sliding velocity, are used to determine the friction coefficient between the tread blocks and the road.

In addition to the temperature model, a tread wear model, air vibration model, and flexible rim model is available with FTire. The tread wear model affects the tyre cross-section geometry, contact pressure distribution, radial tread stiffness, tread shear stiffness, tyre mass, and the tread's heat capacity. The air vibration model can be used to determine the fluctuations of air density, air pressure, and air flow velocity inside the tyre. The unbalanced tyre pressure results in an uneven reaction force on the tyre structure and rim and thus influences the tyre forces in

higher-frequency ranges. The flexible and viscoplastic rim model determines the flexible and/or viscoplastic rim flange displacements and deformations from the spatial forces, exerted by the tyre on the left and right rim flanges. The rim can further undergo permanent plastic deformation.

Parameterisation of the tyre model is generally done with the FTire/Fit code [cosin scientific software, 2017d]. The code provides several optimization routines to minimize the error between measured results and the corresponding simulation with a FTire model. FTire/fit begins with an initial tyre estimate. The user can subsequently improve the tyre behaviour by supplying the parameterisation program with general tyre data and experimental test data.

The first stage in the parameterisation process is the tyre model preparation stage. In the preparation stage, a new tyre model is created from general tyre data. The general tyre data comprises of the tyre dimensions, operational pressure, mass, and other physical properties. The user can then “check in” various test results to optimize the model to better represent the physical model. Additional data that can be used to improve the accuracy of the tyre model, include tyre footprint images, static tyre stiffness, static cleat tests, side force slip angle measurements, dynamic cleat tests and various other test results. During the “check-in” process FTire/fit automatically determines the kind of measurement, depending on the operating conditions, inflation pressure, etc., and saves information on how the validation and/or identification is to be performed. The model parameterisation is done by minimizing the mean square deviation between the measurements and simulation results. Occasionally model parameters, such as radial, longitudinal, lateral, and torsional tyre stiffness, are directly extracted from the test data. If no test data, or only limited test data is available, the program will use the same parameter set that was loaded as the initial estimate. FTire/fit automatically generates diagrams during the parameter identification process showing the comparison between the simulation and measurement. The diagrams can be automatically compiled into a comprehensive parameterisation report.

2.6. Chapter summary

A review of a set of commercially available tyre models were discussed in this section. The discussed models can be subdivided into three modelling approaches. The first modelling approach is a descriptive approach. For this approach a selection of mathematical models, that describe isolated tyre properties, are superimposed on top of each other to describe the nonlinear tyre behaviour. These models may include an analytical solution based on a flexible or rigid ring to describe the frequency response of the tyre body. A simplified contact model is used to describe the tyre road interface. One of the biggest disadvantages of this modelling approach is that the models cannot be safely extrapolated to conditions that have not been measured experimentally. Advantages of this modelling approach include the accessibility of scaling factors for parametric studies and the short processing times.

The second modelling approach is based on the physical modelling approach. This modelling approach focuses on modelling the underlying cause of the tyre behaviour rather than capturing the effect. The physical description of the tyre inherently allows the model to extrapolate to various conditions. The tyre contact pressure distribution is realistically embedded in these models. Tyre models of this group tend to rely heavily on experimental results to extract the model parameters. The accuracy and validity of a tyre model is thus also dependent on the accuracy, and availability, of the measurements used to parameterise the model.

Research has also shown that the FTire model can be used to accurately predict the tyre behaviour of large tyres during off-road simulations. The biggest challenge is however to obtain the parameterisation test data to parameterise the tyre models. Specialized test laboratories, including the Vehicle Dynamics Group at University of Pretoria, have developed various test rigs to perform tests on large tyres. The limitations of the tests equipment and the large range of OTR tyres that are available, increase the complexity of parameterising large OTR tyre. An introduction into the FTire modelling and parameterisation procedure was presented.

The literature review has identified two alternative methods that can be used to obtain data that can be used to extract model parameters. The first alternative approach is the use of FE tyre models. Researchers have developed and used FE tyre models for a wide range of applications, including performing simulations to overcome limitations of laboratory test equipment. The required input data of a FE tyre model comprises of the tyre geometry and material properties. The test equipment, and testing effort, required to obtain these properties is largely independent of the test tyre size, and thus has the potential to broaden the range of tyres that can be parameterised. It should be investigated whether it is possible to obtain an accurate FE tyre

model with only the measured geometry and material properties as input to the model, without the need to tune the model parameters. This would improve the confidence in the FE model, especially if no measured tyre test data is available to validate the finite element model.

The second alternative approach that could be used to obtain parameterisation data is the use of Digital Image Correlation (DIC) technique. Researchers have successfully measured the full field tyre deformation during laboratory and field tests. Very little work has however been published where this technique has been used for tyre testing. Nevertheless, developers of tyre model parameterisation tools have included functions to extract model parameters from tyre carcass deformation results. In this approach, the attempt is made to extract stiffness parameters from local tyre deformation data. This approach is only feasible for tyre models based on a physical model approach.

Chapter 3

Investigated tyre

3. Investigated tyre

The tyre that was analysed for this project is the Michelin XZL 16.0R20 all-terrain tyre. The tyre could be used for on or off-road vehicles [Michelin, n.d.]. The Michelin XZL tyre was designed with a self-cleaning, open shoulder tread design with offset elements to increase traction on various terrains such as snow, sand, and mud. Figure 3-1 shows the tyre and its tread pattern.



Figure 3-1 Left: Michelin 16.00R20 XZL. Right: thread pattern [Michelin, n.d.]

Full width steel belts and a protector ply help to protect the tyre against off-road hazards. The tyre could be used with or without a tube. The weight of the tyre carcass is 154kg and the complete wheel, including the carcass, run flat insert and rim, was weighed at 240kg. The tyre specifications and dimensions are summarized in Table 3-1.

Table 3-1 Michelin XZL specification (Michelin, n.d.)

Size description	Load Range	Max. Speed [km/h]	Loaded Radius [mm]	Overall Diameter [mm]	Overall Width [mm]	Max. Load [kg]
16.00R20	M	88	607	1343	438	6595

The DOT identification number indicated that the tyre was manufactured in Kentville, Canada in the 36th week of 2010. The tyre was used for vehicle testing prior to this investigation but was still in operation and structurally undamaged. The remaining tread depth, at the time of the tests, was 22mm.

After testing, the tyre was dissected and measured to create a detailed CAD model of the tyre. The construction of the tyre is shown in Figure 3-2. The figure shows the exposed steel layers of the tread as viewed from the inside of the tyre. A cross section view of the tyre sidewall, presenting the single steel cord layer, is shown in section A of Figure 3-2. The figure shows that the tyre is constructed using a single carcass layer and three belt layers. The carcass layer consists of steel ropes that run from one bead to the other in a radial direction. Two steel belt layers follow the carcass layer. The belt layers are arranged in two different and opposing directions. The fourth layer is a steel rope cap layer. The cords of the cap layer run at a slight angle to the circumferential direction.

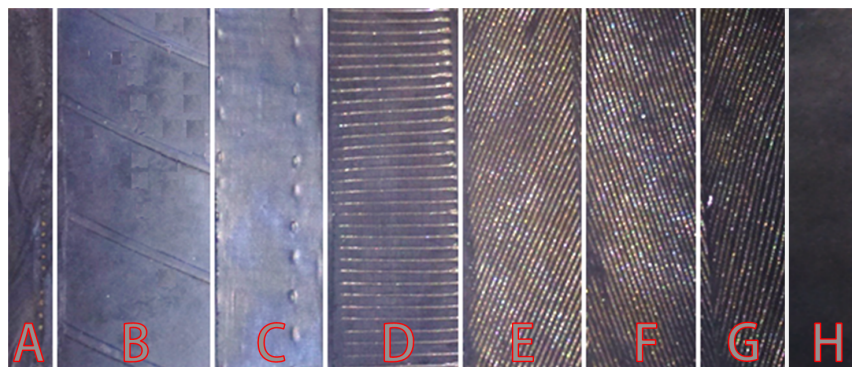


Figure 3-2 Tyre construction

A list describing the rubber layers and structural layers of the tyre is presented in Table 3-2.

Table 3-2 Tyre section description

Section	Layer	Remarks
A	Sidewall	Multiple rubber layers and a single carcass cord layer
B	Inner liner	Rubber layer covering the inside of the tyre
C	Carcass cord liner	Rubber surrounding the carcass cord
D	Carcass cord	Steel cord running from bead to bead
E	1 st belt layer	First steel cord belt layer
F	2 nd belt layer	Second steel cord belt layer
G	Cap ply layer	Cap ply layer
H	Tread rubber	Multiple rubber layers

To illustrate the tyre construction the CAD representation of the tyre, and rim, is shown in Figure 3-3. The tyre bead, indicated in red in Figure 3-3, consists of twisted steel strands. The steel carcass wires are wrapped around the bead on both sides of the tyre. The two steel belt layers, indicated blue and gold, cover the tread area. The final layer, indicated in green, is the steel wire cap layer.

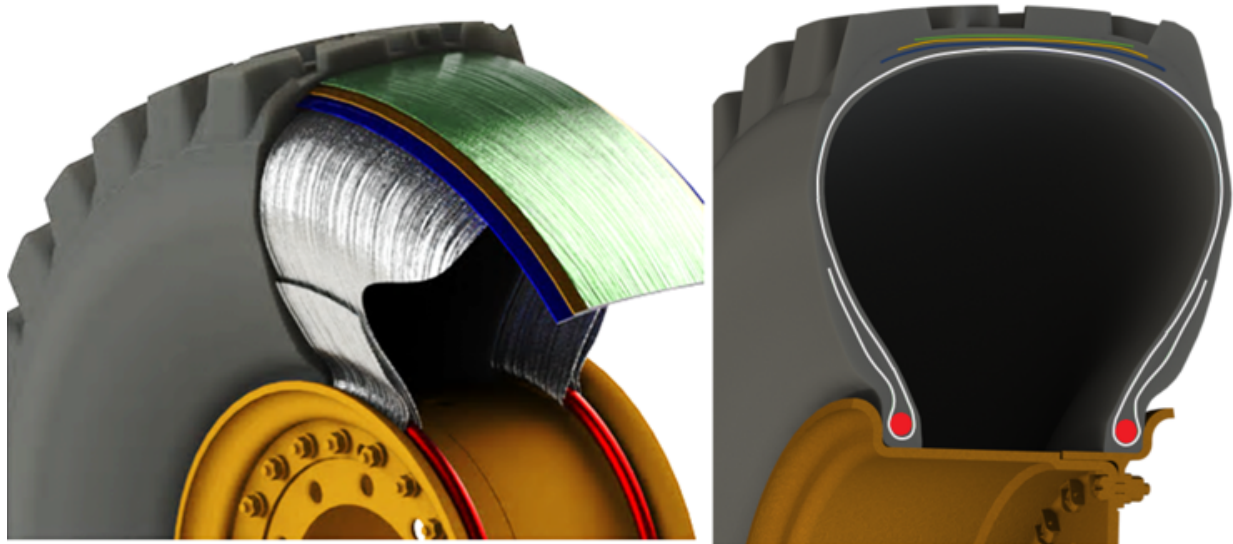


Figure 3-3 CAD representation of the tyre construction

The tyre was selected for this research project due to two main reasons. The first reason is that the tyre was used in a previous investigation [Stallmann et al 2014; Stallmann and Els 2014]. Although a newer tyre was used in this investigation the tyre construction remained the same. Newly obtained experimental test data from the tyre could thus be compared to the previously obtained test results. Not all test results could be repeated with the new tyre and the data was supplemented with test results from the previous investigation.

The tyre was also selected for this investigation as it is large enough to be classified as a large off-road tyre but still small enough to be easily tested in a general laboratory. The tyre construction is also representative of larger truck tyres due to the all steel cord reinforcing layers and the high aspect ratio of the tyre.

Chapter 4

Established FTire parameterisation method

4. Established FTire parameterisation method

The established and most commonly used parameterisation method for FTire models is to use experimental test data to extract the required tyre parameters. This procedure extracts specific tyre parameters from controlled laboratory tyre tests. This procedure is widely used in the industry today and will be used as baseline for this investigation.

In this chapter, the underlying parameterisation methodology will be discussed. The experimental test setups are presented, and the obtained test results are discussed. Not all required parameterisation tests could be conducted in a laboratory. Field tests were conducted, and the test data was used in addition to the standard parameterisation test data. The test results are then used to parameterise a FTire model. Finally, the parameterised tyre model is validated against measurements that were obtained from tests over discrete obstacles as well as on uneven road surfaces.

4.1. Introduction to the established FTire parameterisation method

Due to the complexity of the FTire model, some experience is required to successfully parameterise FTire. Special tools were developed to guide and assist the user through this process. These tools are FTire/fit [cosin scientific software, 2017d], FTire/estimate, included in FTire/fit, and FTire/calc [cosin scientific software. 2017a]. FTire/calc is a tool that may be used to parameterise a FTire model. This tool calculates the structural FTire parameters based on tyre design data that are commonly used as an input for FE models.

FTire/estimate is contained within FTire/fit and is used to estimate some basic tyre parameters. The estimation of the parameters is done by comparing the dimensions, mass and relative radial stiffness of the test tyre to a well-known reference tyre. Mathematic formulae are applied to estimate, or rather scale, some of the required FTire parameters. The quality of the estimated parameters can be improved if the selected reference tyre is similar to the current test tyre.

Parameterisation of the tyre model is generally done with the FTire/fit code. The code provides several optimization routines to minimize the error between measured results and the corresponding simulation with a FTire model. FTire/fit begins with an initial tyre estimate. The user can subsequently improve the tyre behaviour by supplying the parameterisation program with

general tyre data and experimental test data. The suggested FTire parameterisation workflow is shown in Figure 4-1.

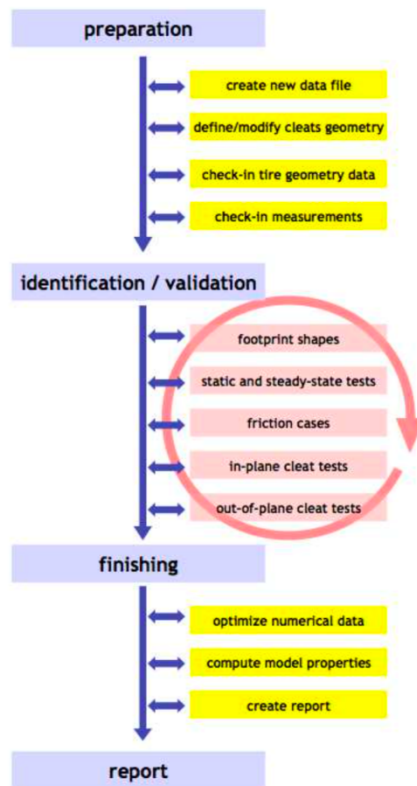


Figure 4-1 FTire/fit workflow [cosin scientific software, 2017d]

FTire/fit identifies tyre model parameters from the proposed set of measurements:

- i. static tyre properties (radial, longitudinal, lateral, and torsional stiffness on different surface geometries – such as flat plate and cleats);
- ii. footprint shapes;
- iii. steady-state rolling tyre tests;
- iv. time- and/or frequency-domain measurements of cleat tests

The first stage in the parameterisation process is the tyre model preparation stage. In the preparation stage, a new tyre model is created from general tyre data. The general tyre data comprises of the tyre dimensions, operational pressure, mass, and other physical properties. The user can then “check in” various test results to optimize the model to better represent the physical model. Additional data that can be used to improve the accuracy of the tyre model, include tyre footprint images, static tyre stiffness, static cleat tests, side force slip angle measurements,

dynamic cleat tests and various other test results. During the “check-in” process FTire/fit automatically determines the kind of measurement, depending on the operating conditions, inflation pressure, etc., and saves information on how the validation and/or identification is to be performed. The model parameterisation is done by minimizing the mean square deviation between the measurements and simulation results. Occasionally model parameters, such as radial, longitudinal, lateral, and torsional tyre stiffness, are directly extracted from the test data. If no test data, or only limited test data is available, the program will use the same parameter set that was loaded as the initial estimate.

The proposed tests were designed to highlight a specific tyre behaviour that is influenced by a selected number of FTire parameters. The tyre footprint tests, at zero-degrees camber, for example are predominantly dependent on the tyre geometry and belt lateral and in-plane stiffness. The shape and size of foot prints at a high camber angle are in turn mostly dependent on the belt twist and torsion stiffness. The full set of proposed parameterisation measurements can be used to identify the FTire parameters. If a measurement is not available, the parameter will either be estimated by FTire/estimate or will be directly adopted from the reference tyre file. It is thus recommended to obtain all the proposed measurements to ensure that the parameters match the test tyre.

The proposed set of measurements are intended for passenger car tyres and are based on tests that can easily performed be performed on existing test equipment. Similar tests are required for larger tyres. The measurement conditions need to be adapted to compensate for the larger tyre dimensions and rated operating loads. Some tests can however not be adapted or scaled due to test rig limitations. Alternative test procedures need to be performed or developed to extract FTire parameters from. The dynamic cleat tests fall into this category as no equipment is currently available to accurately preform these on drum or flat track test rigs.

4.2. Experimental test setup

Specially constructed test equipment was used to obtain the required parameterisation measurements. A static tyre test rig was constructed to obtain static tyre test data and a tyre test trailer was used to obtain some dynamic test data.

Static tyre test rig

To perform the static (non-rolling tyre) tests the test tyre was mounted to a static camber adjustment test rig. The test setup is shown in Figure 4-2. The camber adjustment test rig was designed to perform static tyre tests at various camber angles. The camber angle could be varied

between -6 and 6 degrees in one-degree increments. The rim was bolted to a non-rotating hub adaptor. A 250kN Shenck hydraulic actuator was used to apply a load to the tyre. A 75mm thick steel plate, which was connected with two linear bearings to the actuator, was used as a rigid contact surface. The linear bearings could be locked to avoid a sliding motion of the plate. A second actuator can be attached to the steel plate to perform lateral and longitudinal tyre stiffness tests.



Figure 4-2 Static tyre test setup

Cleats could be mounted to the steel plate to investigate the tyre behaviour on an obstacle. The steel plate can be rotated to test cleats in the lateral and longitudinal direction. The test setup with a square 50mm longitudinal cleat is shown in Figure 4-3.

During the tests, the applied loads, as well as the resulting tyre deflection, were recorded. A pressure sensor was also installed to record the tyre inflation pressure during the tests. All tests were conducted in an air-conditioned laboratory at a temperature of 22 degrees Celsius.

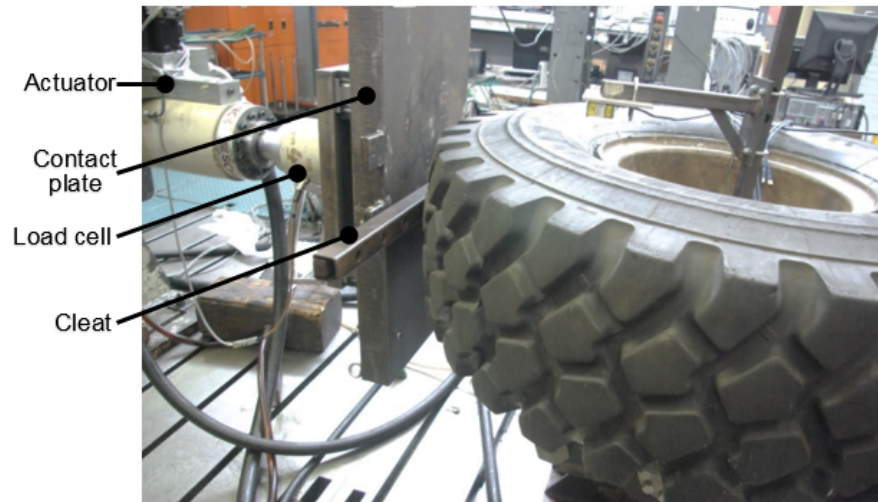


Figure 4-3 Longitudinal cleat test setup

Dynamic tyre test rig

A tyre test trailer was used in this investigation to obtain test results of a rolling tyre. The test trailer, as shown in Figure 4-4, comprises of two core structures, the main-frame, and a sub-frame. The test tyre is mounted to the sub-frame on the right-hand side of the tyre test trailer. The sub frame is connected to the main-frame by six universal tension/compression load cells. The load cells are positioned in such a way that all the forces and moments acting on the wheel can be determined (see Figure 4-4). Since the tyre test trailer has no suspension, all the forces acting on the load cells, connecting the main-frame to the sub-frame, could be related to the forces and moments that are generated in the tyre contact patch.

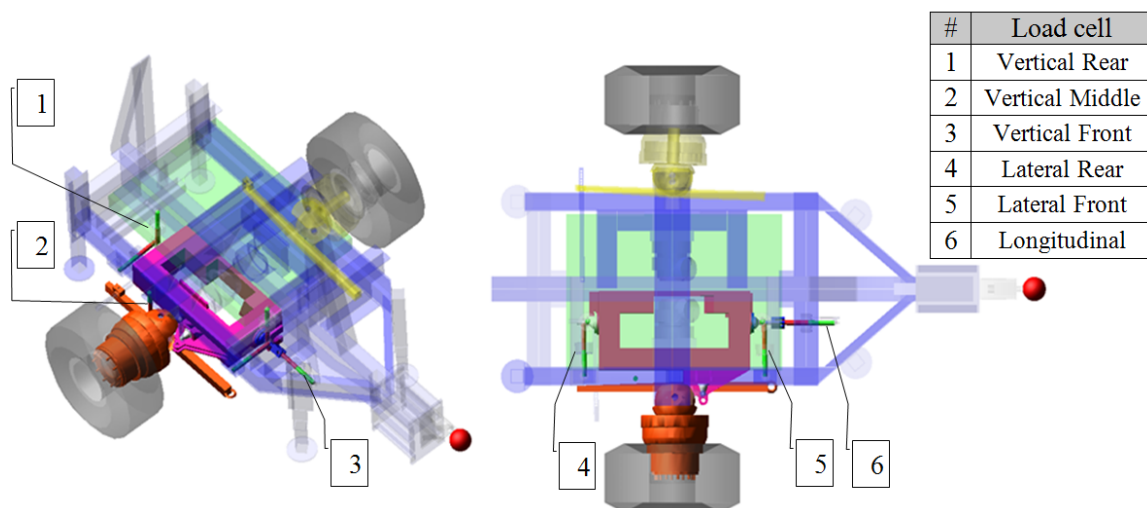


Figure 4-4 Load cell location of the tyre test trailer

The tyre track width of the tyre test trailer was wider than the track width of the towing vehicle. This allowed the towing vehicle to avoid obstacles while the test trailer was towed over these obstacles. Figure 4-5 shows a dynamic cleat test.



Figure 4-5 Tyre test trailer during a 50x50 mm dynamic cleat test

During the tests, the forces acting on the tyre test trailer load cells, the trailer velocities as well as roll, yaw and pitch velocities of the test trailer were recorded. Figure 4-6 shows typical measured forces and moments that are generated in the test tyre during the cleat test.

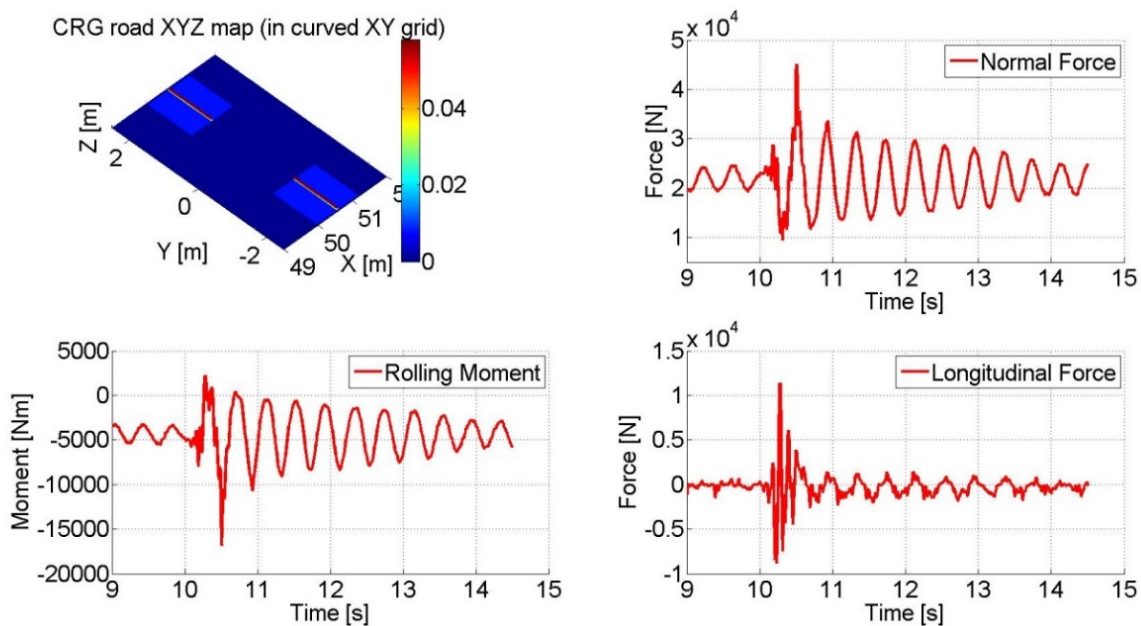


Figure 4-6 Experimental results of a 50 mm lateral cleat test

To investigate the tyre behaviour at different loading conditions the test trailer can be loaded with ballast so that the load on the tyre ranges from 2400 kg to 5200 kg. To determine the side-force slip characteristics of the test tyre the slip angle of the tyre test trailer can be changed. The actual slip angle of the tyre test trailer was recorded with a Correvit optical slip sensor. A braking torque can also be applied to determine the longitudinal force versus wheel-slip characteristics. The kingpin angle could not be varied and was kept fixed during all tyre tests.

4.3. Parameterisation Procedure

The FTire model is parameterised by comparing measured test results to the corresponding simulation results. A set of optimisation algorithms is used to determine the tyre parameters that best match the measurements. FTire/fit uses specific tests to optimise a predefined set of tyre parameters. These parameters are selected by the influence the parameter has on the specific test.

Parameterisation test were conducted at tyre inflation pressures of 1.0 and 3.0 Bar. An inflation pressure of 1.0 Bar is often used for manoeuvres on soft deformable terrain, such as sand, while a higher inflation pressure is needed for high speed driving on un-deformable road surfaces.

The first test that was conducted on the test tyre were footprint tests. The footprint size and dimensions are used by FTire/fit to identify various in-plane and out-of-plane tyre stiffness's. The footprints were obtained using the dye method [Els et al., 2016]. For the tests, a smooth surface is covered with a non-drying dye. The tyre is pressed against the surface until the desired load is reached. The load is then released. The tyre removes the dye in the areas where contact was made. A footprint test result, at zero degrees camber, is shown in Figure 4-7. A digital camera is used to capture the footprint. The obtained image is digitally modified to obtain a calibrated black and white image of the footprint. A red line with a known length of 100mm is also added to simplify the check-in procedure of the footprints in FTire/fit. Various footprint tests were conducted at 0 and -4 degrees camber angle.

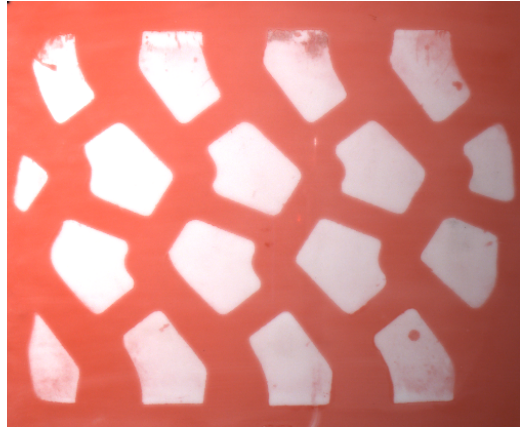


Figure 4-7 Footprint measurement, 3.0 Bar, 56.3 kN

The scaled footprint images, at 0 degree camber, were used to identify the belt lateral and in-plane bending stiffness parameters. The negative 4 degree camber angle footprint measurements were used to determine the belt twist and torsions stiffness. The footprint results, for a tyre with an inflation pressure of 1.0Bar, is shown in Figure 4-8.

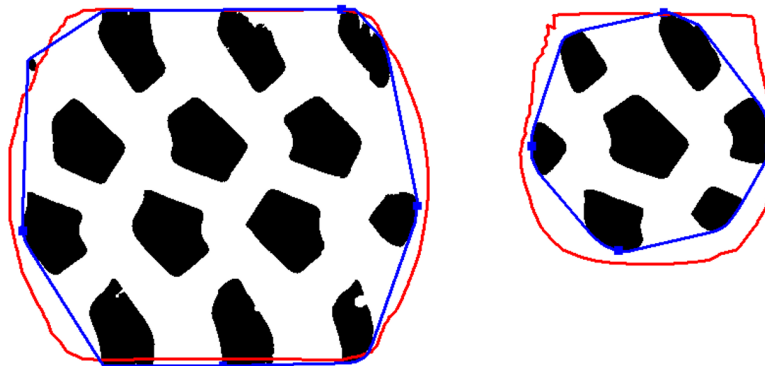


Figure 4-8 1.0 Bar footprint validation. Left: 19.2 kN. Right: 7.3 kN -4.0 deg camber

The blue outline indicates the measured footprint outline while the red line represents the predicted footprint outline of the current FTire model. Figure 4-8 shows that FTire is capable to accurately predict the shape and size of the footprint at 0 degrees camber. The correlation between the measurement and the model is slightly decreased for tests at low loads. The overall correlation is however acceptable as the underlying tyre behaviour is accurately represented.

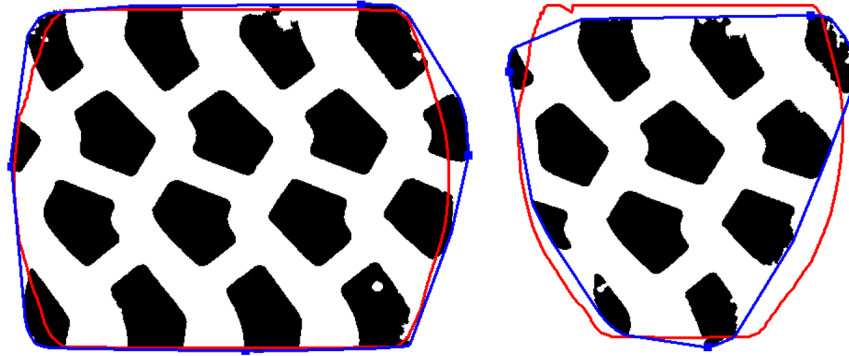


Figure 4-9 3.0 Bar footprint validation. Left: 56.3 kN. Right: 30.9 kN -4.0 deg camber

Figure 4-9 shows the measured and predicted tyre footprints for two loading conditions at an inflation pressure of 3.0 Bar. The figure shows that the model is capable of accurately predicting the tyre footprint for this higher inflation pressure.

The second stage of the parameterisation process is to identify the parameters that influence the tyre behaviour during steady state tests on a non-rolling tyre. These parameters describe the stiffness behaviour of the tyre carcass. The measured and predicted radial tyre stiffness, on a flat plate, is shown in Figure 4-10. Good correlation was again found for both inflation pressures.

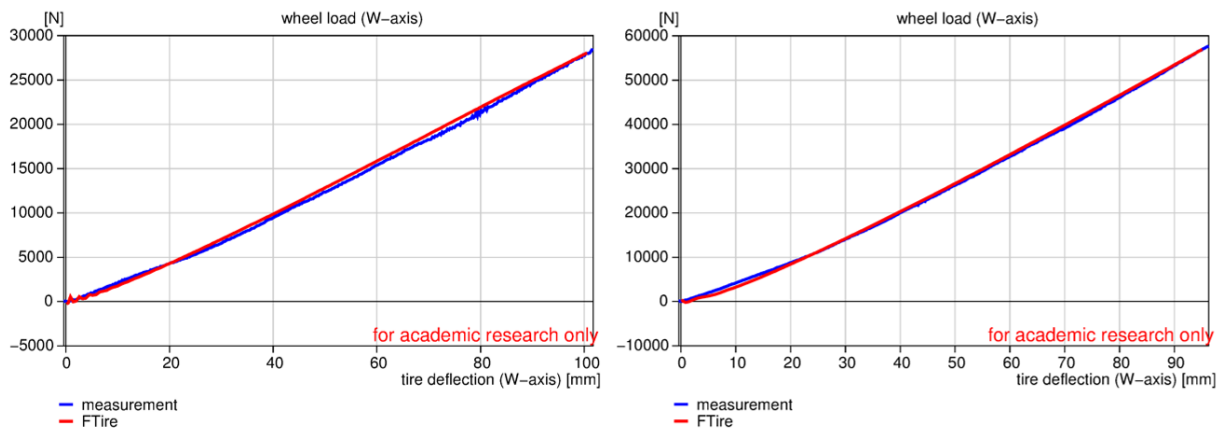


Figure 4-10 Radial stiffness validation. Left: 1.0 Bar. Right: 3.0 Bar

Figure 4-11 shows the radial tyre stiffness at a negative 4 degree camber angle. The model is again capable to accurately predict the wheel load during the camber tests. It should be noted that the vertical stiffness does not decrease during non-zero tyre camber tests as is the case for many passenger car tyres. The stiffness of a camber test is almost identical to the tyre stiffness during a zero-degree camber tests. This behaviour is attributed to the construction as well as the large aspect ratio of the tyre.

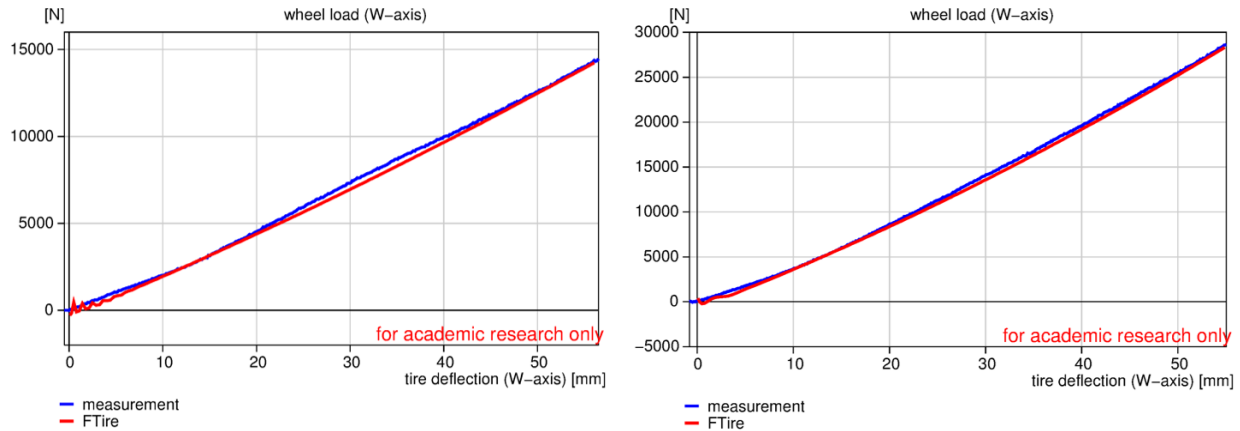


Figure 4-11 Radial stiffness -4.0 deg camber validation. Left: 1.0 Bar. Right: 3.0 Bar

The in-plane bending stiffness parameters of the tyre model can be identified with the use of transversal cleat tests. Transversal cleat tests at a camber angle can also be used to identify the belt twist stiffness parameters. The measured and predicted tyre load during a square 50 mm transversal cleat test at a negative 4 degree camber angle and an inflation pressure of 1.0 Bar is shown in Figure 4-12. Test results on a flat plate is added as reference. The percentage deviation between the vertical force on a flat surface and the vertical force during a cleat test is shown on the right-hand side of the figure. The tyre reaction force decrease shows a similar trend in the measurement compared to the simulation results.

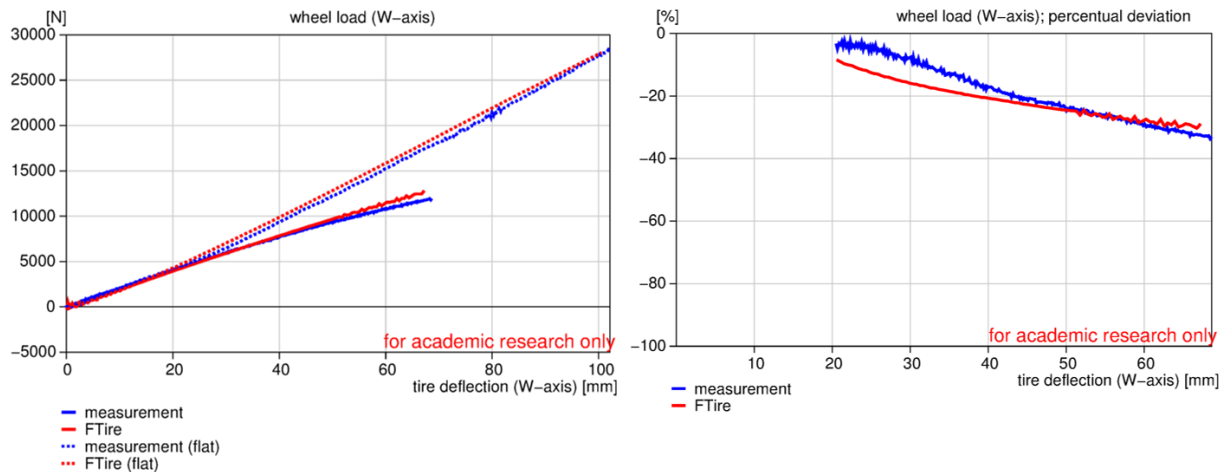


Figure 4-12 50mm transversal cleat validation, 1.0 Bar

Figure 4-13 shows the measured and simulated tyre load during a 50mm longitudinal cleat test. The presented test was conducted at an inflation pressure of 3.0Bar. The percentage deviation in the wheel load indicates that the lateral belt bending stiffness is lower at lower deflections but

increases as the tyre deflection increases. The figure shows that the model behaviour deviates from the measured response, especially at very high tyre deflections (>80mm). The correlation between the measurement and simulation is however acceptable.

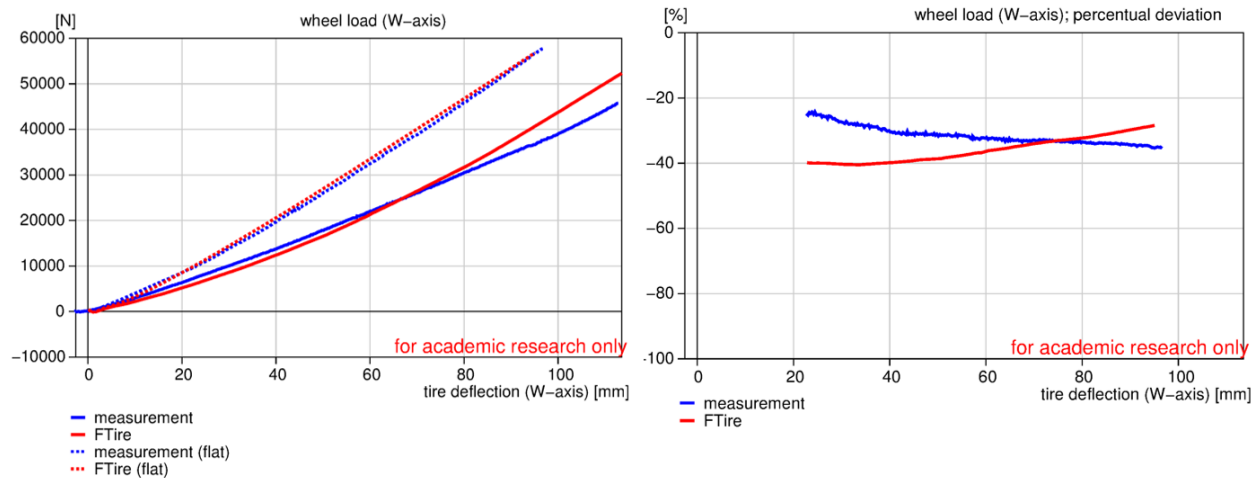


Figure 4-13 50mm longitudinal cleat validation, 3.0 Bar

The lateral and longitudinal tyre stiffness of the test tyre is shown in Figure 4-14. The tyre model is also capable to accurately predict these force displacement characteristics. The model is slightly over estimating the lateral tyre force for deflections between 10 and 40mm lateral rim displacement.

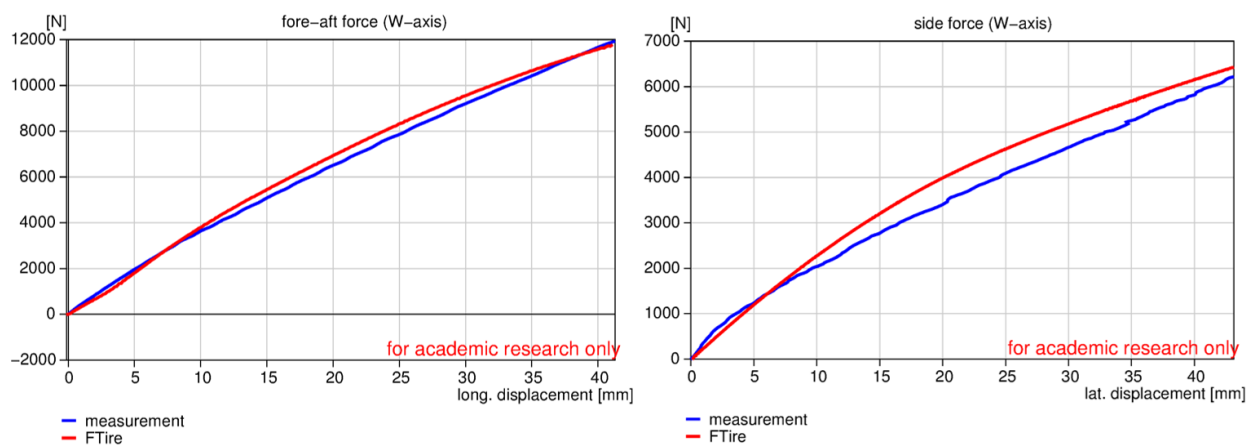


Figure 4-14 Left: Longitudinal tyre stiffness. Right: Lateral tyre stiffness 1.0 Bar

The handling parameters of the tyre model can be identified from side force versus side slip angle measurements. The braking and traction behaviour can be parameterised with longitudinal force versus slip test results. The results of the lateral force versus slip parameterisation, at an inflation

pressure of 3.0 Bar, are shown in Figure 4-15. The parameterisation of the handling parameters does not fall into the scope of this investigation but is discussed in Babulal et al. [2015].

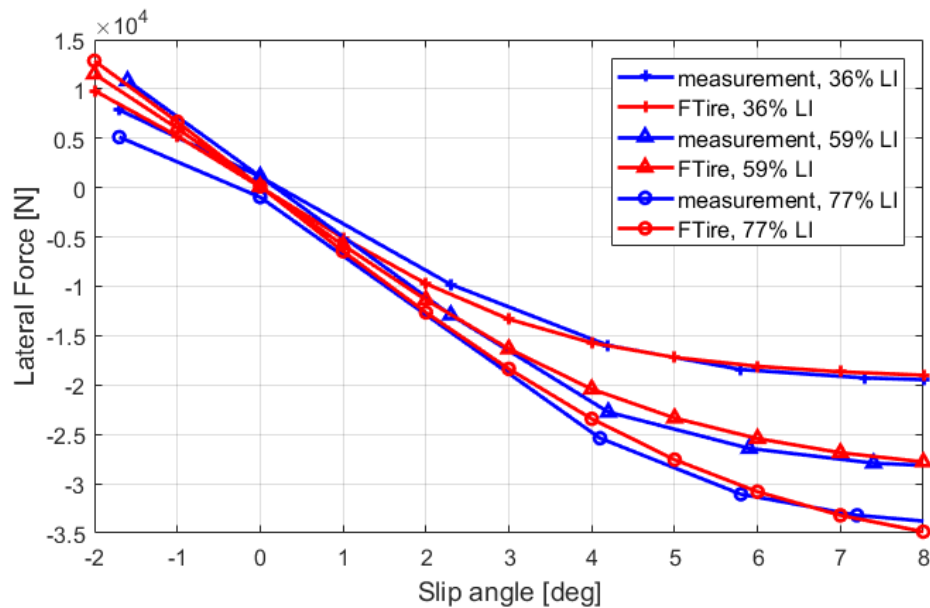


Figure 4-15 Tyre handling characteristics, 3.0 Bar

The final parameters that need to be identified are the damping parameters. The radial hysteresis characteristics of the tyre can be analysed by applying a sinusoidal displacement to the test tyre. Due to the hysteresis effect, the loading cycle will result in a larger radial force than during the unloading cycle. The result of a vertical stiffness test with a sinusoidal displacement is shown in Figure 4-16. Good correlation was found between the measurement and the simulation results.

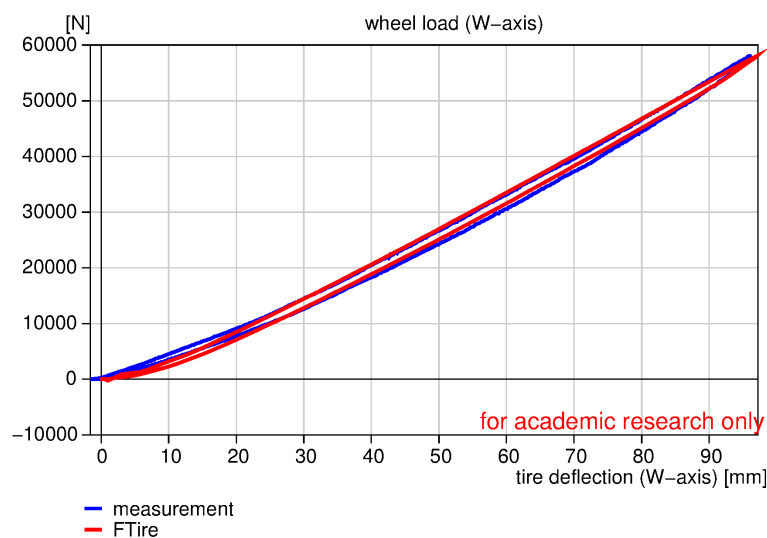


Figure 4-16 Radial hysteresis characteristics

The damping and inertia properties of FTire model are usually identified using drum test measurements from a rolling tyre while rolling over a clearly defined obstacle, such as a cleat. During these tests all degrees of freedom, except the spin axis to allow the tyre to roll freely, are fixed. These tests could however not be conducted for the test tyre due to the size and high operating load condition. Dynamic cleat tests were however conducted with a tyre test trailer. The limitation of these tests is that the obtained data cannot be used directly in FTire/fit. An ADAMS model of the trailer was created and used to simulate the cleat tests with the FTire model. The simulation results were compared to the obtained measurements. The logarithmic decrement was used to compare the damping behaviour of the test tyre to the tyre model. The logarithmic decrement is given by:

$$\delta = \frac{1}{n_p} \ln \frac{x(t)}{x(t + n_p T_s)} \quad (4.1)$$

where $x(t)$ is the amplitude at time t and $x(t + n_p T_s)$ is the amplitude of the peak n_p periods away, where n is any integer number of successive peaks. The relevant damping parameters in FTire were then manually tuned until good correlation between the measurements and the simulated results were found. The logarithmic decrement of the test data was calculated as 0.174. The damping parameters of the tyre model were tuned until the simulation results showed a decrement of 0.1662. This resulted in a relative error of 0.7%. The test and simulated damping response is shown in Figure 4-17.

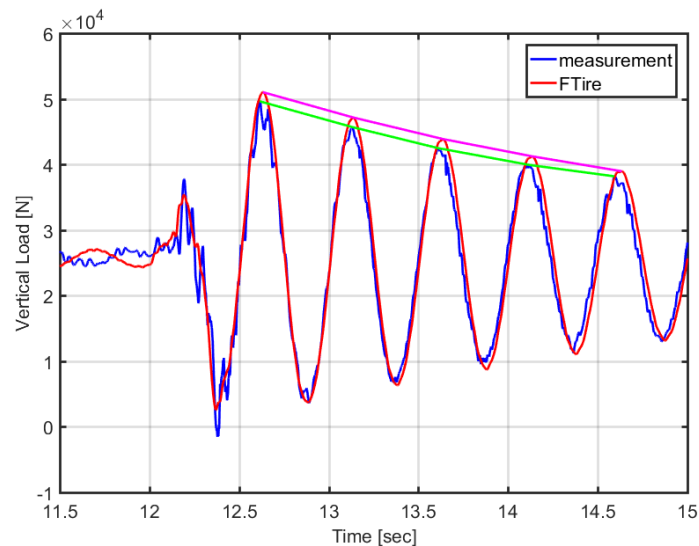


Figure 4-17 Tyre damping parameterisation

4.4. FTire Validation

Model validation is an important part of any model development process. It ensures that the model can accurately represent the modelled system and thus increases the confidence in the model. The increasing dependence on simulation results, in all areas of engineering, requires that no analysis, or the interpretation of the results, should be conducted without validating the model. Thacker et al. [2004] defines the validation process as “the process of determining the degree to which a model is an accurate representation of the real world from the perspective of the intended uses of the model”. The validation process is thus a process of collecting evidence of the model correctness or the accuracy of the model for a specific set of scenarios. During the validation process, experimental results of the real-world system are often compared to the corresponding numerical solutions. These conducted experiments, called validation experiments, are defined by Thacker et al. [2004] as “Experiments that are performed to generate high-quality data for the purpose of validating a model”. Experimental results, obtained from a highly-controlled test environment, is thus a prerequisite to validate the numerical model. The validation experiments should furthermore be a collection of tests that are representative of the intended use of the model.

The validation process is an important step to ensure that the parameterised tyre model accurately captures the tyre behaviour. Validation tests are often conducted for conditions that replicate the operating conditions for which the tyre model would be used. These tests are thus often of a dynamic nature as they are performed on a rolling tyre. Conducting these tests on large off-road tyres is however a major challenge. Due to the high loading conditions, as well as the size of the tyre, these tests need to be performed on specially constructed test equipment, such as tyre test trailers. Alternatively, in-situ tyre test can also be performed to obtain the necessary validation dataset. Tests are often conducted on various uneven roads to validate the tyre response due to road disturbances. The recorded tyre forces are thus not only a result of the road disturbances but are also affected by the test setups response to the generated tyre forces.

To validate the parameterised tyre model, tests were conducted with the test tyre rolling over a discrete obstacle and on various hard uneven terrains. It should be noted that the validation tests were conducted with a tyre test trailer, as was shown in Figure 4-4. The measured forces and moments that are presented in this section are the forces as measured by the load cells connecting the sub-frame of the trailer to the main-frame. Due to the dynamic nature of the test the tyre forces cannot be isolated from the data. The presented test results should thus be

interpreted as the systems response to various road disturbances. To achieve good correlation between the measurements and the corresponding simulation the entire system needs to be modelled accurately. The results are thus not only dependent on the accuracy of the tyre but also depend on the accurate representation of the tyre test trailer, the road as well as the applied boundary conditions. Although every effort was made to accurately represent the trailer in the simulation environment some errors might still be present and might influence the results.

Care should be taken to accurately model the test equipment in the simulation environment. Figure 4-18 shows the measured and simulated yaw, pitch, and roll velocities of the tyre test trailer. The test was conducted at the same speed and the same road conditions were used. During the initial investigation, it was assumed that the assumption of a fixed towing hitch can be made. The simulation results however show that the system response, of the trailer, is not accurately modelled when this assumption is made.

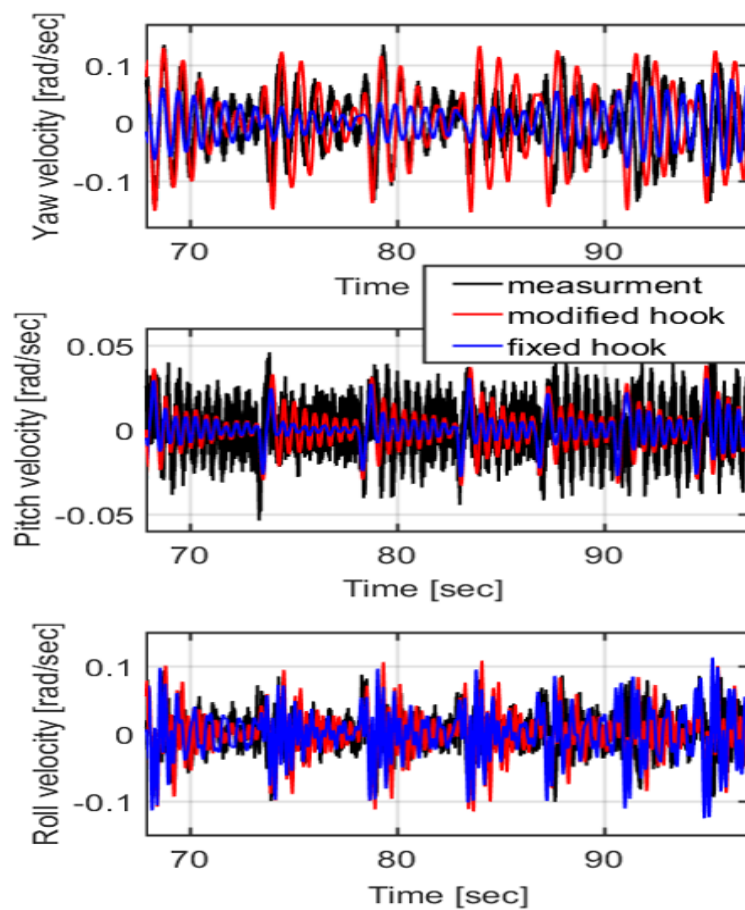


Figure 4-18 Trailer yaw, pitch and roll velocities during validation test.

The modelling approach was altered to allow the hook to move or deflect. A spring damper system, with stiffness and damping parameters in the longitudinal, lateral, and vertical direction, was added to the model. The simulation results, with the modified hook, showed that this modification greatly alters the system response. The model better represents the test equipment when the modifications were made to the hook. The correlation between the measured and simulated tyre forces were also dramatically improved.

Tyre validation tests should be conducted with extreme caution if tests of this nature is used to validate the tyre model. The tyre forces should not be looked at in isolation, but the response of the entire system should be analysed. If this is not done deviations between the measurements and simulation results may be interpreted as errors in the tyre model which might not be the case.

4.4.1. Discrete obstacles

Comparing measured and simulated tyre forces while rolling over a single discrete obstacle allows for direct time domain comparison of the results. The tyre test trailer was instrumented to obtain force measurements of the test tyre while rolling over a 50mm cleat. These tests were conducted at various axle loads and towing speeds. The longitudinal and vertical reaction forces during a 50mm transversal cleat test is shown in Figure 4-19. The shown test was conducted at a constant speed of 18km/h.

The test conditions were replicated in the ADAMS simulation environment. The simulation results are shown in Figure 4-19. It should be noted that the figures show the measured and simulated forces acting between the sub-frame and the main-frame of the tyre test trailer to include the inertial forces of the sub-frame and the rim. The forces thus represent the forces acting on the load cells that is used to connect the sub-frame to the main-frame. This was done to be able to directly compare the test and simulation results. The sub-frame forces can however be related to the generated tyre forces.

From Figure 4-19, it is evident that the model can predict the measured forces while clearing a discrete obstacle. During the experiments the right tyre of the tyre test trailer cleared the cleat slightly before the tyre on the left-hand side, resulting in a disturbance that is not modelled in the ADAMS environment. As a result, the test result shows a spike in the test data while clearing the cleat and at 8.22 seconds. This behaviour thus shows the difficulty to accurately control the test conditions. The overall correlation between the test and simulation results is however very good.

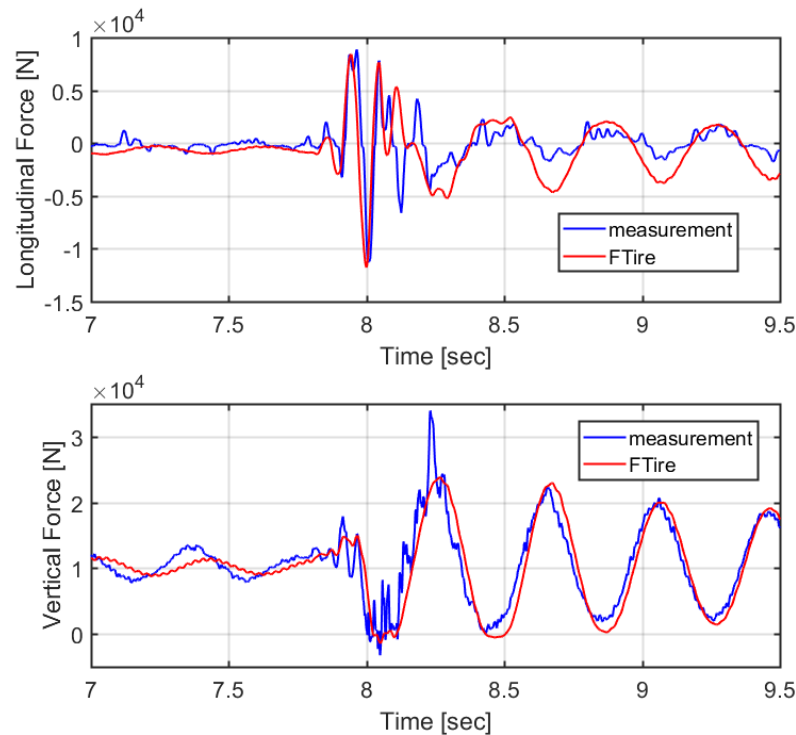


Figure 4-19 Discrete obstacle validation, 50mm transversal cleat. 18 km/h, 3.0 Bar.

4.4.2. Uneven road

Test tracks

The tests were also conducted on various test tracks at the Gerotek Test Facilities [Gerotek Test Facilities, 2017] to validate the model for simulations on uneven terrain. The test tracks have a length of one hundred meters and a width of about four meters. The road profiles of the test tracks were measured using the “Can-Can road profiling machine” [Becker and Els, 2014]. The “Can-Can machine” is a road profiling device that was developed at the University of Pretoria, which drags profiling arms over the road surface. By measuring the angle of these arms, a digital three-dimensional road profile can be created. The Can-Can road profiling machine is shown in Figure 4-20. The figure also shows the superimposed results of the post processed data that was obtained during the road profiling measurement.



Figure 4-20 Can-Can road profiling machine

The sensing arms were spaced 40 mm apart and during the tests the angle of the arms were recorded every 12 mm in the direction of travel. Using this technique, the road profiles of the test tracks were measured with a resolution of 40 mm by 12 mm. The measurements were used to create curved regular grid road definition files, better known as CRG road files [OpenCRG, 2011]. Figure 4-21 shows the CRG road representation of the Increasing frequency cleats test track. The test track consists of 50 mm high trapezoidal cleats that are spaced at various intervals. The spacing of the obstacles is reduced from an initial spacing of 10 m down to 0.7 m.

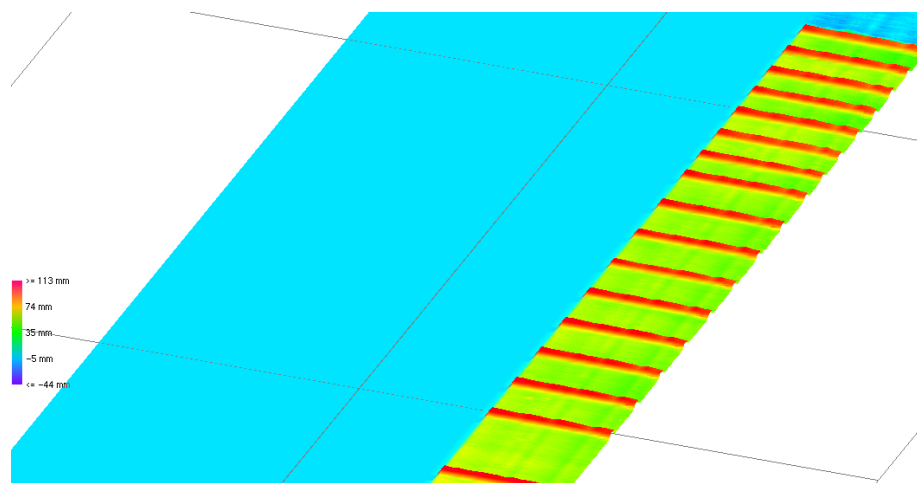


Figure 4-21 Increasing frequency cleat test track CRG road representation

The Belgian paving, also known as the Belgian block road, is often used to test the durability and ride comfort of vehicles. The blocks on the track have a random width but a regular length of 134 mm perpendicular to the direction of travel. Figure 4-22 shows the tyre test trailer during a test on the Belgian paving. During the validation tests, only the right wheel of the test trailer was on

the test track while the left wheel and the tyres of towing vehicle were rolling on a smooth concrete surface next to the test tracks.



Figure 4-22 Belgian paving validation test

The Displacement Spectral Density, DSD, is often used to describe the roughness of a terrain. A Power function or Inverse Power Law is often applied to DSD's of random roads using an equation of the following form:

$$S_z = A_x \varphi^{-n} \quad (4.2)$$

The spatial frequency range for φ , for off-road profiles, should be between 0.05 cycles/m (wavelength = 20m) and 10 cycles/m (wavelength = 0.1m) according to the ISO 8608 [International Organisation for Standardization, 1995] standard. The Roughness coefficient, A_x , and the Road exponent, n , can then be used to classify the roughness of the road. The method to obtain the Roughness coefficient and the Road exponent is discussed in Becker [2008].

The Roughness coefficient, A , of the test track is determined to be $3.48\text{E-}05 \text{ m}^2/\text{cycles/m}$ while the Road exponent, n , is 1.6. The Displacement Spectral Density of the Belgian paving is shown in Figure 4-23.

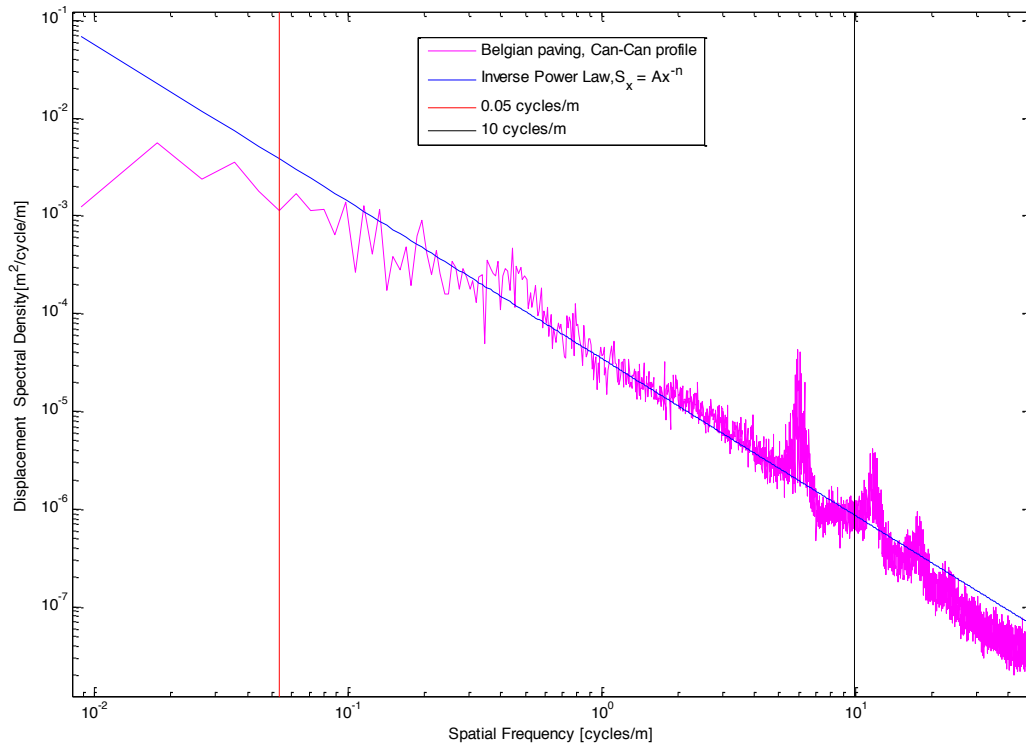


Figure 4-23 Displacement Spectral Density of the Belgian block road [Becker, 2008]

Validation results

The measured and simulated forces acting between the sub-frame and main-frame of the tyre test trailer while it is being towed over the increasing frequency cleats test track is shown in Figure 4-24. The figure shows that the longitudinal force is accurately represented, while the predicted lateral and vertical peak forces are slightly lower than the measured results. The lateral forces are generated due to the non-symmetric test track. The tyre on the right-hand side is pulled over the obstacles while the tyre on the left is rolling on a smooth road surface. A rolling and yawing motion of the test trailer is thus induced, which results in the lateral force being generated. Overall good correlation is found for all three force components.

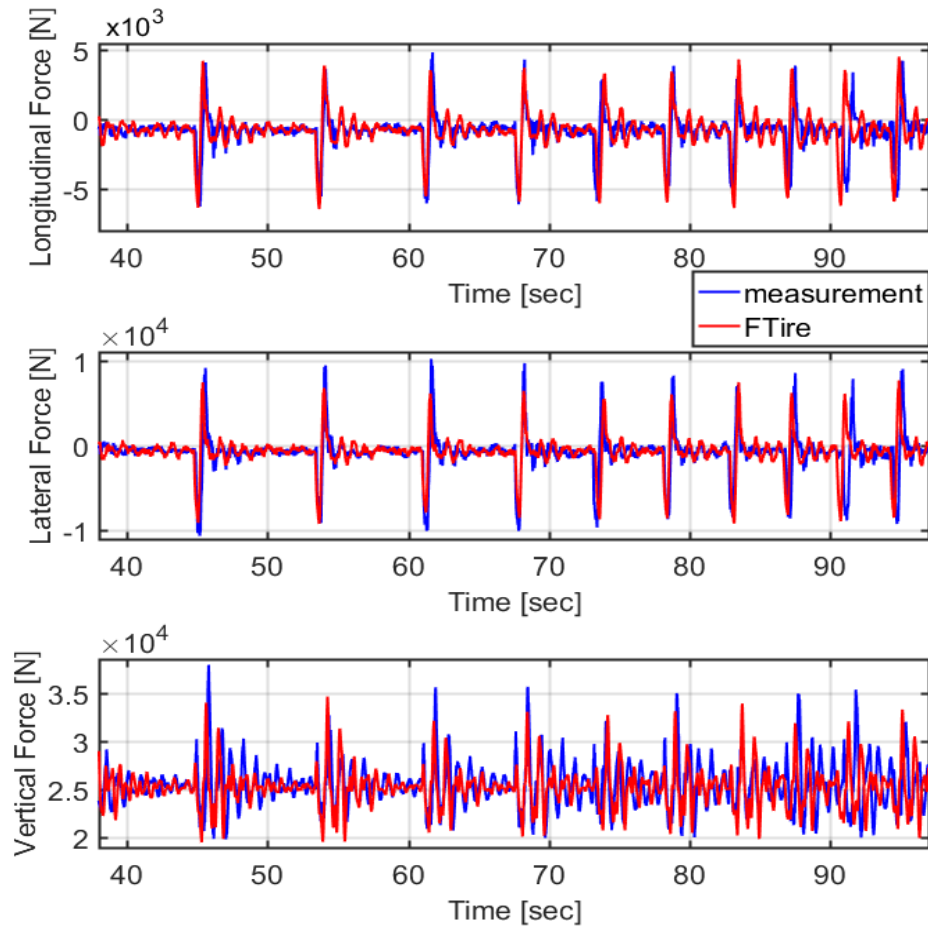


Figure 4-24 Validation results of the increasing frequency cleat test.

Time domain comparison of the test results is often difficult as it is extremely difficult to exactly repeat the test conditions in the simulation environment. One of the biggest problems is to drive over the exact part of the test track at the same speed. This is especially true for test tracks with random road unevenness such as the Belgian paving. Other ways of analysing the data should thus be used. Analysing the data with a statistical approach, rather than comparing the time domain results, gives greater insight into the system response due to the road disturbances. One of the methods is to determine the force histogram of the entire test. The force histogram shows the probability that a load condition is found during the test. The force histogram of the lateral and vertical forces are shown in Figure 4-25. The test was conducted at a speed of 5km/h. The figure shows that the measured lateral force, due to the road unevenness, can accurately be replicated with the simulation model. The vertical force histogram shows that the simulation model experiences vertical loading conditions that are slightly higher than the loading conditions during the experimental testing. The overall correlation between the two systems is however very good.

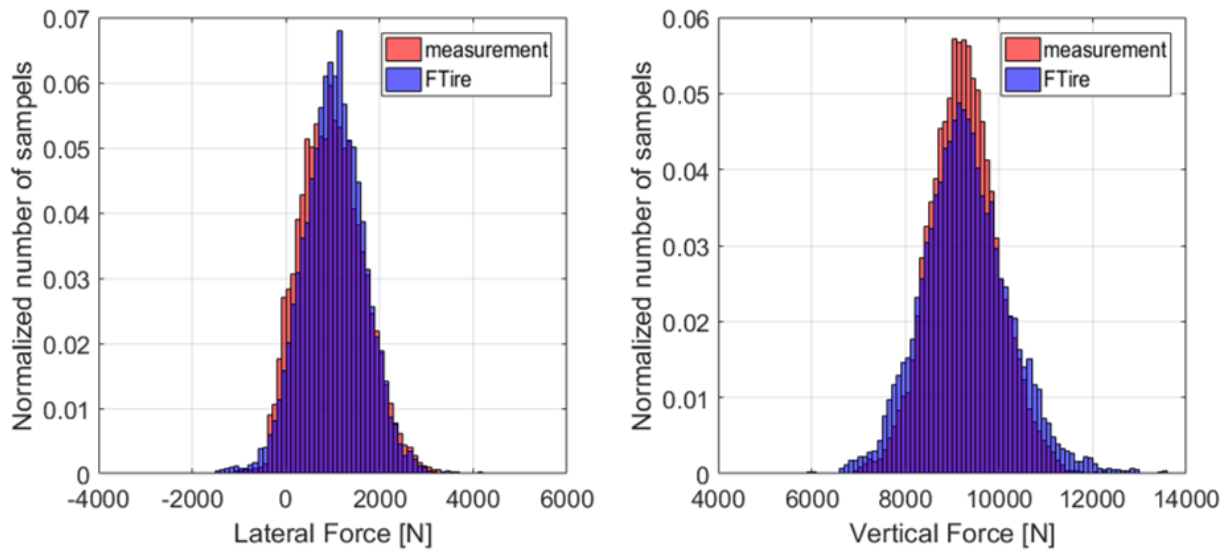


Figure 4-25 Force Histogram, Belgian paving

A second approach, to compare the data sets, is to analyse the data in the frequency domain. A Power Spectral Density (PSD) analysis is often used. The Power Spectral Density describes how the average power of a signal is distributed over the frequency domain. It can therefore be utilised to formulate a better understanding in which frequency bands the response exhibits most energy.

The PSD results of the tyre forces while driving over the Belgian paving is shown in Figure 4-26. As expected, no distinct peaks are visible in the lateral force signal. This can be explained by the smaller obstacle size and the random unevenness of the test track. The lateral force predictions of the model correlate well with the measured results up to a frequency of about 14Hz.

In the vertical direction, the force signals with frequencies up to 40Hz are relatively well captured in the simulation model. The peaks at 20Hz and 60 Hz in the vertical spindle forces are not present in the simulation results. These peaks are present in all test results and might indicate that ADAMS trailer model is incomplete. The reason for this discrepancy could however not be determined.

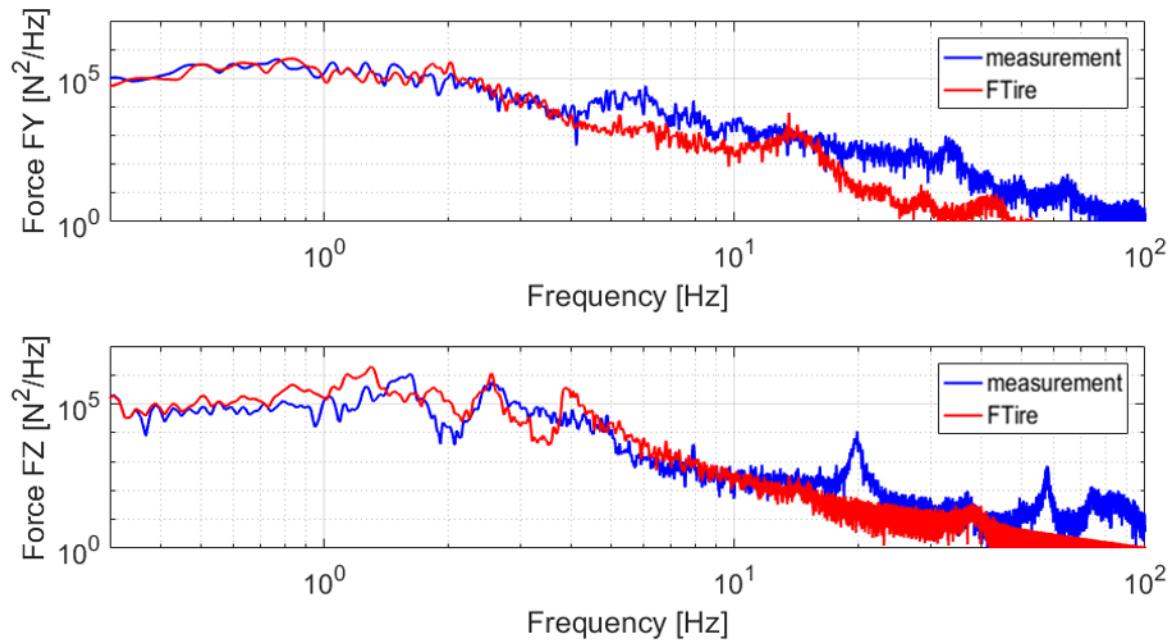


Figure 4-26 Force PSD validation, Belgian Paving

4.5. Chapter Summary

This chapter described the most commonly used parameter identification method for FTire models. This method identifies the required model parameters from experimentally obtained test results. This procedure is almost exclusively used in the industry today and will be used as reference model for this investigation.

Due to the size and load rating of the tyre, many of the standard methods had to be adapted to use the test data that could be measured. The experimental test setups were presented, and the obtained test results were discussed. Laboratory tests, on a static tyre test rig, were conducted to determine the force deflection characteristics of the test tyre for various conditions. Test conditions included various tyre inflation pressures and camber angles as well as tyre tests on cleats and flat road surfaces. A tyre test trailer was used in this investigation to obtain test results of a rolling tyre. The tyre test trailer was used to conduct cleat tests and validation tests on various road surfaces.

The test results are used to parameterise a FTire model. The FTire model was parameterised by comparing the measured test results with the predicted simulation results. The FTire/fit built-in optimisation algorithm was used to determine the tyre parameters that best match the measurements. Dynamic cleat tests could not be used directly to extract the damping and inertia

properties of the tyre. A multi body dynamics model was rather used, in conjunction with a trial and error routine, to obtain these parameters. The results of the parameter identification procedure were presented and discussed.

The parameterised tyre model was validated for simulations over discrete obstacles and uneven road profiles. The model was validated by comparing simulation results to experimentally obtained results. The investigation found that the measured and simulated tyre test trailer forces correlated well for tests over a single 50mm cleat.

The simulation model was also validated for undeformable uneven roads. Tests and simulations were conducted on various test tracks that are available at the Gerotek Test Facilities. The model was validated by comparing the force signals in the time domain and by comparing the force histogram of the entire test. The power spectral density of the force measures was also determined to validate the frequency response of the system. Overall good correlation was found for all road profiles.

It can thus be concluded that an accurate FTire model, of a large off-road tyre, can be parameterised from experimentally obtained test data. A comprehensive list of test data needs to be available for the investigated tyre. Available test equipment at the University of Pretoria can be used to obtain the required parameterisation test data.

Using experimental data, to parameterise large off-road tyre models, pose some challenges that need to be addressed to improve the accuracy of the model and to reduce the cost of conducting these tests. The biggest challenge is to accurately control the testing conditions to acquire accurate and repeatable test results. The second challenge is that these tests are expensive to conduct. Specialized equipment and trained staff is required to conduct these tests and to analyse the data. The large range of tyre sizes and load ratings, of these tyres, further complicate the testing procedure as the test equipment needs to be adapted to accommodate these tyres. Further scaling of the test equipment, to test even larger tyres, might also be challenging due to an increase of the applied tyre test load. Due to these challenges, it is suggested to investigate other methods to acquire tyre data that can be used to extract tyre model parameters.

Chapter 5 investigates the use of finite element tyre models to generate parameterisation data. Finite element models have been used in the past to investigate tyre behaviour. The required input data, geometry, construction and material properties, can also be obtained regardless of the

tyre size and operating load condition. The cost of the required test equipment is significantly lower and more readily available.

Chapter 6 investigates the use of carcass deformation data to extract the required tyre model parameters. The measurements can be done in-situ, reducing the cost of the tests. Using computer stereographic vision to conduct these tests, full field tyre deformation tests can be conducted with inexpensive camera equipment.

Chapter 5

Finite element tyre model parameterisation

5. Finite element tyre model parameterisation

One of the options to parameterise models of large tyres, if test data is not available, may be the use of FE models. The required model properties, material properties and geometry, can be obtained with the same test equipment regardless of the tyre size.

5.1. Material testing for FE analysis

One of the biggest challenges of modelling the tyre in a FE environment is to obtain the necessary geometry and material properties. These properties are not readily available, and manufacturers tend not to share this proprietary information. Hyper-elastic and viscoelastic material properties can be obtained from physical material tests. The Experimental results are used to fit various material models. To successfully extract the required material model parameters from the test data, tests must be conducted for multiple states of strain under carefully considered loading conditions [Miller, 2000]. Miller [2000] notes that the required experiments, for defining material models, are not yet clearly defined by international standard organisations. Miller proposed that tests should be conducted to test the simple tension, equal biaxial, and planar shear strain state of the material.

5.2. Material models

Tyres consist of various materials such as rubber, steel, Kevlar fabric etc. Material models are required to describe the material behaviour of all these compounds. Rubber is generally considered to be a non-linear, nearly incompressible, and hyper-elastic material. Constitutive relationships to describe the stress strain relationship for rubber materials, need to be found. The relationships need to account for the nonlinear stress-strain behaviour and be valid for large deformations. A short derivation summary of some of the constitutive relationships that were developed by researchers are discussed below [Ali et al., 2010].

The deformation gradient of a solid subjected to a displacement field, $u_i(x_k)$, is given by:

$$F_{ij} = \delta_{ij} + \frac{\partial u_i}{\partial x_j} \quad (5.1)$$

Where δ_{ij} is the Kronecker delta, and $\frac{\partial u_i}{\partial x_j}$ is the displacement gradient tensor. The left Cauchy-Green deformation tensor can then be defined as:

$$\mathbf{B} = \mathbf{F}\mathbf{F}^T \quad (5.2)$$

The elastic properties of rubber can be explained in terms of a strain energy function based on the strain invariants I_1 , I_2 and I_3 of \mathbf{B} . The most common invariants are:

$$I_1 = \text{tr}(\mathbf{B}) = \lambda_1^2 + \lambda_2^2 + \lambda_3^2 \quad (5.3)$$

$$I_2 = \frac{1}{2} [(\text{tr} \mathbf{B})^2 - \text{tr}(\mathbf{B}^2)] = \lambda_1^2 \lambda_2^2 + \lambda_2^2 \lambda_3^2 + \lambda_3^2 \lambda_1^2 \quad (5.4)$$

$$I_3 = \det(\mathbf{B}) = \lambda_1^2 \lambda_2^2 \lambda_3^2 \quad (5.5)$$

Where λ_1 , λ_2 , λ_3 are the corresponding principal stretch ratios and thus the square roots of the eigenvalues of \mathbf{B} . The total strain energy is given by the sum of the deviatoric strain energy and hydrostatic strain energy

$$U = U_d + U_h \quad (5.6)$$

Where U_d is the strain energy due to distortion, and thus deviatoric strain energy, and U_h is the strain energy related to volume change or hydrostatic strain energy. The elastic properties of rubber can be explained in terms of a strain energy function based on the three strain invariants:

$$U = f(I_1, I_2, I_3) \quad (5.7)$$

The strain energy, in terms of the strain invariants, can be represented as an infinite power series:

$$U = \sum_{i+j+k=1}^{\infty} C_{ijk} (I_1 - 3)^i (I_2 - 3)^j (I_3 - 1)^k \quad (5.8)$$

The stress-strain law is deduced by differentiating the strain energy function. It can further be shown that the stress in terms of the strain invariants is given by [Bower, n.d]:

$$\sigma_{ij} = \frac{2}{\sqrt{I_3}} \left[\left(\frac{\partial U}{\partial I_1} + I_1 \frac{\partial U}{\partial I_2} \right) B_{ij} - \frac{\partial U}{\partial I_2} B_{ik} B_{kj} \right] + 2\sqrt{I_3} \frac{\partial U}{\partial I_3} \delta_{ij} \quad (5.9)$$

Researchers have developed numerous models to describe the strain energy of rubber like materials. These models include the Neo-Hookean, Mooney-Rivlin, Ogden and Yeoh models.

Generalized Neo-Hookean model: The Neo-Hookean model is one of the simplest hyperplastic material models and depends on only two parameters, or only one if the material is assumed to be incompressible. The strain energy is defined as [adapted from Bower, n.d].:

$$U = C_{10}(I_1 - 3) + \frac{K_1}{2}(J - 1)^2 \quad (5.10)$$

Where $J = \sqrt{I_3} = \lambda_1\lambda_2\lambda_3$ and C_{10} and K_1 are material constants. This is a rubber elasticity model, for rubbers with very limited compressibility, and should be used if when material data is limited [Ali et al., 2010]. It can be shown that the stress-strain relation is given by [based on Bower, n.d]:

$$\sigma_{ij} = \frac{2C_{10}}{J^{\frac{5}{3}}}\left(B_{ij} - \frac{1}{3}B_{kk}\delta_{ij}\right) + K_1(J - 1)\delta_{ij} \quad (5.11)$$

Generalized Mooney-Rivlin model:

The strain energy for the Mooney-Rivlin model is defined as [adapted from Bower, n.d]:

$$U = \sum_{i,j=0}^N C_{ij}(I_1 - 3)^i(I_2 - 3)^j + \sum_{i=1}^N \frac{K_i}{2}(J - 1)^{2i} \quad (5.12)$$

C_{ij} and K_i are material constants and with $C_{00} = 0$. The more common two term Mooney-Rivlin model is given by:

$$U = C_{10}(I_1 - 3) + C_{01}(I_2 - 3) + \frac{K_1}{2}(J - 1)^2 \quad (5.13)$$

To improve the fit the three term Mooney-Rivlin model may also be used. This is a rubber elasticity model, for rubbers with very limited compressibility, and should be used with $K_1 \gg C_{10}$. The stress-strain relation is given by [adapted from Bower, n.d]:

$$\sigma_{ij} = \frac{2C_{10}}{J^{\frac{5}{3}}}\left(B_{ij} - \frac{1}{3}B_{kk}\delta_{ij}\right) + \frac{2C_{01}}{J^{\frac{7}{3}}}\left(B_{kk}B_{ij} - \frac{1}{3}[B_{kk}]^2\delta_{ij} - B_{ik}B_{kj} + \frac{1}{3}B_{kn}B_{nk}\delta_{ij}\right) + K_1(J - 1)\delta_{ij} \quad (5.14)$$

Generalized Ogden model:

The Ogden energy density function is defined using the principle stretches directly and is given by [Ali et al, 2010]:

$$U = \sum_{i=1}^N \frac{2\mu_i}{\alpha_i} J^{-\frac{\alpha_i}{3}} (\lambda_1^{\alpha_i} + \lambda_2^{\alpha_i} + \lambda_3^{\alpha_i}) - 3 + \sum_{i=1}^N \frac{K_i}{2}(J - 1)^{2i} \quad (5.15)$$

where μ_i , α_i and K_i are material property constants. The constants μ_i and α_i are used to describe the shear behaviour of the material while the constant K_i describes the compressibility of the material. The Ogden hyperplastic rubber elasticity model is intended to be used with $K_1 \gg C_{10}$.

The Yeoh model:

This model differs from the above higher order models in that it only depends on the first strain invariant [Ali et al., 2010]:

$$U = \sum_{i=1}^N C_{i0} (I_1 - 3)^i + \sum_{i=1}^N \frac{K_i}{2} (J - 1)^{2i} \quad (5.16)$$

Ghosh et al. [2003] showed that this simple model can predict the stress strain behaviour under different deformation modes even if the model is fitted to data from a simple uniaxial extension test.

5.3. Experimental testing and results

For the FE tyre model, the following information is required:

1. Geometry
 - a. Tyre outline
 - b. Tyre construction
2. Material properties
 - a. Base material, rubber
 - i. Uniaxial tension test
 - ii. Equi-biaxial tension test
 - iii. Planar shear
 - b. Reinforcing material, steel cords
 - i. Uniaxial tension test

This section describes the testing method and procedure that was used to obtain the input data. All the material tests were conducted at a controlled room temperature of 20 degrees Celsius.

5.3.1. Tyre geometric properties

The geometric properties were determined with a set of measurements. The first measurement that was conducted was to determine the inflated tyre geometry. The inflated cross section of the test tyre was determined with a laser measurement technique. Multiple measurements were taken at various tyre orientations and locations. The measurements were post-processed to realign the measurements. Figure 5-1 shows the result of two tread carcass sections and the tyre sidewall. The figure depicts the relationship between the section height and the tread width.

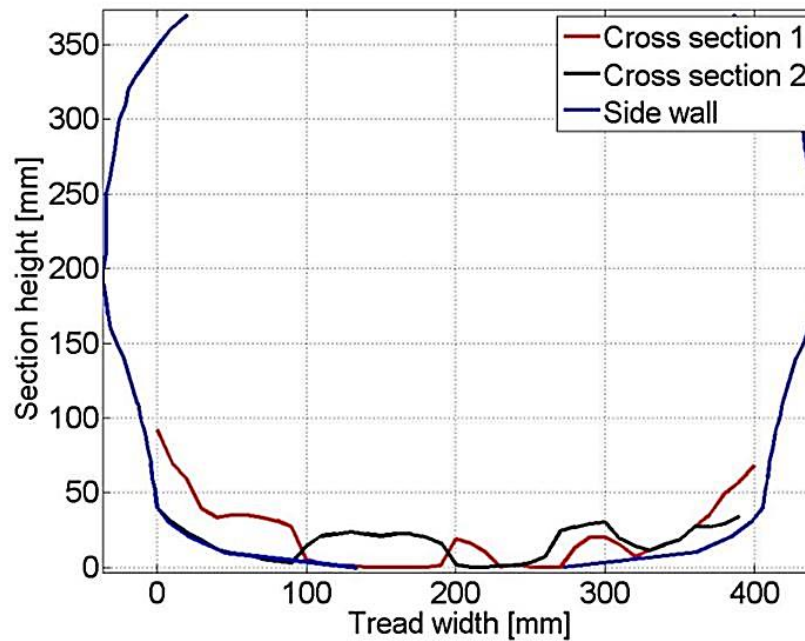


Figure 5-1 Outer contour test results

In a second test a cross section was cut from the tyre. The sample was used to determine the sidewall width, carcass base thickness, and tread depth. The sample was also used to determine the relative positions of the steel reinforcing layers and steel bead of the tyre. Footprint measurements, as discussed in section 4.3, were used to determine the shape and size of the tread blocks. Measurements were also conducted to determine the rim geometry.

The measurements were used to construct a detailed CAD model of the tyre and the rim. The CAD model of the Michelin 16.00R20 test tyre is shown in Figure 5-2.



Figure 5-2 Michelin 16.00R20 CAD model

It is well known that a pneumatic tyre usually consists of multiple layers of rubber each consisting of different chemical compounds. Each layer thus displays a different material characteristic. It is unknown, however, precisely how many diverse rubber compounds are found in the investigated tyre. Identifying the layers accurately poses a challenge. In an attempt to identify, and classify, the different rubber layers, various specimens were cut from the tyre. Some of the samples are shown in Figure 5-3. From the figure, it can be seen that some of the rubber compounds can be identified due to a distinct colour change between the rubber sections. A fading red “dot-dashed” line is superimposed onto the image to indicate the different material boundaries. Numerous rubber compounds were identified using this method. It is however unknown if all rubber compounds used can be visually identified.

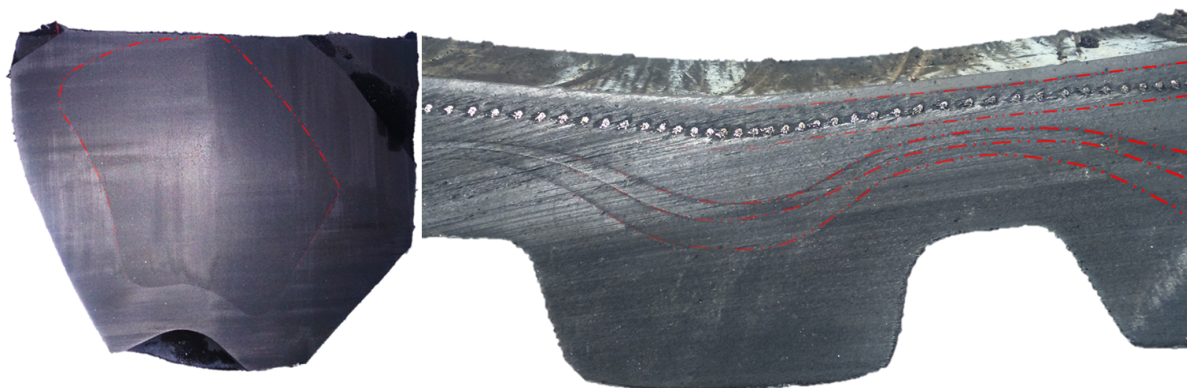


Figure 5-3 Tyre rubber layers, Left: tread block, Right: carcass section near tyre sidewall

Some rubber layers were also too thin or uneven to successfully cut a material sample from it. A total of five layers were identified that were suitable to cut material samples from. These layers

were defined as: Sidewall outer, sidewall inner, inner liner, tread outer and the carcass liner. The CAD model was updated to include the identified rubber layers.

5.3.2. Tyre material properties

Uniaxial tension, equibiaxial tension, shear, and ShoreA hardness tests were conducted to extract the rubber material model coefficients. Tests were also conducted to determine the Young's Modulus of the reinforcing steel cords as well as the tyre bead.

To determine the stress and strain relationship of the rubber under various loading conditions the applied load and resulting deformation needs to be recorded. The applied load is measured using a calibrated load cell and a data acquisition device. The rubber deformation is measured with a non-contacting digital image correlation technique. Digital Image Correlation (DIC) is an image analysis method, based on tracking features in recorded digital images [Botha, 2015]. DIC is used to perform full field surface measurement using sub-pixel registration between the left and right images of a stereo camera setup. Using triangulation techniques, the 3D locations and deformation of features in the image can be determined. DIC measurement is taken without any contact with the material, and therefore, it does not disturb the local displacement measurements. During the material tests the full kinematic field is measured. The technique is therefore well adapted to the identification of rubber mechanical properties. To perform DIC on the test samples, the samples were sprayed with a random speckle pattern. A stereo camera setup was used to capture synchronised images during a test.

Shore Hardness

The hardness of the rubber was also determined. The hardness of rubber is commonly measured by a Shore hardness test. The method determines the hardness by measuring the resistance of rubber toward an indentation [Qi et al., 2003]. The ShoreA hardness tests uses a hardened steel rod with a diameter of 1.4 mm. The tip of the rod is truncated with a 35° cone so that the tip has a 0.79 mm diameter. A load of 8.06N is applied and the indentation is determined. To accurately measure the hardness of the rubber the test material should have a minimum thickness of 6 mm [ASTM D2240]. A Bs-392A Bondtec Shore hardness tester was used for the tests. The hardness tester had a range of 10-90H with a resolution of 0.1H. The measurement deviation of the tester is rated to be less than 1H.

To accurately measure the ShoreA hardness the test specimens must be thicker than 6mm. The carcass cord liner and inner liner had a thickness smaller than 6 mm. Multiple layers were thus

stacked to reach a total thickness larger than 6mm. To determine the hardness ten samples per rubber compound were taken. The extremes and average test results are presented in Table 5-1.

Table 5-1 ShoreA test results

Location	Minimum	Mean	Maximum	Standard deviation
Sidewall outer	65.8	71.1	77.5	3.6
Sidewall inner	56	60.5	65.4	2.9
Tread outer	67.4	71.4	73.8	2.4
Tread inner	55.7	58.8	62.7	2.1
Inner liner	51.4	56.1	58.4	2.2
Carcass cord liner	51.7	55.4	60.0	3.5
Bead filler	75	77.7	80.6	2.2

Uniaxial tension

The first test that was performed was a simple uniaxial tension test. This test is a very popular test and is often used to fit material models of elastomers [Jeong, 2016; Behroozi et al., 2012; Wei et al., 2016; Ghosh et al., 2003; Yang et al., 2010; Song et al., 2008]. For the uniaxial tension test rubber samples were taken from the various rubber layers from the tyre. Large sections of the rubber, from the identified test region, were cut from the tyre. The rubber was glued to a flat surface. Thereafter it was machined and sanded down, resulting in rubber sheets with a uniform thickness. Care was taken to cool the material during processing to avoid melting or excessive heating of the rubber. To perform the uniaxial tension tests, dog bone shaped samples were cut from the rubber sheets. The length of the test section was at least 15 times larger than the width and thickness of the sample. This was done to ensure a state of pure tensile strain. A 5kN LLOYD single column universal materials testing machine was used to test the samples. The test setup is shown schematically in Figure 5-4.

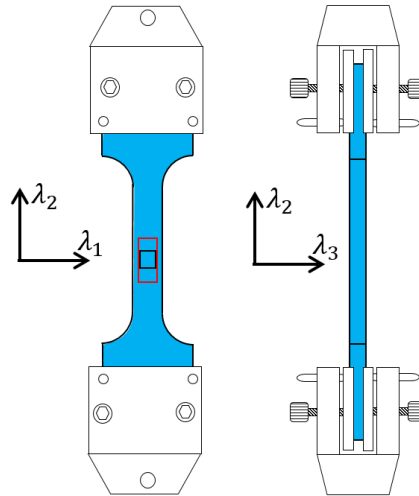


Figure 5-4 Uniaxial tension test

If the material is incompressible, the deformation state during the test is given by:

$$\lambda_2 = \lambda = \frac{L}{L_0}, \quad \lambda_1 = \lambda_3 = \sqrt{\frac{A}{A_0}} \quad (5.17)$$

While the resulting stress state is given by:

$$\sigma_2 = \sigma = \frac{P}{A_0}, \quad \sigma_1 = \sigma_3 = 0 \quad (5.18)$$

The results of the uniaxial tension test are shown in Figure 5-5. Five different rubber sections were tested. The outer sidewall rubber and the outer tread rubber show the highest stiffness while the inner liner has the lowest stiffness of the tested samples. It can further be seen that the outer sidewall rubber shows a very similar stress strain relationship to the outer tread rubber. The Inner liner rubber and the carcass cord liner rubber also show similar results. The material properties of the two samples start to differ slightly at strains higher than 0.3 to 0.4. The test results show that the material properties of the different samples vary significantly. It is thus important to test and determine the rubber properties at various position of the tyre.

To compare the measured ShoreA hardness to the uniaxial tension test, the following relationship is assumed [cosin scientific software, 2017e]:

$$E = 218300(1.0482792^S) = 10^{5.33905+0.020477S} \quad (5.19)$$

Where S is the ShoreA hardness value. The results are shown in Figure 5-5. The relationship between the two measurements correlate well for strain values below 0.1.

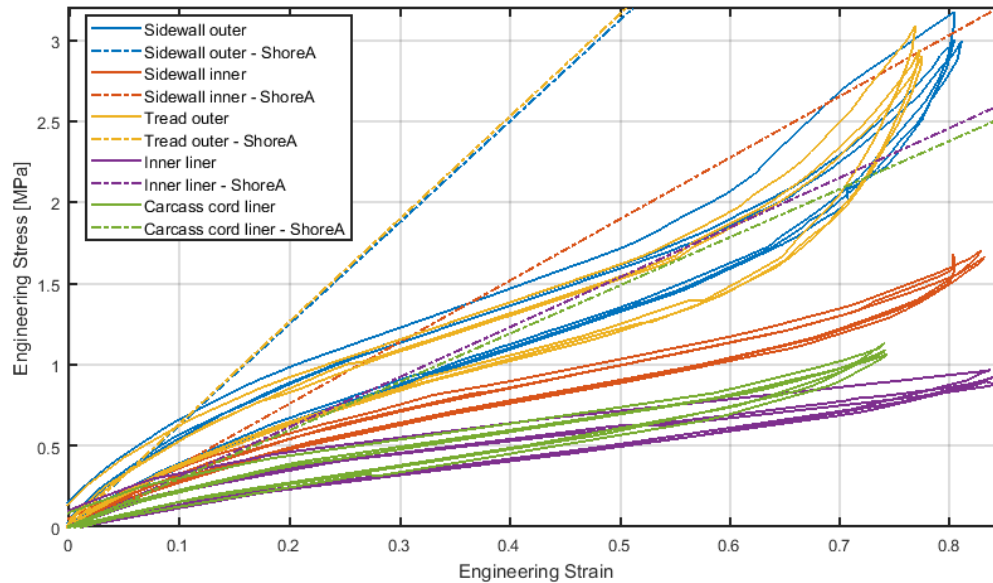


Figure 5-5 Uniaxial tension test results

The figure also shows that the rubber is a great deal stiffer during the first loading cycle. The stiffness of the rubber however decreases when the loading cycle is repeated. This effect is known as the Mullins' effect. After multiple cycles, the stress strain relationship of the rubber converges to a stable hysteresis loop.

Equibiaxial tension

The second material test that was performed was the Equibiaxial tension test. The test was conducted to achieve an equal biaxial strain state. Biaxial tension tests are often conducted using circular or square specimens. The outside edges of the specimen are deformed to form a larger circle or square. Special equipment is required to perform these tests. Seibert et al [2014] investigated different specimen shapes to perform a biaxial test. The test specimens investigated, had a cross like shape and thus only required four points to be stretched. Specimens were cut according to the recommendations from Seibert et al. [2014]. The stress and strain state was achieved by applying the same load to all four ends of the specimen by means of weights. The test setup is shown schematically in Figure 5-6. The test setup did not allow for cyclic tests to be conducted due to the manual loading and unloading of the weights. The strain of the test specimen was measured using a DIC technique. Strain measurements were taken in three directions, two

in the direction of the clamps and one at a 45-degree angle to the clamps. This was done to ensure an equal strain in all directions is applied to the test specimen.

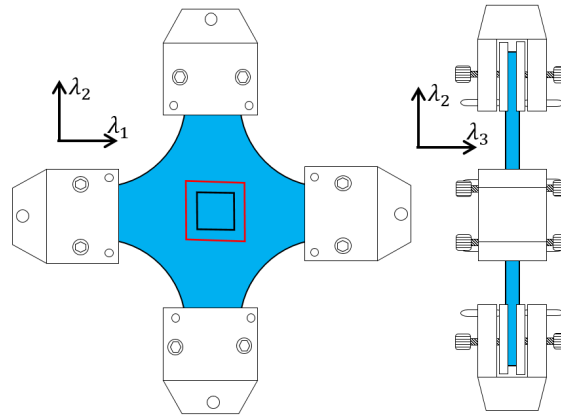


Figure 5-6 Equibiaxial tension test setup

Deformation state for the Equibiaxial tension test is given by:

$$\lambda_1 = \lambda_2 = \lambda = \frac{L}{L_0}, \quad \lambda_3 = \frac{t_t}{t_0} \quad (5.20)$$

The corresponding stress state:

$$\sigma_1 = \sigma_2 = \sigma = \frac{P}{\pi D t_0}, \quad \sigma_3 = 0 \quad (5.21)$$

The test results are shown in Figure 5-7. From the figure, it can again be seen that the outer sidewall and the outer tread rubber show a very similar stress strain behaviour during the test. The inner liner and carcass cord liner had the lowest stiffness and showed a similar stress strain relationship. The tests could not be conducted at strains higher than 0.5 due to the small differences in the clamping positions resulted in an unequal strain field. This is due to different

elongations of the “arms” of the test specimen. Usable results, with equal strain in all directions, were however obtained for strains up to 0.35.

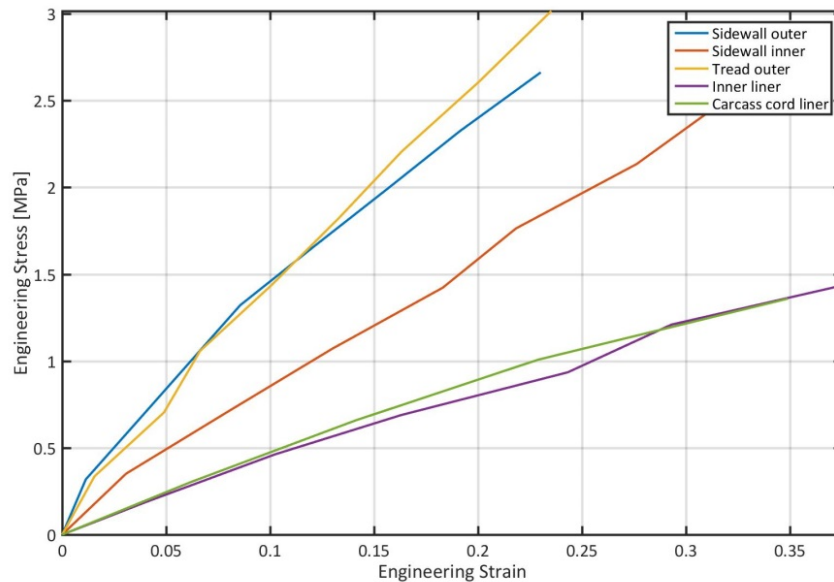


Figure 5-7 Equibiaxial tension test results

Shear

Rather than performing a simple shear test, a planar shear tests was conducted [MSC Software Corporation, 2016]. The planar shear test was conducted on the 5kN LLOYD single column universal materials testing machine. To perform the test a rubber specimen was cut from the rubber that was 15 times wider than its length in the stretching direction. The specimen was clamped in special jaws to perfectly constrain the sample in the lateral direction. The same test setup was used as was described in the uniaxial tension test. A DIC technique was used to determine the strain state of the specimen. During the tests the specimen was stretched in the vertical direction but not in the lateral direction. Due to the constraint in the lateral direction a state of planar shear exists in the specimen at a 45-degree angle. The test setup is shown schematically in Figure 5-8.

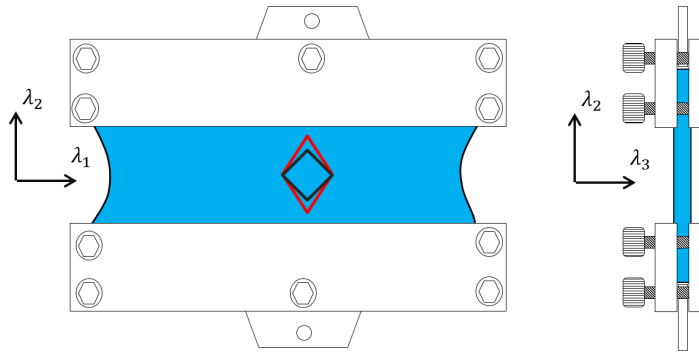


Figure 5-8 Planar shear stretch diagram

The test results of the primary stretch ratios, λ_1 and λ_2 , are shown in Figure 5-9. The figure shows that the stretch ratio λ_1 only changes 0.001 while the stretch ratio λ_2 changes by more than 0.45. The assumption of no deformation in the lateral direction is thus valid.

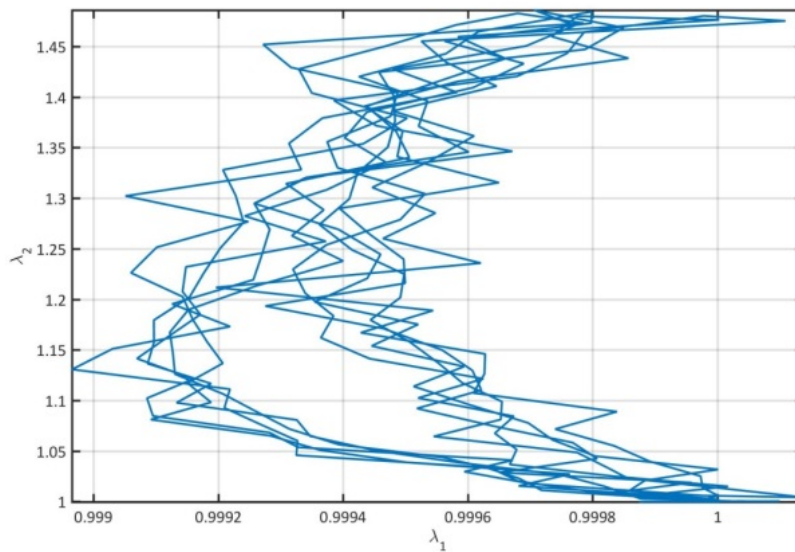


Figure 5-9 Comparison of principal stretch ratios λ_1 and λ_2

The deformation state of the planar shear test is given by:

$$\lambda_1 = 1, \quad \lambda_2 = \lambda = \frac{L}{L_0}, \quad \lambda_3 = \frac{t_t}{t_0} \quad (5.22)$$

The corresponding stress state is given by:

$$\sigma_1 \neq 0, \quad \sigma_2 = \sigma = \frac{P}{A_0}, \quad \sigma_3 = 0 \quad (5.23)$$

The test results are presented in Figure 5-10. It can again be seen that the material samples cut from the outer layers of the tyre show similar stress-strain characteristics. The same is true for the inner liner and carcass cord liner rubber samples.

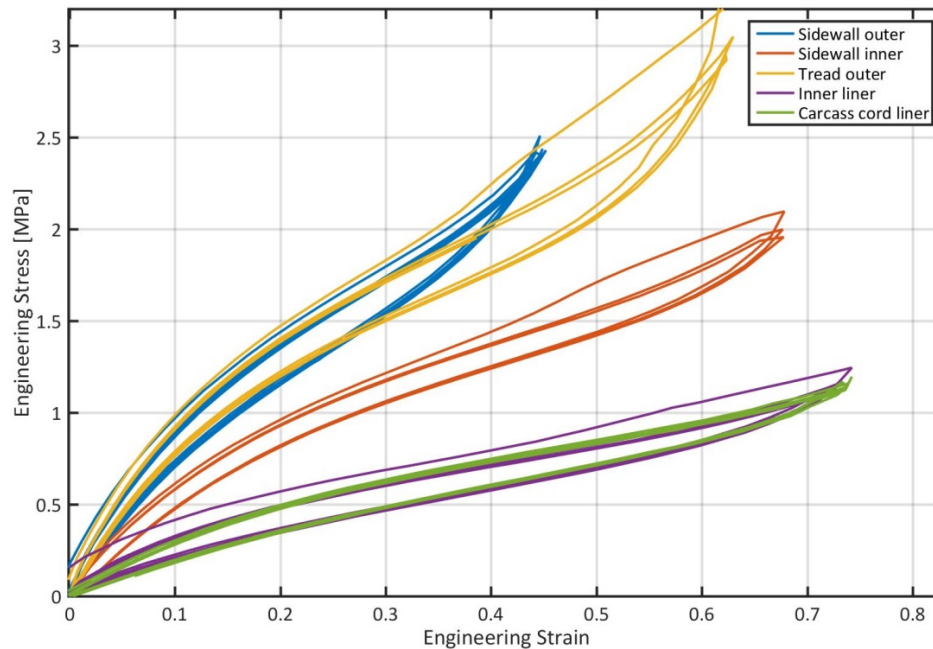


Figure 5-10 Planar shear test results

5.3.3. Reinforcing material

The reinforcing cords of the test tyre were also tested. Individual cords were cut from the tyre. The samples were tested with the 5kN LLOYD single column universal materials testing machine. To determine the strain of the test specimens, markers were glued to the cords. These markers were tracked during the tests, using a DIC technique, and the strain was calculated. The deformation state of the sample is given by:

$$\lambda = \frac{L}{L_0} \quad (5.24)$$

And the corresponding stress state:

$$\sigma = \frac{P}{A_0} \quad (5.25)$$

The calculated elastic modulus, or rope modulus, of the reinforcing cords and the measured cord diameters are presented in Table 5-2. The table clearly shows that the elastic modulus of the test cords is significantly lower than that of steel. The construction of the cords can explain this. The cords consist of several individual strands that are twisted or helically bend together to form a cord. The lay of the wire cord is influencing the elastic modulus of the cord.

Table 5-2 Reinforcing material test results

Location	Elastic modulus kN/mm²	Area mm²	Diameter mm	Cord direction degrees
Bead strand	187.86	2.89	1.92	-
Carcass cord	115.19	1.49	1.38	0.0
1st Belt ply cord	134.55	1.53	1.4	120.9
2nd Belt ply cord	134.55	1.53	1.4	74.4
Cap ply cord	65.22	1.45	1.36	110.9

5.4. MARC finite element tyre model

The full three-dimensional tyre was modelled in the MSC MARC environment. MARC is a powerful, general purpose, nonlinear analyses software that allows for fully nonlinear finite element analyses. The software is capable of modelling material and geometric nonlinearities, nonlinear boundary conditions as well as contact and self-contact. All these capabilities are required to accurately model a pneumatic tyre.

5.4.1. Material model fit

To fit the hyperplastic material models the measured test data was post processed. Firstly, as the material models don't incorporate a hysteresis model, the hysteresis must be ignored and a stable upload cycle needs to be isolated. An equilibrium curve, or the mean between the upload and unload curve, may also be considered and used to fit the hyperplastic material models. This is especially useful if hysteresis needs to be considered. The modelling of the hysteresis effect does

however not fall into the scope of this project as only static simulations will be considered. For the purpose of this thesis only a single stable upload curve was used during the fitting process. The hysteresis effect would thus not be captured with this model. Secondly the data needs to be shifted to the origin so that the material has a zero stress state at zero strain. Finally, the test data was subsampled. The subsampling of the data was done in such a way that the final data set has more data points in the region of interest. It is assumed that the engineering strain in the rubber would rarely exceed 0.3. This assumption was later confirmed by the FE simulation results. This is done to improve the accuracy of the fitted models in the region of the expected operating conditions of the material. The test data was subsampled in such a way that at least 50% of the data points were between zero and 0.3 Engineering strain, 30% between 0.3 and 0.6 Engineering strain and the remaining 20% between 0.6 and 1 Engineering strain.

The pre-processed test data from the different tyre sections was used to determine the material model fits. Two of the test sections were eliminated from the fitting process due to their similar stress-strain behaviour. The processed test data from the outer tread layer, inner sidewall layer and the inner liner was selected and used to extract the required model coefficients. The material coefficients were determined with the “Experimental Data Fit” tool supplied with the MARC Mentat software from MSC Software. The coefficients are determined by minimizing the relative error between the measured and predicted material stress-strain behaviour. The calculated material model coefficients are presented in Table 5-3 to Table 5-5. Conditional stability is ensured for engineering strains ranging between -0.85 and 1 .

Table 5-3 Tread outer material properties

Tread outer	Coefficient	Value (MPa)	Mean percentage error [%]	
Neo-Hookean	C10	1.035	8.4	
Mooney (2)	C10	0.000	4.0	
	C01	1.135		
Yeoh	C10	1.161	7.6	
	C20	-0.418		
	C30	0.191		
Ogden (4)		Moduli	Exponents	2.9
	1	5.334	5.201	
	2	13.799	1.187	
	3	-2.790	-0.384	
	4	-8.874	4.532	

The material coefficients of the outer tread layer are shown in Table 5-3. The best fits were found with a four term Ogden material model. The Ogden model has a error of 2.9% while the second best performing two term Mooney model had a error of 4.0%. The Neo-Hookean and Yeoh model failed to accurately represent the material behaviour during uniaxial tension, planar shear and biaxial tension tests.

The sidewall inner rubber behaviour can best be represented with a three term Ogden model. The three term Ogden model was selected as the relative error of a four term Ogden model was only marginally better than the error of the three-term model. The Mooney model again showed good correlation between the measured and simulated material behaviour. The Yeoh and Neo-Hookean models performed the worst with both having a error of 5.3%.

Table 5-4 Sidewall inner material properties

Sidewall inner	Coefficient	Value (MPa)	Mean percentage error [%]	
Neo-Hookean	C10	0.667	5.3	
Mooney (2)	C10	0.110	1.6	
	C01	0.584		
Yeoh	C10	0.667	5.3	
	C20	0.000		
	C30	0.000		
Ogden (3)	Moduli		1.4	
	Exponents			
	1	16.128		5.059
	2	-18.282		-0.261
	3	-16.660	5.011	

Table 5-5 shows the material coefficients that were determined from the inner liner rubber tests. The three term Ogden model again could best predict the material behaviour. The relative error of the fit was 2.7. The Mooney model had an error of 3.0% while the Neo-Hookean and Yeoh models had errors of 6.5% and 6.4% respectively.

Table 5-5 Inner liner material properties

Inner liner	Coefficient	Value (MPa)	Mean percentage error [%]	
Neo-Hookean	C10	0.393	6.5	
Mooney (2)	C10	0.126	3.0	
	C01	0.270		
Yeoh	C10	0.407	6.4	
	C20	-0.023		
	C30	0.002		
Ogden (3)		Moduli	Exponents	2.7
	1	0.000002	19.911	
	2	-26.419	-0.304	
	3	70.422	-0.091	

Validation of model fits

To validate the accuracy of the determined material parameters and material model coefficients, a four-point bending test was conducted. Two samples were cut from the test tyre. The first sample was cut from the tyre tread in the lateral direction and the second was cut in the longitudinal direction. The carcass cords were orientated along the length of the sample in the lateral test specimen and across the width in the longitudinal specimen. The samples were cut from the centre of the tyre so that all the rubber and steel layers were present in the sample. The samples had a width of about 100mm and a length of about 330mm.

A stereo-vision camera setup was used to determine the outer geometry of the test specimens. The three-dimensional point cloud was imported into CAD software to create a solid model of the specimens. The rubber layers of the solid were divided into three sections, namely: tread outer, middle and inner liner. The acquired Ogden material coefficients were assigned to the different rubber layers. The rubber layers of the finite element model were modelled with Tetra10 elements using the Full Hermann formulation.

The carcass, belt and cap steel cord layers were modelled with Tria6 membrane elements. The meshing of the solid and membrane elements was conducted in such a way that the nodes of the membrane elements were shared with the corresponding nodes of the solid Tetra10 elements. The membrane elements were orientated according to the different steel layer orientations. The elastic-plastic orthotropic material properties of the cord layers were calculated using the slab model. The slab model could be used to calculate the equivalent Young's and shear moduli of

long fibre composites. The resulting Finite element model of the lateral four-point bending test is shown in Figure 5-11. The purple wire frame model indicates the un-deformed test specimen. The solid model indicates the deformed state of the lateral four-point bending test specimen.

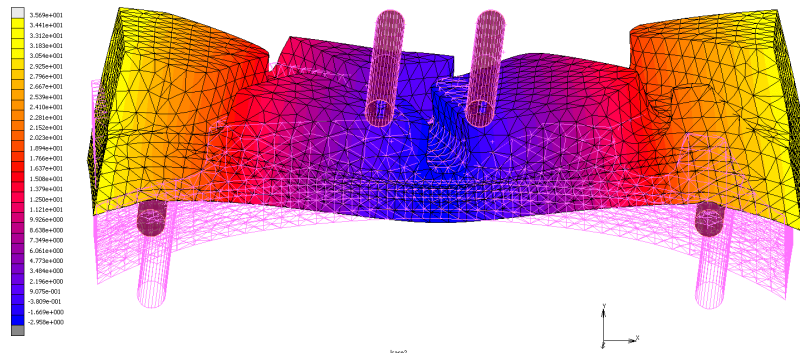


Figure 5-11 Finite element model of the lateral four-point bending test

Figure 5-12 shows the measured and simulated force-displacement characteristics of the lateral four-point bending test specimen. The reaction force for a displacement less than 15mm is slightly lower during the simulation as compared to the measured results. The reaction force is however higher for deflections above 15mm. The overall correlation is however acceptable.

To investigate the stiffness contribution of the rubber to the bending test, a simulation was conducted where the steel cords were removed from the finite element model. The results of the rubber only test is also shown in Figure 5-12. From the figure, it's clear that the rubber stiffness contribution is relatively small compared to the "overall" stiffness.

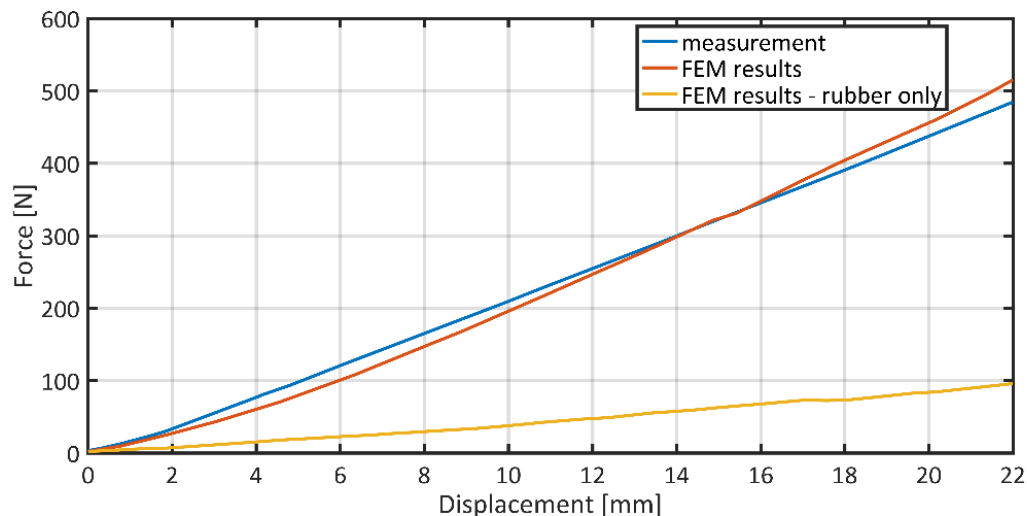


Figure 5-12 Lateral four-point bending results

The force-displacement results of the longitudinal specimen are shown in Figure 5-13. The results show that the overall bending stiffness in the longitudinal direction of the finite element model is slightly lower than the bending stiffness of the test specimen. The error between the experimental results and the simulation results was determined to be 12%. Part, or all, of the error can be attributed to the incorrect boundary conditions that were applied to the model. During the simulation, as well as the physical test, the specimen moved relative to the test equipment, and thus altering the applied boundary conditions. The trend and overall correlation between the test and simulation specimen is however very good.

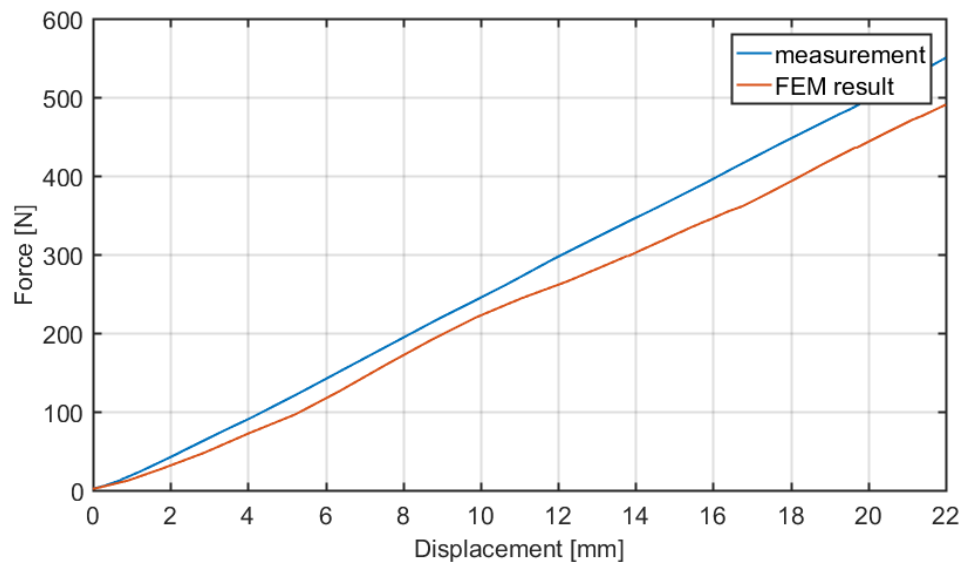


Figure 5-13 Longitudinal four-point bending results

5.5. FE tyre model

It is generally accepted that hexahedral, or brick elements, are superior to tetrahedral elements [Cifuentes and Kalbag, 1992; Bussler and Ramesh, 1993]. This is especially true for incompressible or nearly incompressible materials where mesh locking can occur [Benzley, et al., 1995]. Both the error and CPU time tend to be lower for models using quadratic hexahedral elements compared to quadratic tetrahedral elements. The disadvantage of the hexahedral element is that meshing is more work intensive as it requires that the geometry consists of Iso or paver meshable solids when automatic mesh generation is required. Complex geometry thus needs to be sub-divided into simple geometric sections. These sections are individually meshed with an Iso or paver mesher. The meshes are then equivalenced, to remove overlapping nodes, to create a single continuous hex mesh. Tetrahedral meshes can be created much quicker and

easier using a standard tet-mesher. Almost any geometric shape can be meshed with a tet-mesher without the need to subdivide the geometry into simple geometric sections.

Although a finer mesh would potentially result in a more accurate finite element model, two aspects should be considered. The first aspect is the availability of computer memory. A finer mesh would require more memory. The second aspect is the solving time. Again, an increase in elements would increase the CPU time. Although this model would not be used for time sensitive simulations a solving time of hours, rather than days or weeks, would be beneficial and improve turnaround time. The number of elements of the model should thus be kept to a minimum while ensuring that the model is still an accurate representation of the tyre.

To keep the number of elements to a minimum, while ensuring an accurate model and tread representation, it was decided to mesh the tyre carcass and the tread separately. This would allow the carcass of the tyre to be modelled with hexahedral elements while the tyre tread blocks can be modelled with tetrahedral elements.

To create the carcass mesh, a planar section was created from the 3D CAD model. The planar cross-section was divided into different rubber regions to create an axisymmetric FE model. Different rubber material properties will later be assigned to these regions. The carcass was divided into four regions (Figure 5-14). The first region is the sidewall-inner rubber region and combines the inner liner and carcass liner rubber regions. The second region is the sidewall outer rubber region. The model also includes a bead filler rubber region as well as the bead itself. The modelled rubber regions were thus the sidewall inner, sidewall outer and bead filler rubber section. Eight node quadrilateral elements were used to mesh rubber regions of the planar tyre carcass model. The bead was meshed with a combination of eight node quadrilateral elements and six node triangular elements. A combination of these elements had to be used to allow the outer nodes of the bead to tie up with the neighbouring bead filler element nodes.

The tyre reinforcing layers, consisting of steel cords, were modelled in Marc/Mentat with rebar elements. Rebar elements are hollow elements that can be used to accurately model reinforcing material within a filler material. Rebar elements are embedded into solid elements, called the host elements, to represent the reinforcing material. Rebar elements are capable of representing small as well as large strain behaviour of the reinforcing cords. Multiple rebar layers may be added to a single host element. The locations of the reinforcing layers were imported as splines from the CAD model of the tyre. The 2-D Rebar meshing tool of Marc/Mentat was used to mesh the splines with rebar elements. Special attention was given to the orientation of the host elements to ensure

that the orientation of the layers was modelled correctly. In conjunction with the location and the orientation of the reinforcing materials the rebar area, density and material properties needed to be specified. These input parameters were experimentally obtained as discussed in section 5.3.1 and 5.3.2.

Figure 5-14 shows that the element size near the bead is smaller than the element size of the rest of the tyre carcass. This was done to ensure that the model is capable of accurately representing the tyre rim contact. The rest of the tyre carcass was modelled with a rather coarse mesh to achieve a good aspect ratio of the elements when the axisymmetric model is later expanded to a three-dimensional model.

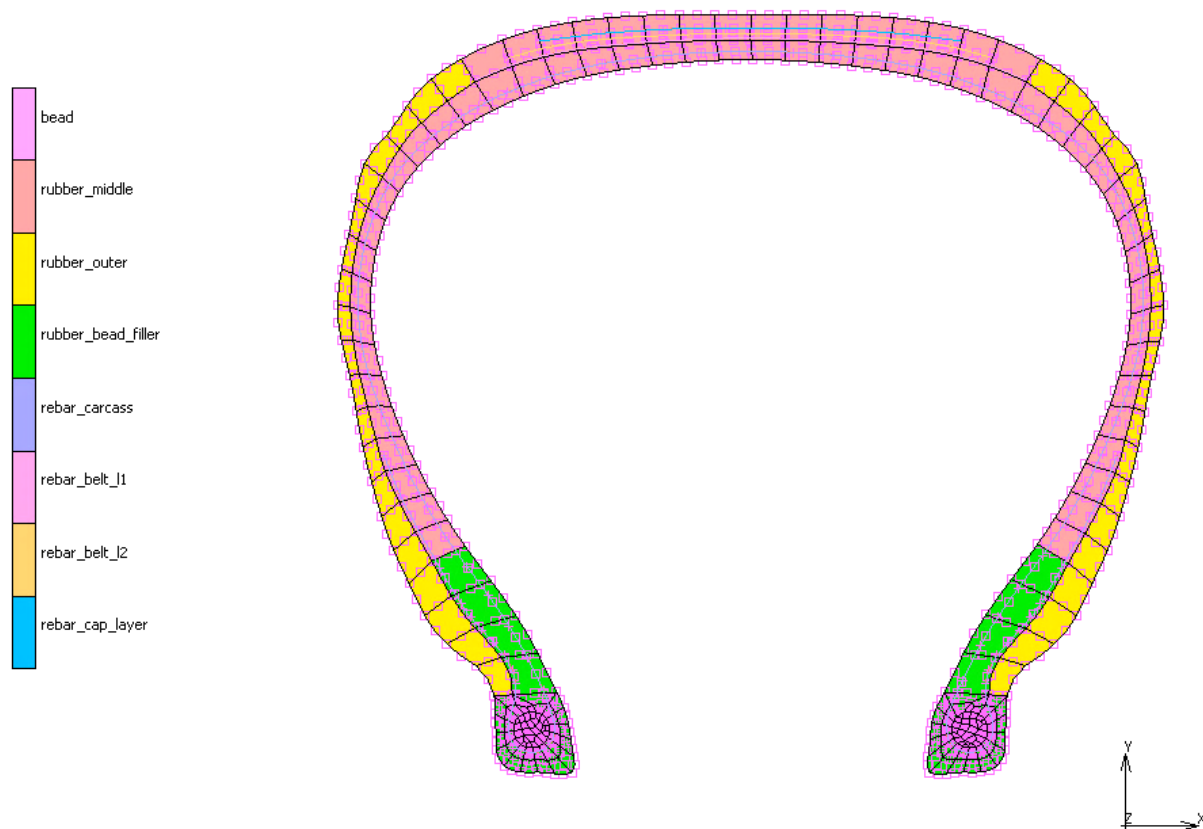


Figure 5-14 Tyre axisymmetric FE model

The axisymmetric tyre carcass model was expanded to a three-dimensional tyre model. The process converts the eight node quadrilateral rubber elements to 20-node hexahedral solid brick elements. The element types were chosen to include the perturbed Lagrangian variationally principle, based on the Herrmann Formulation, to model the nearly incompressible rubber of the tyre. The rebar elements were converted into eight node rebar membrane elements. The

elements representing the tyre bead were converted into 20-node hexahedral elements and 15 node pentahedral elements.

Due to the complex geometry of the individual tread blocks the tread was meshed with 10-node tetrahedral elements. The element type was again chosen to include the Herrmann formulation to ensure an accurate representation of the nearly incompressible rubber. The tread elements are permanently glued to the carcass elements to form the complete FE tyre model. The glued contact suppresses all relative motions between the tyre carcass and the tyre tread elements. This contact method is an efficient way to join two differently meshed bodies permanently together. Care is taken to remove all gaps and overlays between the two bodies. The glued tread elements are shown in Figure 5-15. The colour of the elements indicates the contact status of the elements. A yellow colour specifies a permanent contact between two elements from the two differently meshed contact bodies. A finer mesh was used for the tread blocks that would contact the test surface. This was done to reduce the number of elements of the finite element model and thus reduce the CPU time whilst maintaining good fidelity in the important contact region. This approach can only be adopted for tests on a non-rolling tyre. For simulations on a rolling tyre the mesh size should be kept constant.

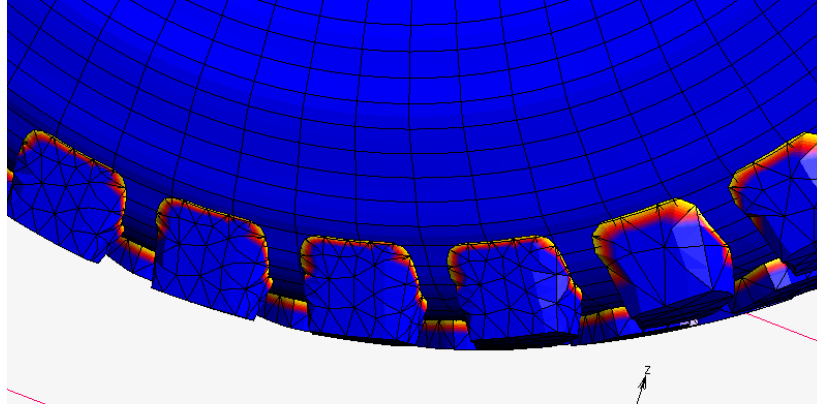


Figure 5-15 Glued tread elements

The complete three-dimensional finite element tyre model is shown in Figure 5-16. The model on the left-hand side of Figure 5-16 shows the tyre model that was created with an equal axisymmetric expansion. A total of 72 repetitions, with a 5 degree spacing, was used to create the three-dimensional tyre model. The model on the right-hand side of the figure was created with a variable mesh spacing in the circumferential direction. This was done to investigate whether a finer mesh near the tyre contact patch would yield higher accuracy results. A circumferential element spacing of 2 degrees was used for the lower section of the tyre model. The spacing was

increased to 4 and 5 degrees resulting in a total of ninety eight sections. The same tread mesh was used for both models.

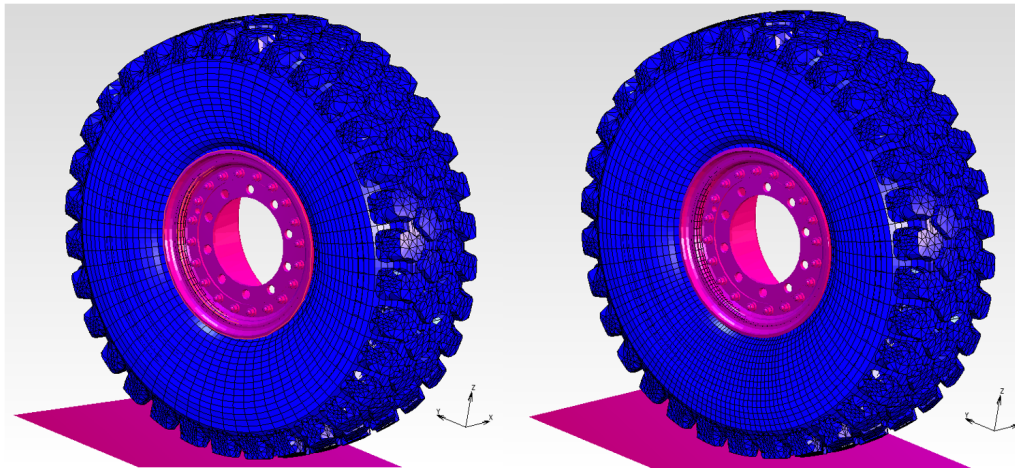


Figure 5-16 Left: Equal mesh spacing. Right: Variable mesh spacing

The finite element tyre model with the equally spaced carcass section consists of 41778 elements. The variable spaced carcass mesh model has about 25% more nodes and elements compared to the equally spaced model. The number of elements and nodes of these two models are summarized in Table 5-6.

Table 5-6 FE tyre model number of elements

Location	Number of Elements	Number of Nodes	Reference
2D axisymmetric model	382	1135	Figure 5-14
3D equally spaced model	41778	147222	Figure 5-16 (left)
3D variable spacing model	51710	188464	Figure 5-16 (right)

Three boundary conditions need to be defined before an analysis can be conducted using the finite element model. The first boundary condition is the tyre inflation pressure. Two options are available to model the tyre inflation pressure. The first option is to model the inflation pressure as a surface pressure that is applied to the inner tyre surface. The surface pressure is applied perpendicular to the element face. Any change to the internal air volume is disregarded resulting in a constant inflation pressure. Due to the flexible structure of the tyre it is known that the internal volume may change during loading of the tyre. A second option would be to model an air cavity

on the inside of the tyre. This option would take a change in air volume, resulting in a change in inflation pressure, into account. The disadvantage of this method is however that the internal volume, and resulting air pressure, needs to be calculated during each iteration. This increases the solving time of the model. From experimental tests, it is known that the variation of the inflation pressure is however small and a constant inflation pressure may be assumed.

The second boundary condition that needs to be defined is the contact between the tyre and the rim. Again, two options are available. The first option is to define the contact with a touching contact model. During a simulation, the position and motion of the contact bodies with respect to each other, is determined. When the bodies come in contact the area of contact, contact normal force and friction stresses are calculated. The friction between the two contact bodies can be modelled with stick-slip or continuous friction models. The second option would be to fix the contact nodes during the simulation. A seating simulation needs to be conducted to determine the nodes that are in contact with the rim after the tyre is seated on the rim. The nodes that are in contact with the rim are fixed in three-dimensional space during the following simulations. This method decreases the CPU time but would ignore any changes in the contact definition that might occur during the simulation. The disadvantage of this method is that the force and moment transfer between the tyre and the rim is not accurately modelled. This research is focused on the forces and moments that are generated in the tyre contact patch and not how the forces are applied to the rim. The fixed node approximation is thus deemed sufficiently accurate for this research project.

The final boundary condition that needs to be defined is the tyre to road contact. The road surface can be a deformable or non-deformable surface. For static analyses the contact is modelled with a rigid plate or cleat. A friction model may be used to model the friction behaviour of the two contact bodies.

To determine the influences of the boundary conditions and the effect of the mesh resolution on the simulation outcome, three simulations were conducted. A vertical stiffness test on a smooth rigid surface was conducted. The first model is a simplified model comprising of the equally spaced finite element tyre model with a fixed rim contact. The friction coefficient between the plate and tyre is set to zero and is thus neglected. The second simulation comprises of the FE tyre model with a variable mesh spacing. The contact between the rim and the tyre is modelled with a touching contact algorithm. A friction factor of 0.7 is assumed for the contact. The friction between the tyre and the contact plate is set to zero. The last model is the complete model and is like the

second but with a friction coefficient of 0.7 between the tyre and the contact plate. The results of the investigation are shown in Figure 5-17. From the figure it is clear that the boundary conditions only have a minor influence on the outcome of the performed simulation. It was thus decided to use the simplified model for the rest of the investigation due to the reduced computation time while the accuracy of the results is not compromised.

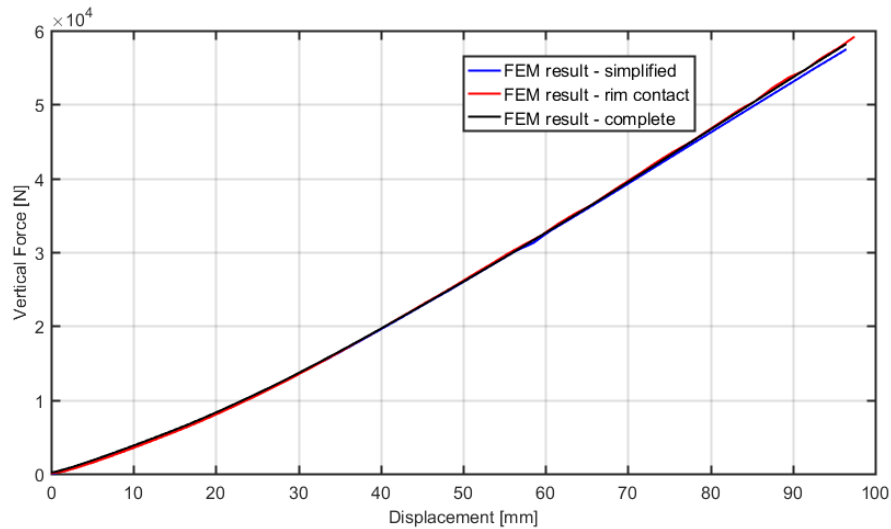


Figure 5-17 FE result comparison between the simplified model and the complete model

The final boundary conditions, as applied to the simplified model, are shown in Figure 5-18. For illustration purposes, the boundary conditions are applied to the axisymmetric tyre model. Equivalent boundary conditions are applied to the three-dimensional model. The tyre inflation pressure was modelled with a face load that is determined by a pressure. The face loads are determined based on the current geometry and is thus influenced by the deformation of the tyre carcass. The rim contact is modelled by fixing the translational degrees of freedom of the nodes that are in contact with the rim after a seating simulation.

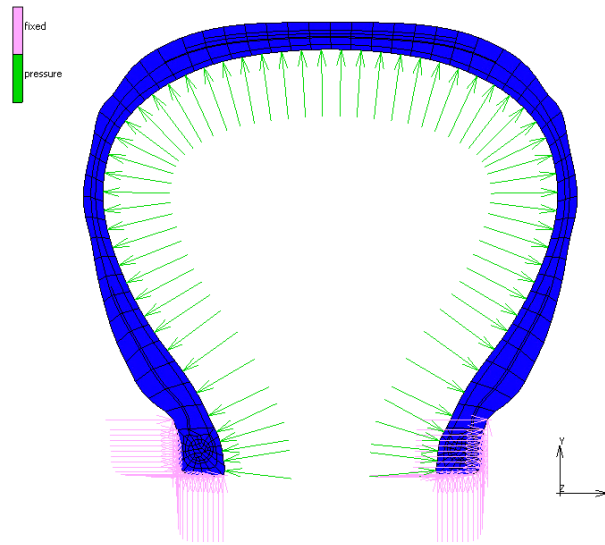


Figure 5-18 FE tyre model boundary conditions

5.6. FE tyre model validation

Researchers are using a wide range of experiments to validate finite element tyre models. Hölscher et al. [2004] and Barbani et al. [2012] developed FE tyre models and validated the models by comparing the predicted vertical force deflection characteristics to experimental results.

To investigate an aircraft tyre and wheel assembly Guo [2014] created a detailed finite element model of the two components. To validate the FE tyre model Guo compared the measured change in section width and outer diameter, due to an increase in inflation pressure, to the simulation results. Guo further uses a static tyre loading test to validate the model. A similar approach is used by Wei [2015] to validate a FE model of a passenger car tyre. Wei extends his validation to include test at various inflation pressures. Wei motivates this step due to the convenience to conduct further static tyre tests at lower inflation pressures. The measured and simulated footprint areas are also compared. The author further compares the footprint shapes at various static loading conditions and inflation pressures.

Kurunovic et al. [2011] created a FE tyre model to investigate the tyre behaviour to static loading conditions. The author validates the model by comparing the vertical load deflection curves, as well as the footprint shapes, of the test tyre to the numerically obtained results. The tests were conducted at a single inflation pressure.

Fervers [2004] creates a 2-D FEM tyre model to investigate the tyre-soil interaction. The author validates the model by comparing the tyre contour under load. The author also compares the dynamic rolling radius, for various inflation pressures, of the model to test results. The vertical load deflection characteristics at various inflation pressures are also used to validate the model. A step climbing manoeuvre is also conducted to investigate the belt bending behaviour.

Obtaining accurate experimental results is however not always possible for large off-road truck tyres. It is thus not always possible to validate the model and the obtained simulation results need to be trusted. This section is also intended to give the researcher an indication of the accuracy that can be expected of a finite element tyre model that was created with the same method as was discussed earlier in this section. If the finite element tyre model is capable of accurately reproducing the experimental results, without the need to tune any model parameters, this method could be used to create accurate finite element models of other large off-road tyres. This would thus improve the level of confidence in the finite element tyre model even if only limited or no validation test data is available.

Static experimental results are available for the test tyre and a validation process of the finite element tyre model can be conducted. For the validation process the experimental tyre tests were replicated in the finite element environment. The simulated test results were compared to the experimentally obtained results. The experimental test setup was discussed in section 4.2 and the obtained experimental results were presented in chapter 4.3.

The first validation test conducted was a vertical tyre stiffness test on a flat surface. The tyre inflation pressure was reduced to 0.1 Bar for this test. The inflation pressure could not be reduced to zero as tests at an inflation pressure lower than 0.1 Bar resulted in the unseating of the tyre during the test. A tyre with this low inflation pressure has no practical application as the tyre would not be able to support any significant load. This test is however very useful for validation purposes. Firstly, due to the low inflation pressure the carcass stiffness is dominating the tyre behaviour. At higher inflation pressures the stiffness contribution of the tyre carcass is reduced and is dominated by the internal pressure on the carcass. This test can thus be used to validate the material properties, construction and geometry of the finite element tyre model. The second advantage of conducting a validation test at a low tyre inflation pressure is that the tyre loads are significantly lower than at higher inflation pressures. Large carcass deformations can thus be tested even at relatively low loads. The lower reaction forces have numerous advantages for the testing of tyres with a higher load index. Firstly, a tyre with a much higher load index can be tested

on a test setup that is rated for much lower loads. The test setup is thus only limited by the size and dimensions of the tyre and not the loads that could be applied. Secondly due to the lower loads more sensitive test equipment may be used. Another advantage is that the deformation of the test setup is kept to a minimum due to the lower applied loads. This supports the assumption of an infinitely stiff test setup that is often made.

During the experiments, a trapezoidal loading cycle was used to apply a vertical force. The tyre was loaded to 6 kN, 8 kN and 10 kN resulting in a rim displacement of 53mm, 72mm and 85mm respectively. In the FE environment, the load is applied by moving the contact plate 85mm towards the tyre at a constant speed. The test and simulation results of the vertical tyre stiffness test are shown in Figure 5-19. The figure shows that the predicted vertical reaction force is lower than the experimentally obtained reaction force of the loading cycle. It was anticipated that the FE model would follow the force displacement characteristics of the loading cycle as the rubber material models were fitted to data of the loading cycle. The trend of the simulated force displacement curve is however very similar to the measured curve. The relative error, at a tyre deflection of 85mm, of the vertical reaction force is 6.5%. The model is also capable to accurately predict the stiffness increase that occurs at tyre deflections above 28mm.

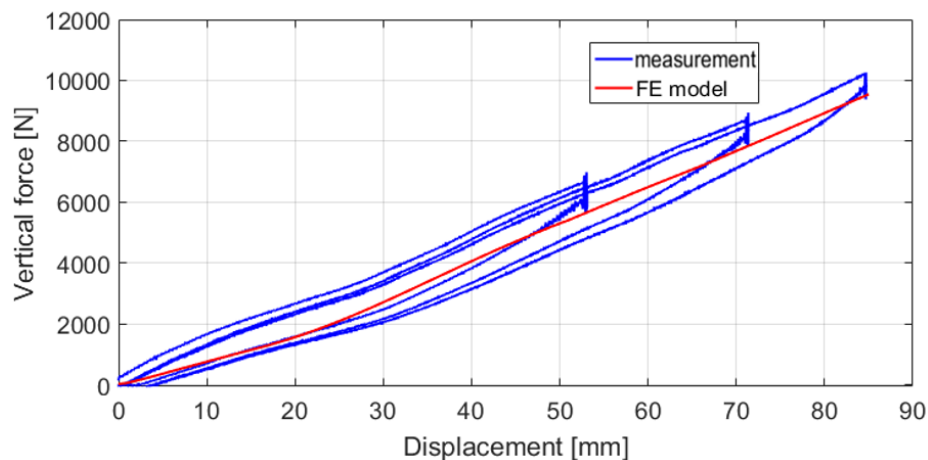


Figure 5-19 Vertical tyre stiffness on a flat surface at 0.1Bar

The tyre footprint can also be used to validate the model. The shape and size of the tyre footprint is not only dependent on the tyre stiffness but also on the stiffness distribution and the geometry of the tyre. To achieve good correlation between the measured and simulated footprints the model must accurately represent all three aspects. The measured and simulated footprints of the test tyre are shown in Figure 5-20. The test was conducted at an inflation pressure of 0.1Bar with a

applied load of 9600 N. The figure shows that the contact area of the individual tread blocks of the FE model are larger than the tread blocks of the test tyre. This is because of a CAD clean-up operation prior to the tread meshing operation. To reduce the number of tread elements all fillets of the solid tread model were removed. This resulted in a significant speedup in the solution time of the model while having a small effect on the overall behaviour of the tyre model. The drawback is that the tread blocks are incorrectly represented. Taking this into consideration, the figure indicates that the calculated footprint of the FE tyre model compares well to the measured result. The FE results indicate that the tyre loses contact in the centre of the tyre. This is however not visible in the measurement due to the measurement procedure. The footprint measurements are conducted using a dye method. The dye is removed from the film when the tyre contacts the film. This means that the measurement will show where the tyre made contact during the entire test. The procedure can thus not capture where the tread lost contact with the test surface.

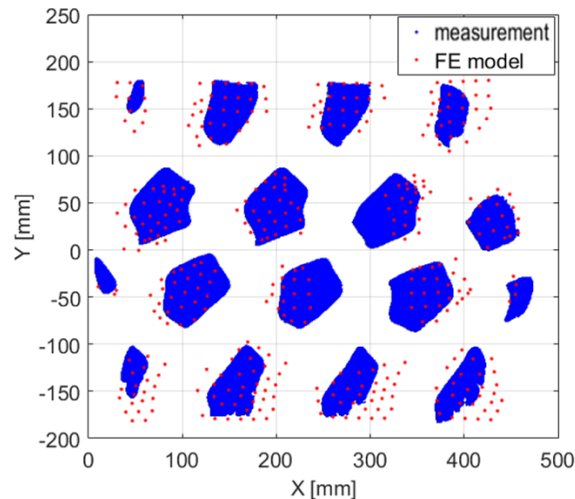


Figure 5-20 0.1Bar footprint validation

The test and simulation results of a vertical tyre stiffness test with an inflation pressure of 1.0 Bar is shown in Figure 5-21. The test was conducted at zero and four-degrees camber. The figure shows that the force displacement characteristic of the tyre is not sensitive to a change in camber. The FE tyre model is capable to predict the tyre behaviour for both test conditions. The predicted vertical stiffness is again slightly lower than the experimentally determined stiffness. The relative error, at maximum displacement, is reduced to 1.8% at zero-degree camber and 3.1% for the test at four-degree camber. The error between the measured and predicted vertical tyre stiffness thus decreases with an increase in inflation pressure. The increase in stiffness for displacements larger than 25mm is again captured by the FE tyre model.

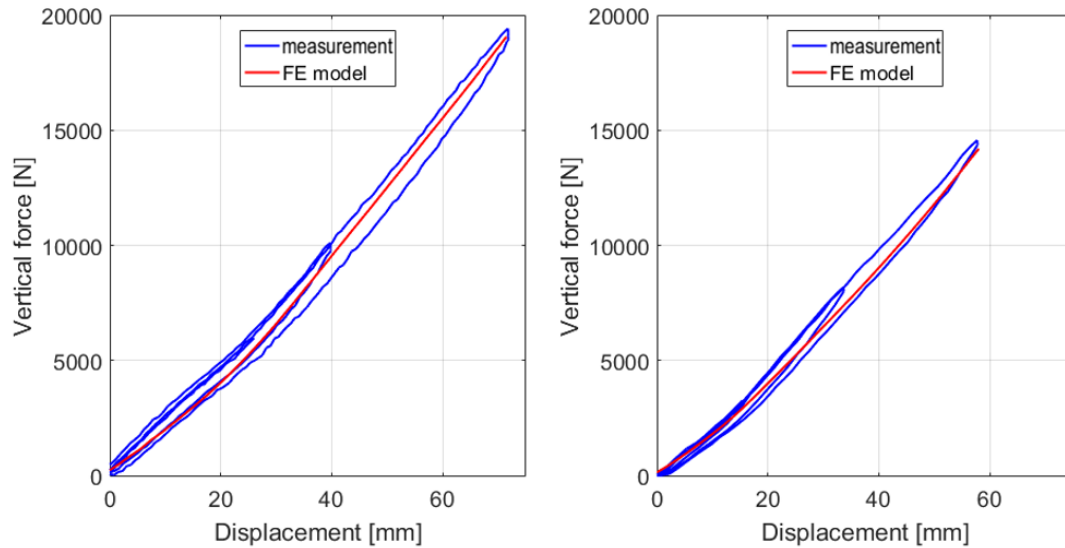


Figure 5-21 Vertical tyre stiffness at 1.0Bar, Left: 0deg camber, Right: 4deg camber

One of the tests that was performed was a static lateral cleat test. A 50mm square cleat was used for the test. The test is replicated in the finite element environment and is shown in Figure 5-22. The scalar plot shows the tyre node displacement resulting from the static cleat test. The figure shows that the largest deformation of the tyre occurs near the contact patch of the tyre while the rest of the tyre shows very little or no deformation.

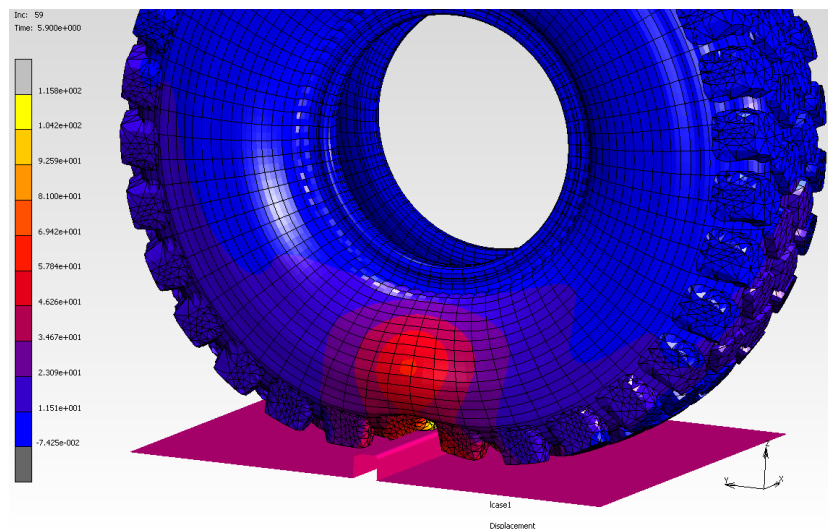


Figure 5-22 Node displacement during a lateral cleat test

Cleat tests were conducted on a lateral and longitudinal orientated cleat. The effect of a four-degree camber on the force displacement characteristics for a lateral cleat test was also investigated. The results of the lateral cleat test are shown in Figure 5-23.

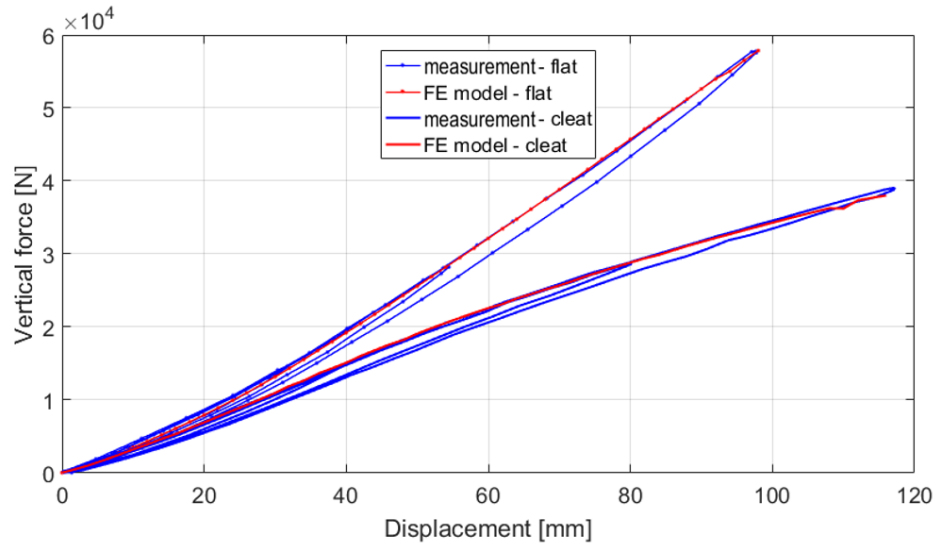


Figure 5-23 Vertical tyre stiffness at 3.0Bar, flat surface and 50mm lateral cleat

The figure also shows the measured and simulated force displacement characteristics of the tyre on a flat surface. The figure shows that the FE model is capable to predict the decrease in vertical stiffness during a lateral cleat test. The FE model is capable to accurately predict the tyre behaviour for both test conditions. The relative error of the vertical stiffness, on a flat surface, was reduced to 0.8% while the error on the cleat, at maximum deflection, was 3.2%.

The measured and predicted tyre footprints, at an inflation pressure of 3.0Bar, are shown in Figure 5-24. The left-hand figure shows the validation results of the zero-degree camber test. The test was conducted at a wheel load of 56300N. The simulated result compares well, in both size and shape, with the measurement. The figure shows that the contact area of the individual tread blocks of the FE model are larger than the tread blocks of the test tyre.

On the right-hand side of Figure 5-24 the measured and simulated footprints of a four-degree camber angle tyre test is shown. A wheel load of 30900N was applied during the footprint test. The predicted footprint shape and size again compares well with the measurement.

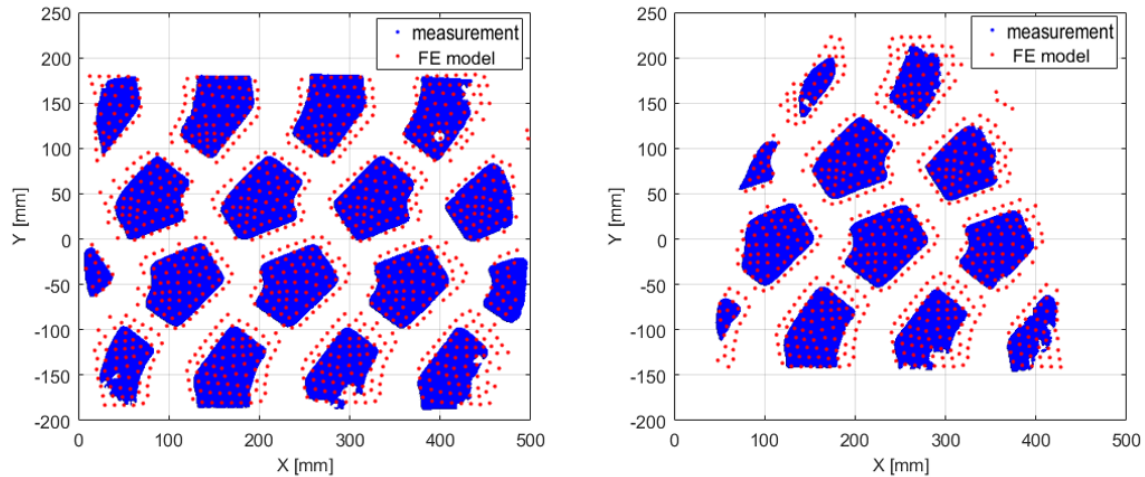


Figure 5-24 Validation of 3.0 Bar footprints. Left: 0 degree camber, Right: 4 degree camber

A lateral and longitudinal test was also conducted. The friction coefficient, used in the FE model, was calculated from the experimental results. The friction coefficient between the tyre and the steel plate as determined to be 0.68. A Coulomb bilinear friction model was used to determine the friction forces during the simulation. The longitudinal force of a longitudinal tyre stiffness test is shown in Figure 5-25. The shown tests were conducted at a tyre inflation pressure of 1.0 Bar. The FE model initially accurately describes the longitudinal stiffness of the tyre. The experimentally determined longitudinal stiffness is however slightly larger than the predicted stiffness for a longitudinal displacement between 2 and 6mm. The predicted longitudinal stiffness, for a longitudinal displacement above 6mm, is however again comparable to the measured stiffness. To illustrate this a 3mm offset was added to the simulation results. With the offset the predicted longitudinal stiffness is comparable to the measured stiffness.

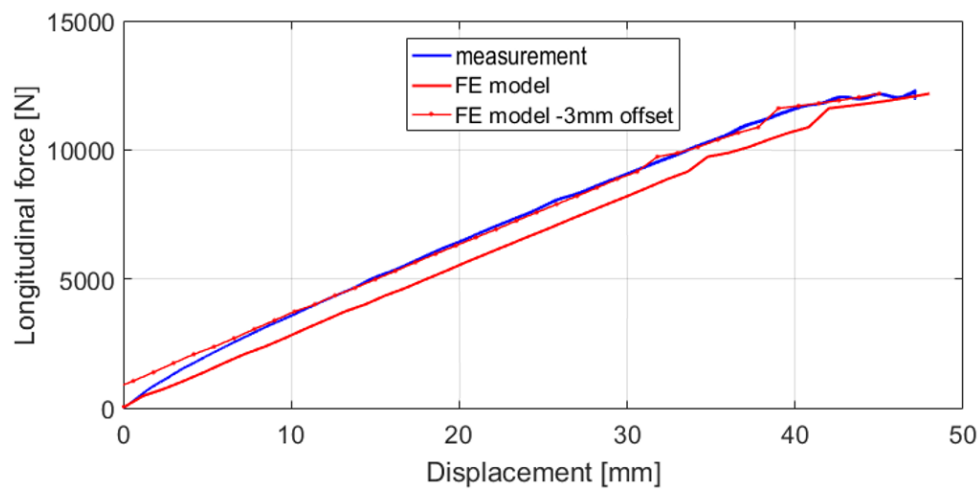


Figure 5-25 Validation of the tyre longitudinal stiffness

The presented results indicate that the finite element tyre model can accurately predict the tyre behaviour of static tyre tests.

5.7. FTire parameterisation using FE simulation results

The finite element tyre model was used to replicate the static and steady-state parameterisation tyre tests that are required to parameterise a FTire model. The simulations were conducted at two different tyre inflation pressures; 1.0 and 3.0 Bar. The obtained simulation results were post-processed to a FTire/fit compatible TYDEX [Unrau and Zamow, 1997] file format. The same parameterisation process as discussed in section 4.3 is followed to parameterise the FTire model. The only difference in this parameter identification process was that all the parameterisation data was obtained from the FE tyre simulation data. The simulation data that was used for the parameter identification process were:

- i. Footprint size and shape at different wheel loads and camber angles
- ii. Vertical stiffness on a flat surface
- iii. Vertical stiffness on longitudinal and transversal cleat
- iv. Vertical stiffness at a camber angle on a flat and transversal cleat
- v. Longitudinal and lateral stiffness on a flat surface

Section 5.6 described the validation process of the FE tyre model. Good correlation was found between the experimental results and the simulation test results. The same static and steady state test data that was used to validate the FE tyre model was used in Chapter 4 to parameterise a FTire model. Section 4.3 described the parameterisation process that was followed in detail. It was shown that the parameter identification process leads to in a FTire model that could accurately represent the tyre behaviour. A similarly good result was obtained when the FTire model was parameterised with the FE simulation data. A summary of the parameterisation results is shown in Figure 5-26 and Figure 5-27. The figures show the vertical force versus deflection characteristics on a flat road and on 50mm cleats, positioned in both transversal and longitudinal direction. Results are shown for simulations at an inflation pressure of 1 and 3 Bar.

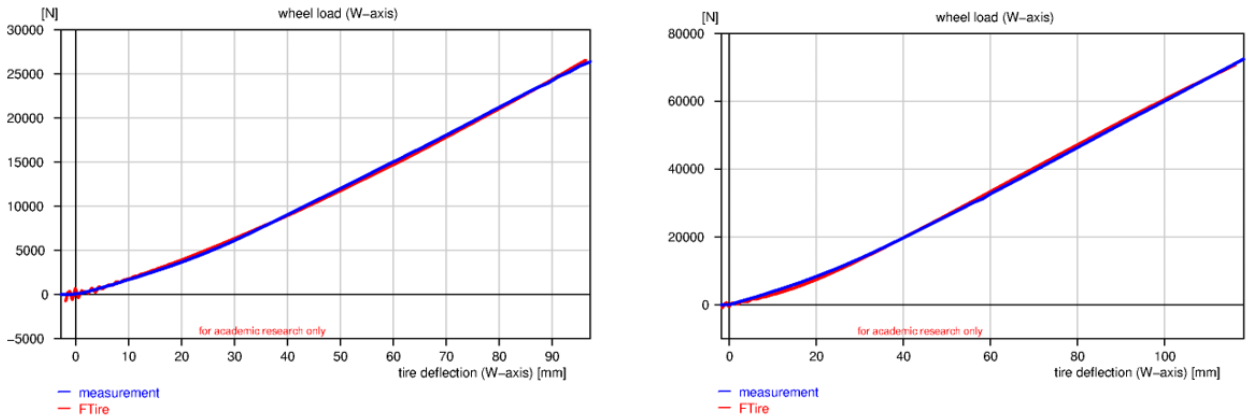


Figure 5-26 Vertical tyre stiffness, Left: 1.0Bar, Right: 3.0Bar

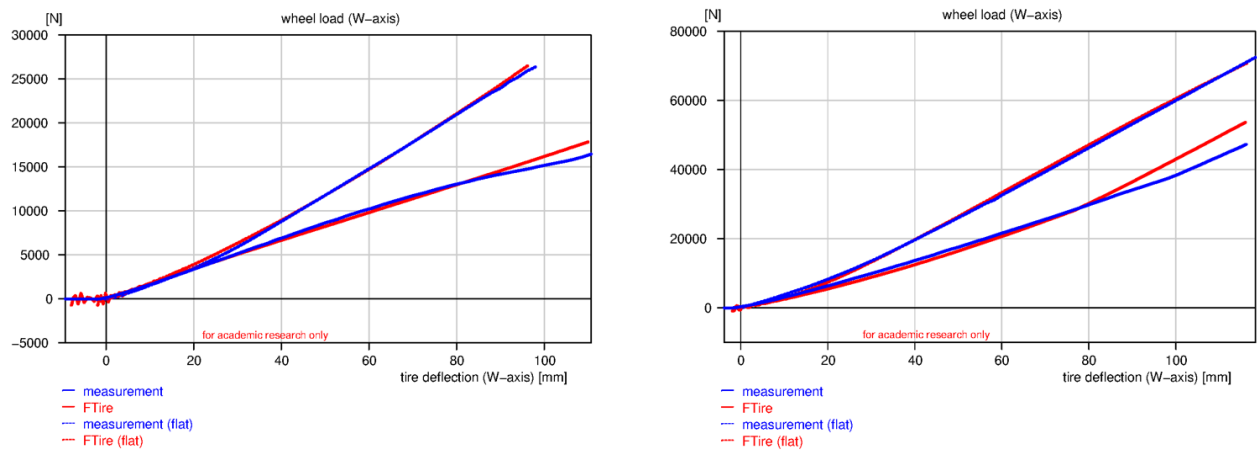


Figure 5-27 Tyre stiffness on cleat, Left: 1.0 Bar transversal, Right: 3.0Bar longitudinal

Due to limitations of the test equipment some parameterisation tests could not be conducted. The challenges that limited the physical testing of the investigated tyre can be circumvented in the FE environment. To extend the parameterisation data set additional simulations were conducted that were not possible to obtain experimentally. These tests included:

- i. Footprint size and shape at high camber angles (>6deg)
- ii. Vertical stiffness at high camber angles on a flat and transversal cleat
- iii. Torsional stiffness

Due to geometric constraints, footprint tests at high camber angles were not possible. This is however not a limitation in the FE environment. Simulations were conducted to determine the footprint shape and size at an eight degree camber angle. The simulation result is shown in Figure 5-28. The figure also shows the predicted tyre footprint shape of the parameterised FTire model. Relatively good correlation is found between the FE footprint and the FTire predicted footprint.

The figure also shows the FE tyre model predicted footprints shape with zero degree camber at a wheel load of 56.3kN. Good correlation is found between the FE tyre model and the FTire model.

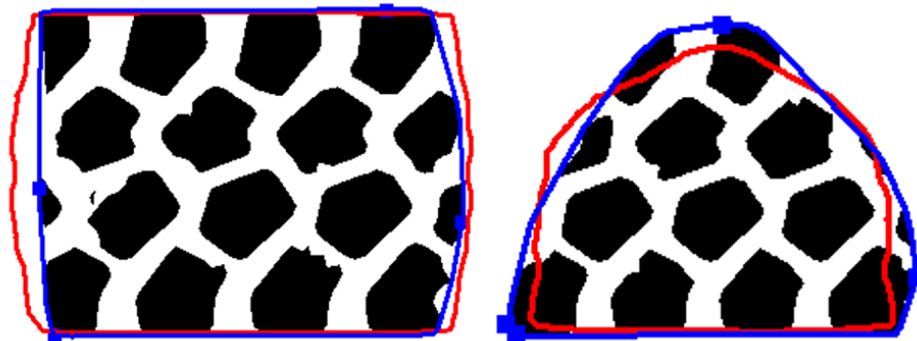


Figure 5-28 3.0Bar footprint. Left: 56.3kN 0deg camber. Right: 41.7kN 8.0deg camber

A vertical stiffness simulation, with a tyre in eight-degree camber position, was also conducted. The FE model prediction and the correlating FTire prediction is presented in Figure 5-29. The FE simulation result is presented as a blue line in the figure and is marked as measurement in the legend. Again, good correlation could be found between the two models.

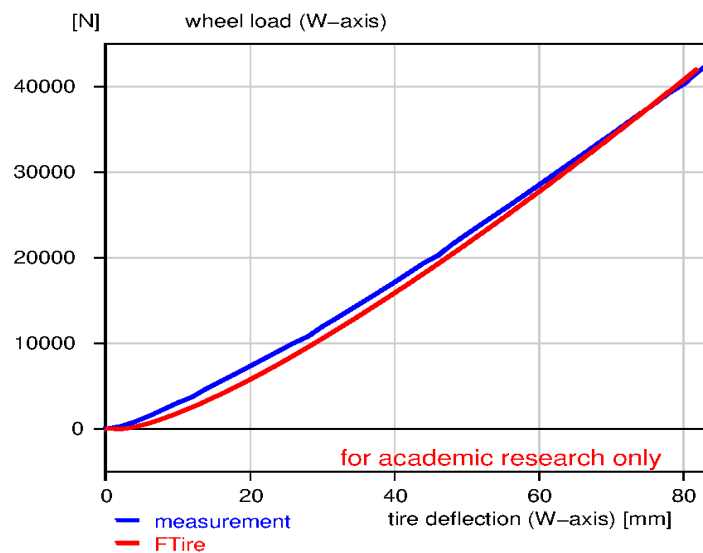


Figure 5-29 Radial stiffness validation: -8.0deg camber, 3.0Bar

A simulation was conducted to determine the tyre behaviour at an 8 degree camber position on a 50mm transversal cleat. FTire parameters could again be found to accurately describe the tyre behaviour under the test conditions. A slight variation between the FE results and the FTire results is found at large tyre deflection. The results of the test are shown in Figure 5-30

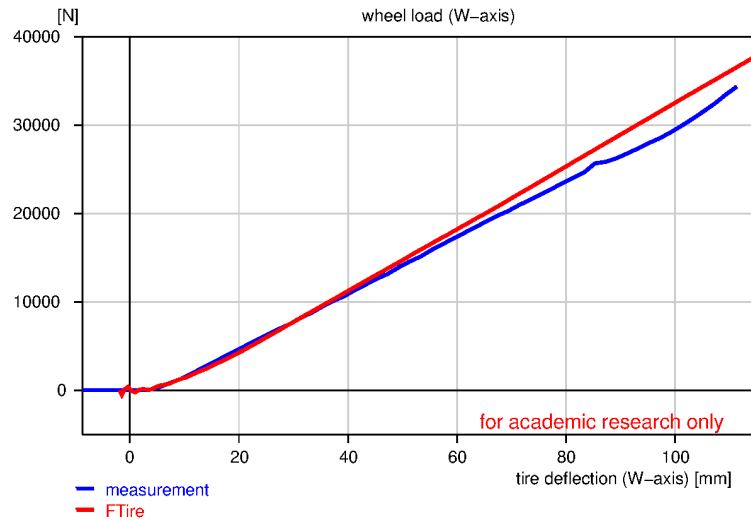


Figure 5-30 50mm transversal cleat validation: -8.0deg camber, 3.0Bar

Finally, a simulation was conducted with the FE tyre model to determine the parking torque tyre behaviour. During the test the aligning torque is recorded for a sinusoidal steering input. The simulation is conducted on a non-roiling tyre. The simulation results, indicated as measurements, are presented in Figure 5-31. Good correlation, between the FE tyre model and FTire, is found.

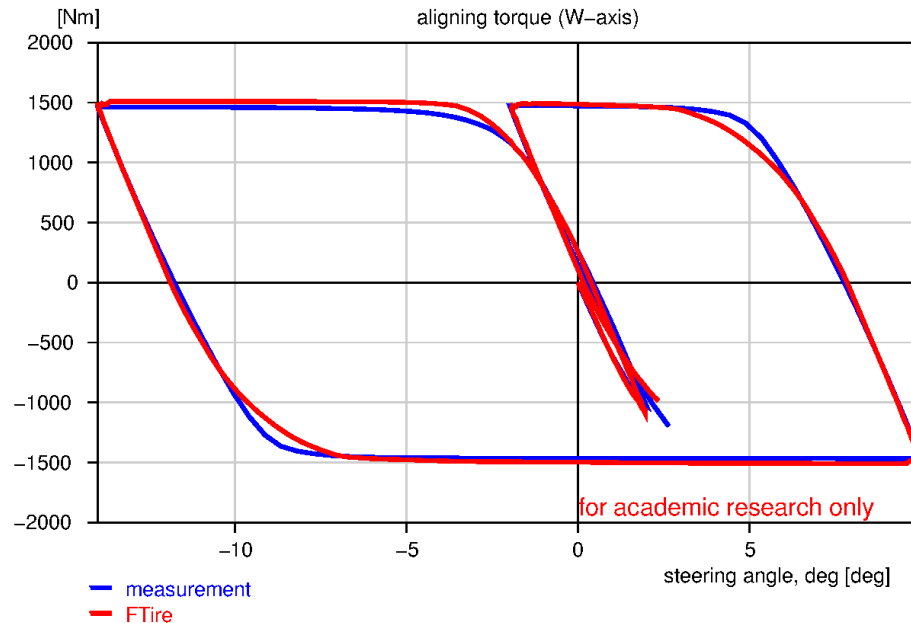


Figure 5-31 Parking torque validation, 29.4kN tyre load

5.8. FTire validation

The parameterised tyre model is again validated against experimental results that were obtained by pulling the tyre test trailer over a set of cleats and over various hard uneven terrains at the Gerotek Test Facility. The same test results that were used to validate the FTire model, that was parameterised with experimental test data, will be used to validate this FTire model.

5.8.1. Discrete obstacle

Figure 5-32 shows the measured and simulated results of the 50mm cleat test. From the figure, it is evident that the tyre model is capable to accurately predict the tyre forces while clearing the discrete obstacle. The figure also shows that the damping of the tyre model is slightly higher than the damping of the physical tyre. This is expected as the damping parameters of the FTire model were not identified from any data but was adopted from the demo truck tyre file that is shipped with the cosin software installer. Knowledge of the damping behaviour of the tyre is required to correctly define the damping parameters of the tyre model. If no data is however available an engineering judgement can be made based on the behaviour of similar tyres or on the user’s experience. Although the damping parameters were only adopted from an available truck tyre model the overall correlation is very good.

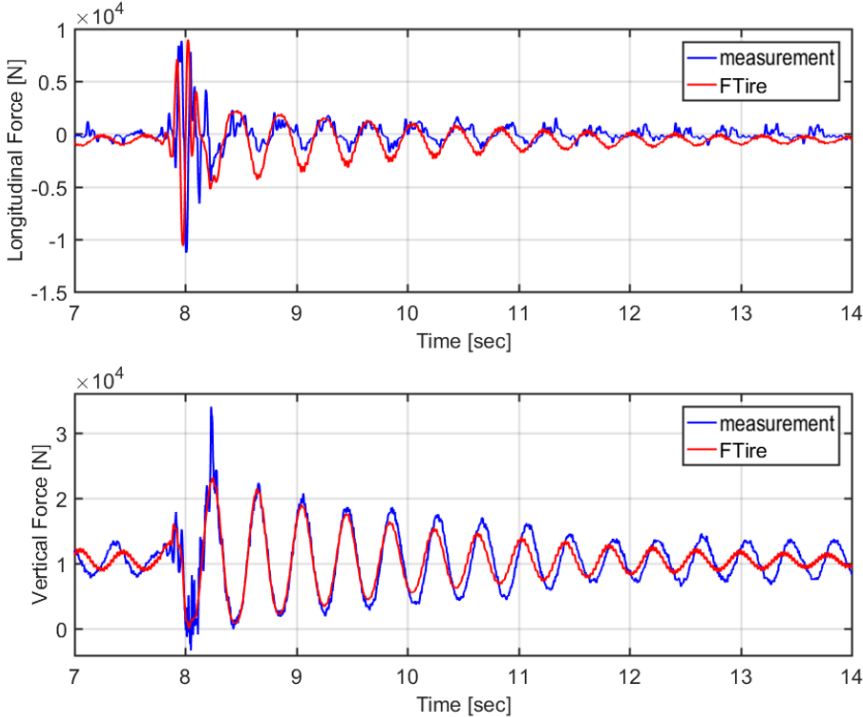


Figure 5-32 Discrete obstacle validation, 50mm transversal cleat. 18km/h, 3Bar.

5.8.2. Uneven road

The measured and simulated forces, acting between the sub-frame and main-frame of the tyre test trailer, while it is being towed over the increasing frequency cleats test track is shown in Figure 5-33. The figure shows that the model accurately represents the longitudinal and lateral loading conditions for this test. Good correlation is also found for the vertical force measurement, although some of the peak loading conditions are slightly lower during the simulation. The FTire model that was parameterised with the FE simulation results performs just as well as the FTire model that was parameterised with the established method (Chapter 4).

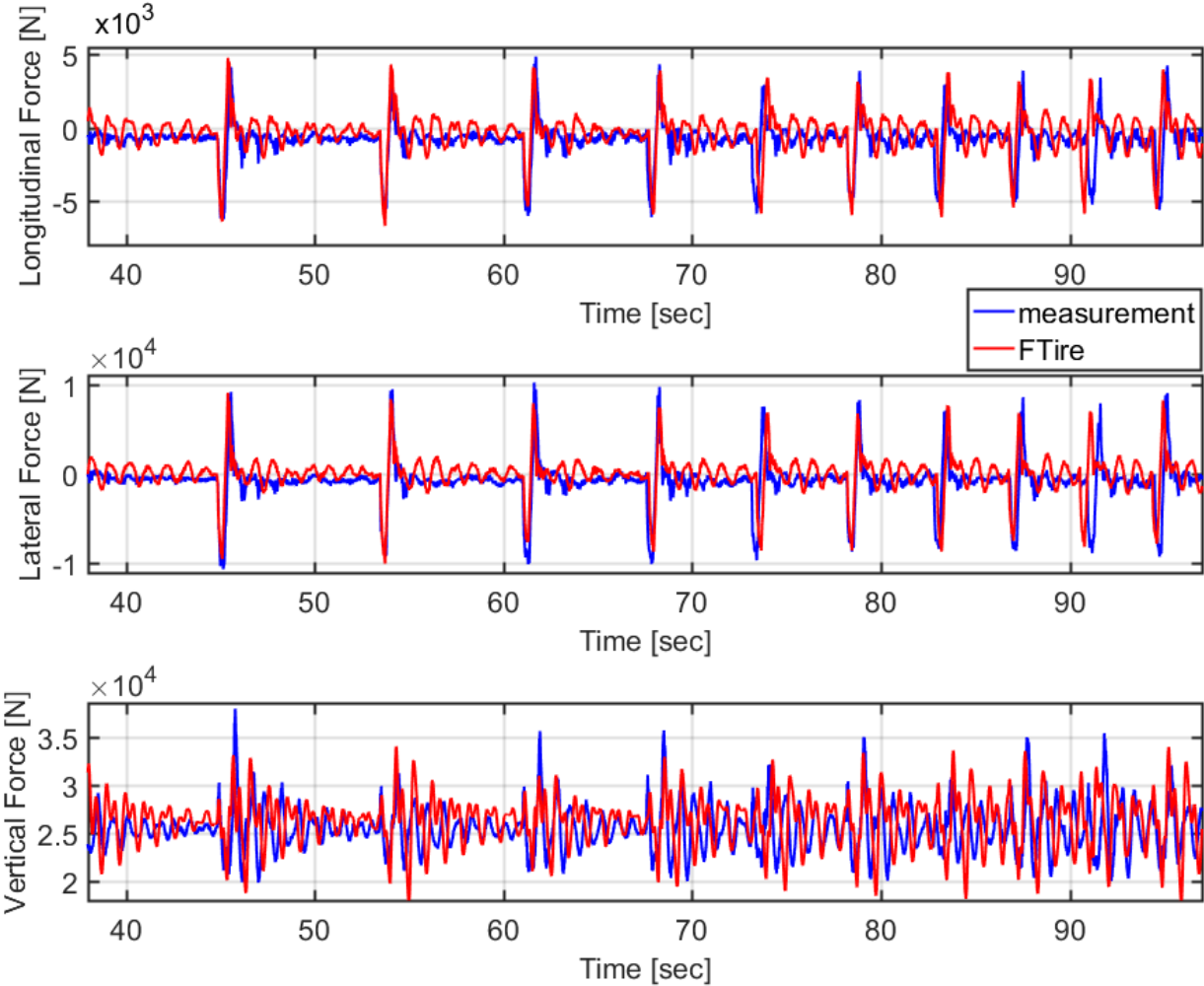


Figure 5-33 Validation results of the increasing frequency cleat test.

The force histogram of the lateral and vertical forces, for the Belgian paving test, is shown in Figure 5-34. The figure shows that the measured lateral force distribution, due to the road unevenness, is slightly lower than the predicted lateral force distribution. The peak lateral force

conditions can however be accurately represented by the simulation model. The vertical force histogram shows that the simulation model experiences peak vertical load conditions that are slightly higher than the load condition experienced during the physical trailer tests. The overall correlation between the two systems is however very good.

The PSD results of the tyre forces while driving over the Belgian paving is shown in Figure 5-35. Between 5 and 10Hz the frequency response of the model is slightly lower than the frequency response of the measurements. The frequency content of lateral force predictions of the model however correlates well with the measured results up to a frequency of about 14Hz.

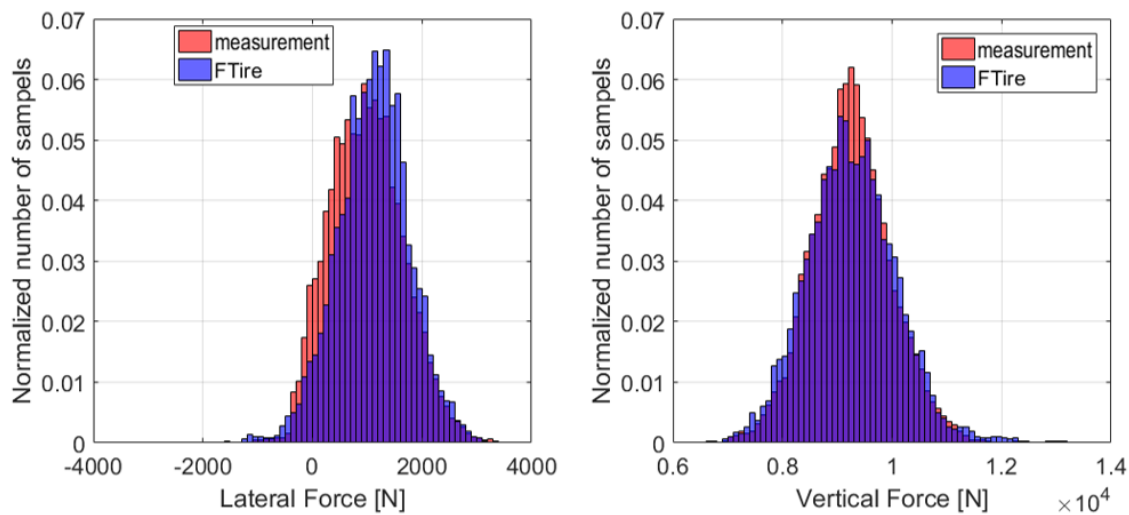


Figure 5-34 Force Histogram, Belgian paving

In the vertical direction, the force signals with frequencies up to 40Hz are relatively well captured in the simulation model. Peaks at 1.6 and 8 Hz, in the measurements are also present in the simulation results but at slightly lower frequencies. The peaks at 20Hz and 60 Hz in the vertical spindle forces are unrepresented in the vertical direction. These peaks are present in all test results and might indicate that MBS trailer model is incomplete. The reason for this discrepancy could however not be identified. The overall correlation between the measured results and the simulation results are however very good.

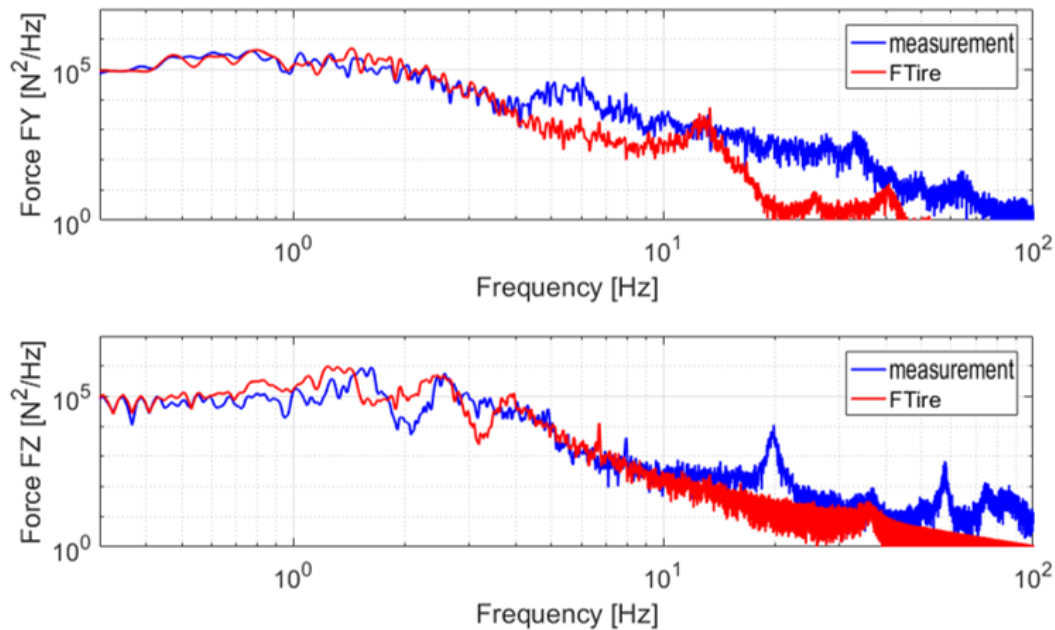


Figure 5-35 Force PSD validation, Belgian Paving

5.9. Chapter Summary

The parameterisation procedure, using finite element simulation results, was discussed in Chapter 5. This investigation was aimed at finding alternative ways to obtain tyre model parameterisation data. The main advantage of this method is that it can easily be scaled to accommodate all tyre sizes and load ratings. This method is thus less dependent on the availability of the test equipment.

The geometric properties of the tyre were determined with a set of measurements. The tyre cross section was determined with a laser measurement technique. The carcass thickness and construction were determined by cutting samples from the test tyre. The measurements were used to construct a detailed geometry (CAD) model of the tyre. The model included various rubber layers and all the tyre steel reinforcing layers.

A comprehensive set of tests were conducted to determine the material properties of the test tyre. Stress strain relationships of several identifiable rubber compounds were determined. A non-contact, full field, digital image correlation technique was used to measure the strain of the test specimen. A set of uniaxial tension, equibiaxial tension, shear, and ShoreA hardness tests were conducted on the rubber samples. The test results were used to fit a set of hyperplastic material models. The tests showed that an Ogden model was best suited to represent the rubber behaviour

of all tested rubber samples. The material coefficients were presented. Tests were also conducted to determine the Young's Modulus of the reinforcing steel cords as well as the tyre bead.

The CAD model and the obtained material properties were used to create a detailed three-dimensional nonlinear finite element tyre model. The tyre model was created in the MSC/MARC simulation environment. The finite element tyre model was validated against a set of measurements. The tyre model was validated for a wide range of inflation pressures and loading conditions. The validation results show the created tyre model could accurately represent the tyre behaviour, without any tuning of any model parameters.

The finite element tyre model was used to replicate the parameterisation tests that are required to parameterise a FTire model. The list of parameterisation tests was extended to include tests at high camber angles and included a parking torque tyre behaviour test. These tests could not be conducted experimentally due to limitations of the test equipment. The FTire/fit tool was used to extract the relevant model parameters from the simulation results. The results of the parameterisation were presented and show that all parameterisation load cases could accurately be replicated with the FTire model. The current finite element tyre model does not include material properties that describe the damping behaviour of the tyre. The damping parameters, of the FTire model, were thus not identified from any simulation data but was adopted from the demo truck tyre file.

The parameterised FTire model was validated against experimentally obtained dynamic tyre test data. The validation showed that the FTire model can be used to accurately predict the tyre forces for a wide range of loading conditions. The validation of the 50mm dynamic cleat test showed that the FTire model is slightly higher damped than the physical tyre. The overall correlation between the measured results and the simulation results as good as the correlation of the FTire model that was parameterised with the tyre measurements.

Chapter 6

Carcass deformation tyre model parameterisation

6. Carcass deformation for tyre model parameterisation

6.1. Introduction to carcass deformation tyre model parameterisation

This chapter discusses a novel method to parameterise FTire models and to validate FE tyre models. A digital image correlation method is used to track predefined points, or markers, on the tyre and to record their three-dimensional position during quasi-static tyre tests. This method will enable the user to compare the measured movement of predefined markers on the sidewall or carcass of the tyre with FTire and FE simulation results. The advantage of this method is that the displacements of a set of nodes during a tyre test can be compared directly to the measured displacements of the corresponding tyre segment.

6.2. Tyre deformation measurements

This section describes the test setup that was used to measure the tyre deformation and presents the obtained results.

6.2.1. Introduction to computer stereographic vision

Computer stereographic vision, or digital image correlation, is the extraction of three-dimensional information from digital images [Grimson, 1981]. In this process, a set of cameras are used to capture images of a scene from two or more viewpoints. By comparing these images, the relative depth information can be obtained. The human eye uses a similar approach for perceiving depth [Qian, 1997]. According to Botha [2015] a fundamental working principal of computer stereographic vision is the principle of binocular disparity. Binocular disparity is the positional difference between a set of images' projection of a certain point in space. The positional difference is due to the translational and rotational separation of the viewpoints. The binocular disparity concept is illustrated in Figure 6-1. The figure shows the projection of objects onto two view planes or image planes. It can be observed that the object closest to the cameras has a high degree of degree of positional separation between the two views. The degree of positional separation of objects decreases with an increase in distance between the camera and the object. Due to this principle, it is possible to determine the three-dimensional position of features from a set of images.

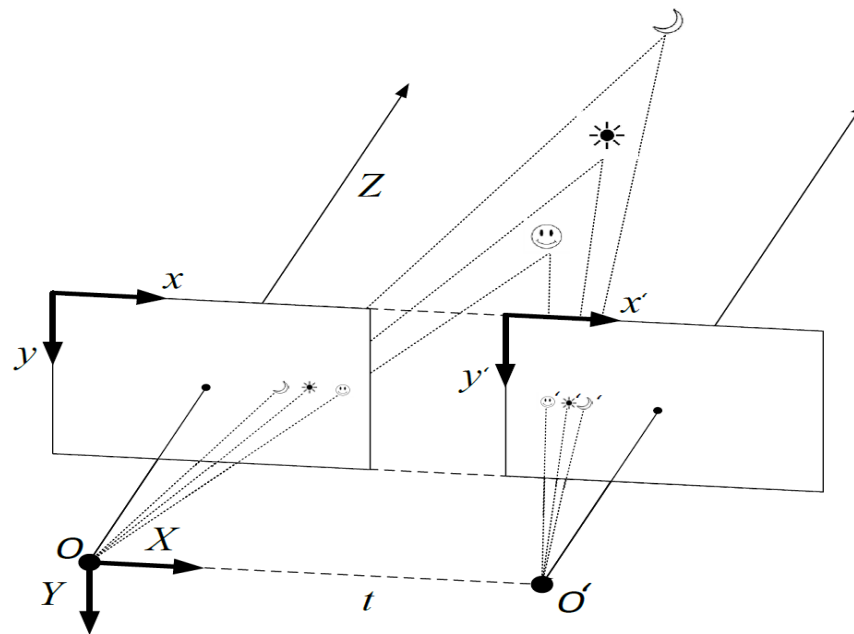


Figure 6-1 Stereovision working principal [Botha, 2015]

The working principle of computer stereographic vision can be summarized as follows:

1. Obtain digital images from differing views of a scene
2. Determine the relative position and orientation of the view points
3. Undistort the images so that the images match the projection of an ideal pinhole camera
4. Rectify the images by projecting the images onto a common plane
5. Create a disparity map of common features in the images
6. Determine three-dimensional point cloud of the image features

6.2.2. Tyre sidewall measurements

To investigate the possibility of using the digital image correlation technique to obtain parameterisation data of large off-road tyres, a preliminary study was conducted. The aim of the initial study was to measure the sidewall deformation of a tyre during a vertical stiffness test. The experimental setup consisted of the test tyre, mounted horizontally onto a specially designed pedestal. A servo-hydraulic actuator was used to apply a load to the test tyre. The applied force was measured using a load cell. The displacement of the actuator, relative to the rim, was measured with a string displacement meter. The measured force and displacements were recorded with a data acquisition system. The test setup is shown in Figure 6-2. A sinusoidal

displacement was applied to the tyre. The amplitude of the sinusoidal input was chosen to be 100mm with a period of 2 seconds.

A set of Point Grey, Grasshopper3 9.1 MP USB 3 [Point Grey, 2016a], cameras were used for this study. The cameras were set to a fixed resolution of 3376x2704 pixels. The cameras were mounted approximately 1200 mm above the tyre. The cameras were calibrated to determine the relative camera position and orientation and to remove the lens distortion. A trigger pulse was generated to externally trigger both camera shutters simultaneously. The trigger was also recorded to synchronize the force and displacement measurement with captured images. The data transfer rate, between the camera and the storage device, limited the frame rate. To avoid missing a frame during the test the frame rate was set to 8 frames per second.

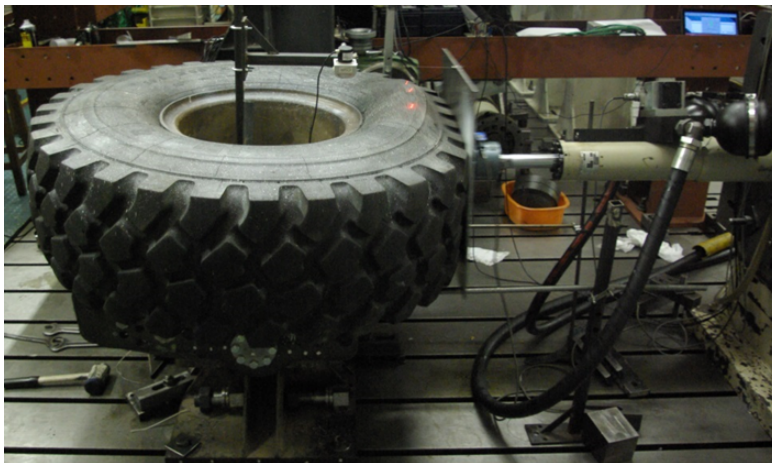


Figure 6-2 Initial experimental setup

The test tyre was labelled with circular markers. These markers were strategically placed on the tyre sidewall and on the tread section of the tyre that was visible to the cameras. The markers were designed to be easily distinguishable from the tyre sidewall. They had a black background with a white circular centre. The placements of the markers are shown in Figure 6-3. Markers were also placed on the steel plate, simulating the road surface, to track the actuator displacement.

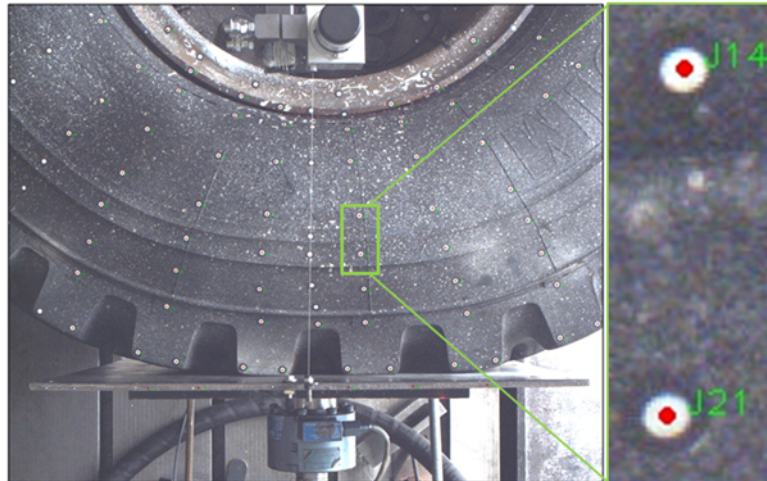


Figure 6-3 Left: Test tyre as viewed from camera, Right: marker close-up (red dot results from post-processing)

The captured video files were filtered and manipulated as discussed earlier. The tracking algorithm was used to track the markers on the test tyre. The image taken by one of the cameras at a deflection of 60 mm is shown in Figure 6-4. The figure also shows the manipulated image that is used to calculate the position vectors of the tracked markers.



Figure 6-4 Left: Test Result, 100mm displacement, 100kPa, Right: Manipulated image

The determined three-dimensional marker positions are shown in Figure 6-5. The markers located on the outer edge of the tyre (the tread section) were connected with a green line to simplify the visual inspection of the image. The markers that were tracked on the steel plate were connected with a black line. The colour of the markers indicates the vertical position of the marker relative to the rim edge at no load. From the figure it can be seen that the markers on the rim moved relative to the camera. This can be explained by the high loads that were applied during the test, causing the rim and pedestal to elastically deform. The measured velocity of the markers is indicated with purple arrows. The scale of the velocity vectors has been exaggerated to make them clearly

visible on the figure. The actual measured velocity is one tenth of the shown magnitude and is given in millimetre per second. The markers closest to the tyre contact patch show the highest change in their displacement while the markers closest to the rim show the smallest change. This tyre behaviour is expected.

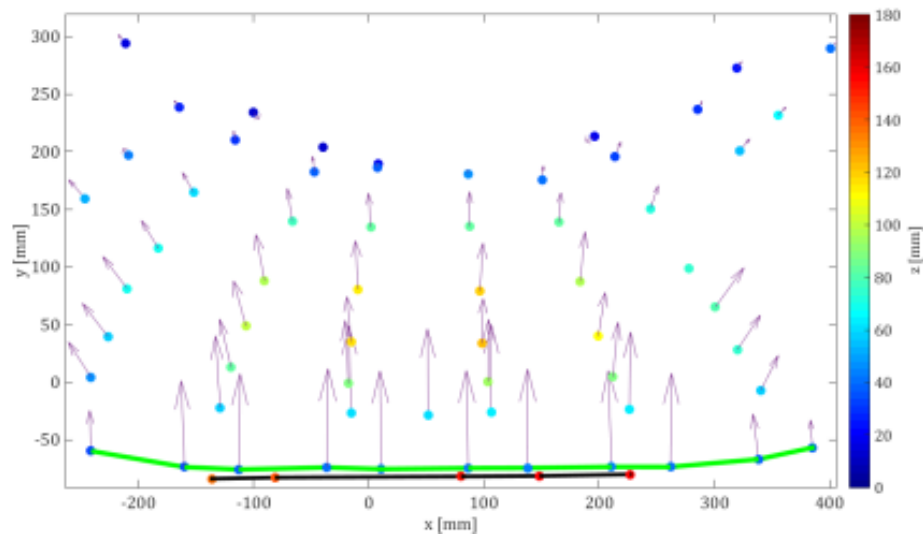


Figure 6-5 Tracked point positions and velocity vectors, 100 kPa

The results show that it is possible to track markers on a tyre sidewall in a three-dimensional Cartesian coordinate system. It is thus possible to compare the measured and simulated tyre structures to determine if the model can accurately represent the tyre behaviour.

With the current test setup, it was not possible to measure the tyre deflections near the tyre contact patch. The deformation of the tyre carcass belt could however be measured from the inside of the tyre as the view is not obstructed. This would also enable the investigation of the entire tyre carcass on an uneven contact surface, such as a cleat. A similar technique has been successfully implemented by Botha et al. [2012].

The camera test rig was modified to fit into the tyre. Only a limited number of camera lenses were available at the time of the investigation. The lenses that were available for the Grasshopper3 cameras were not suitable for the test setup due to the geometric constraints of the tyre and rim. The cameras were replaced by two FLEA3 cameras [Point Grey, 2016b]. The FLEA3 cameras were significantly smaller than the Grasshopper cameras. The resolution of the FLEA3 cameras was lower than the resolution of the Grasshopper camera. The FLEA3 cameras had a maximum resolution of 1.3MP while the Grasshopper cameras had a maximum resolution of 9.1MP.

The initial tests showed that the relative position and orientation of the cameras influenced the accuracy of the obtained results. The accuracy of the test setup was also dependent on the accuracy with which the center of the tracking markers in the captured images was calculated. A camera validation test was conducted to determine the accuracy of the measurement setup.

6.2.3. “Inside tyre camera” test rig validation

A camera setup was constructed that could be mounted on the inside of the Michelin 16.00R20 XZL test tyre. To ensure that the accuracy of the camera setup was acceptable, a validation marker block was created (Figure 6-6). The block was machined from a 250mm by 90mm steel block. Steps, of variable sizes, were machined onto the top surface. The step sizes ranged from 0.1mm to 1mm. The surface was painted with matt black paint to replicate the colour of the tyre. Eighty-six tracking markers were fixed to the painted surface.

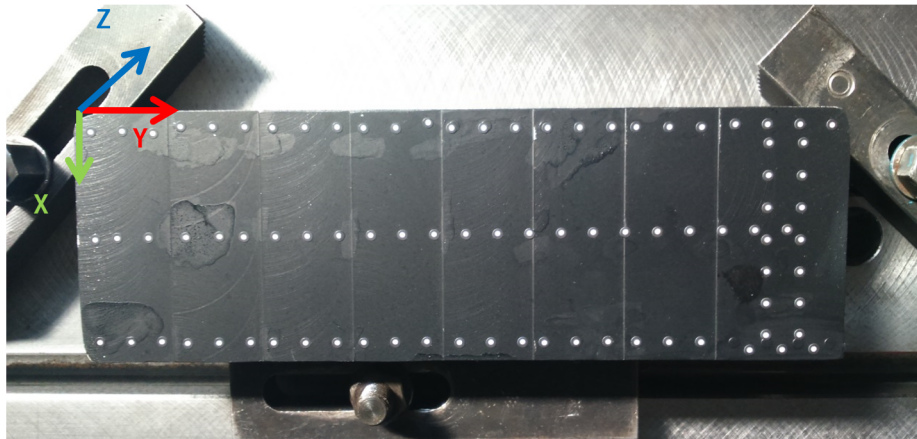


Figure 6-6 Validation test setup

During the validation test the validation block, as shown in Figure 6-6, was mounted to a milling machine. A road profiling laser, with an accuracy of 50 micron, was used to determine the reference position of the markers in a three dimensional space. The laser was mounted to the tool post of the milling machine. The bed of the milling machine was adjusted until the laser was located in the center of the marker. The elevation of the marker was then recorded. Human judgment was used to determine if the laser was positioned in the center of the marker. The lateral (Y) and longitudinal (X) error should thus not be considered as the error might be due to an incorrect reference position.

The camera test rig was used to capture stereo images of the validation block. The position and orientation of the camera test rig, relative to the validation block, was altered to determine the

poorest expected outcome of the tyre test. A sub-pixel edge detection algorithm was developed and incorporated into the postprocessing algorithm in order to improve the accuracy of the test results. The algorithm was proposed by Trujillo-Pino et al. [2013]. The sub pixel edge detection algorithm is derived from the partial area effect. The results of the poorest test outcome are shown in Figure 6-7. From the figure it can be seen that the absolute error is less than 0.31mm in the Z direction. The three dimensional error is also shown for completeness.

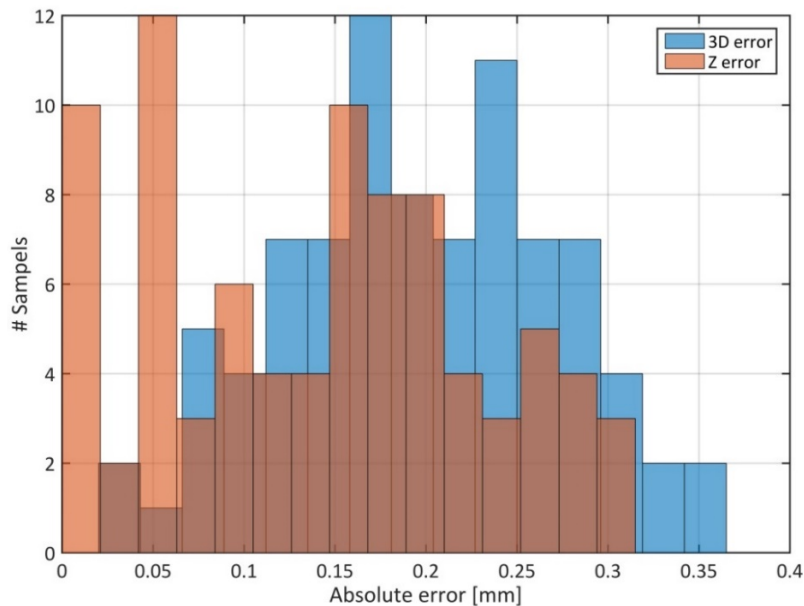


Figure 6-7 Camera setup accuracy

The validation tests thus show that the expected error during the tyre tests would be below 0.4mm. To further improve the accuracy of the measurements higher resolution cameras should be used.

6.2.4. Tyre deformation test setup

The rim of the tyre was adapted so that the camera setup can be mounted to the inside of the tyre. The stereo vision camera test rig was mounted onto the rim, on the inside of the test tyre. The rim was further modified to accommodate the USB, trigger, and power cables. A plug was manufactured to ensure an airtight seal could be achieved where the cables exit the rim. Figure 6-8 shows the camera setup on the inside of the test tyre. During the tests, LED lights were used to illuminate the inside of the tyre. Special care was taken to distribute the light evenly across the observed carcass surface to avoid over exposing sections of the images. All the modifications done to the rim were completed in such a way that they would not influence the behaviour of the tyre.



Figure 6-8 Camera test setup mounted on the inside of the tyre

The marker locations on the inside of the tyre are shown in Figure 6-9. The design of the markers was the same as were used during the validation tests. More than a thousand markers were glued to the inside of the tyre. Only 830 markers were however continuously tracked during the tyre tests.



Figure 6-9 Marker position on tyre carcass (50mm cleat)

The left and right camera views of the markers are shown in Figure 6-10. Due to the camera setup, only a small area of the tyre carcass is visible to both cameras at the same time. The cameras were thus mounted in such a way that slightly more than half of the tyre contact patch,

in the longitudinal direction, is visible to both cameras. It is however assumed that, for tests at 0 degrees camber, the tyre deflection would be symmetrical along the longitudinal direction.

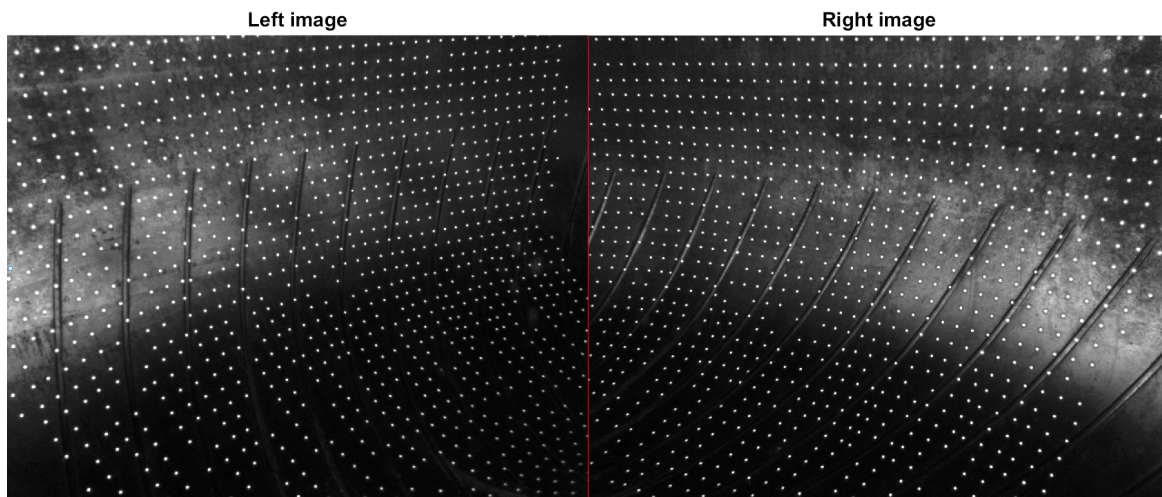


Figure 6-10 Camera view of markers

Figure 6-11 shows the 830 markers that were tracked during the tyre tests. Most markers are located on the tyre carcass near the contact patch of the tyre. Markers were also placed on the side wall of the tyre to capture the sidewall deformation during the tests.

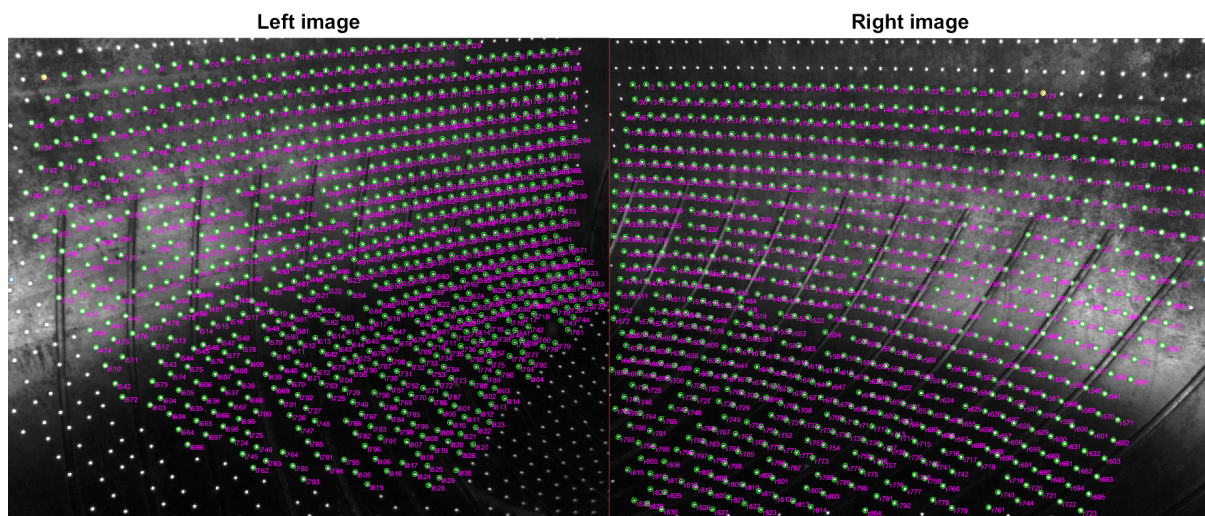


Figure 6-11 Corresponding markers used during post-processing

6.2.5. Tracking algorithm

The marker tracking algorithm played an important role in ensuring the accuracy of the obtained results. The test procedure is outlined in Figure 6-12. Two of the biggest challenges of this

investigation were to accurately determine the pixel location of the markers centre and to accurately determine the corresponding marker in the left and right images. Various checks were also conducted during the process to ensure that the algorithm worked as expected.

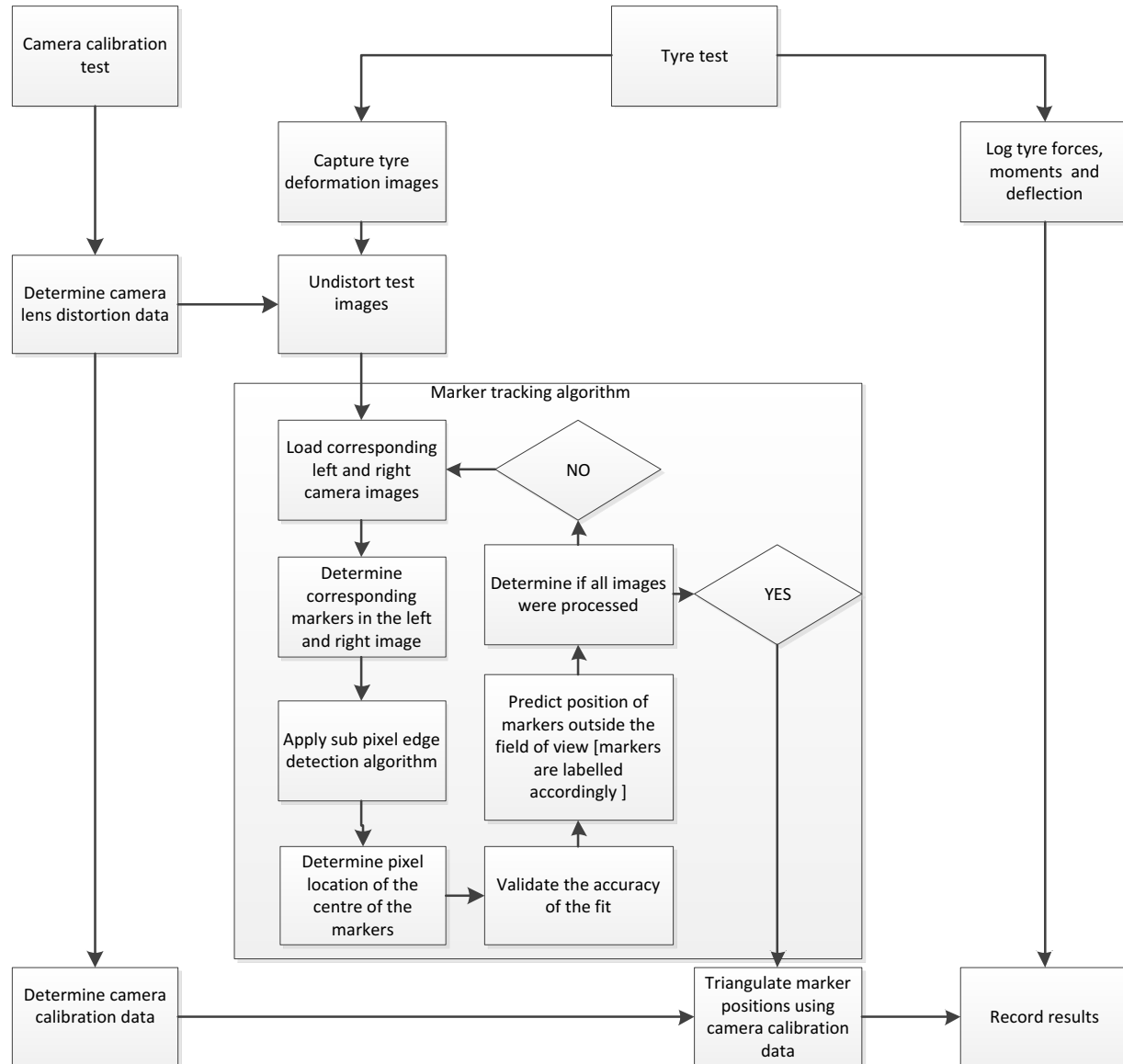


Figure 6-12 Test procedure

To ensure that the centre of the markers was accurately determined, a sub pixel edge detection algorithm and ellipse fitting algorithm were incorporated. The sub pixel edge detecting algorithm was proposed by Trujillo-Pino et al [2013]. The algorithm was based on the partial area effect and did not assume continuity in the image values. The algorithm thus assumed that the pixel values, of an image, were acquired by light sensors where the intensity was proportional to the intensities

and areas on both sides of the edge. The authors showed that the algorithm obtained high accuracy results for ideal images and even for noisy images. This algorithm was thus ideally suited to accurately determine the centre of the marker. An advantage of this algorithm was that the curvature of the edge could be determined. This feature was used as a check to ensure highly accurate results were obtained. The results of the sub pixel edge detection algorithm are shown in Figure 6-13.

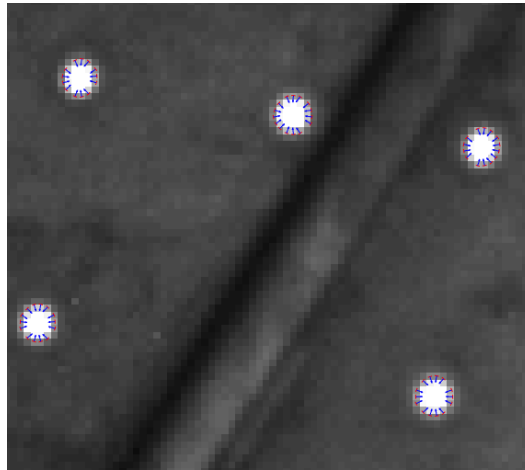


Figure 6-13 Sub-Pixel edge detection algorithm

The edges of the marker, as determined by the sub pixel edge detection algorithm, were used to fit an ellipse. The centre of the ellipse could then easily be found and was used as the pixel location of the centre of the marker. The calculated curvature was used to validate the calculated centre of the marker. When the validation failed, the marker was flagged accordingly. The flagged markers could later be removed from the dataset to ensure a highly accurate test result.

When a marker was not visible in one or both images, a prediction algorithm was used to predict the location of the marker. This was necessary to accurately detect the markers when the markers reappear in both images. The prediction algorithm was based on the nearest neighbour approach and assumes that the relative displacement between markers in a region was rather small. The markers were flagged accordingly to ensure that a distinction between the measured and predicted markers could be made during post processing.

Algorithms were also developed to ensure that the markers in the left image were accurately paired with the markers in the right image. A set of base markers were used to the predicted location of the marker pairs when no carcass deformation was applied. Since the cameras were

fixed to the rim, and the tyre was assumed not to slip on the rim, the pixel position of the markers when no load was applied should remain the same.

The algorithm also checked that the change of the pixel position of the markers, for consecutive images, were comparable to the position change of the nearest markers. If a single markers position changed significantly more than its nearest neighbours, the algorithm had incorrectly paired the markers. The algorithm is then stopped and requests the user to confirm the position of the marker pairs manually. This was however only expected during tests where large tyre deformations occurred between two consecutive frames. The camera frame rate should thus be chosen in accordance with the tyre deflection speed.

6.2.6. Tyre deformation test results

The acquired test results were post processed as described in 6.2.5. The calculated three-dimensional positions of the 830 markers on an un-deformed tyre carcass are shown in Figure 6-14. The markers are coloured according to their distance from the global origin, the wheel centre. To better visualize the inner tyre surface, the scattered data can be interpolated and shown as a surface. The result of the scattered data interpolation is shown on the right of Figure 6-14.

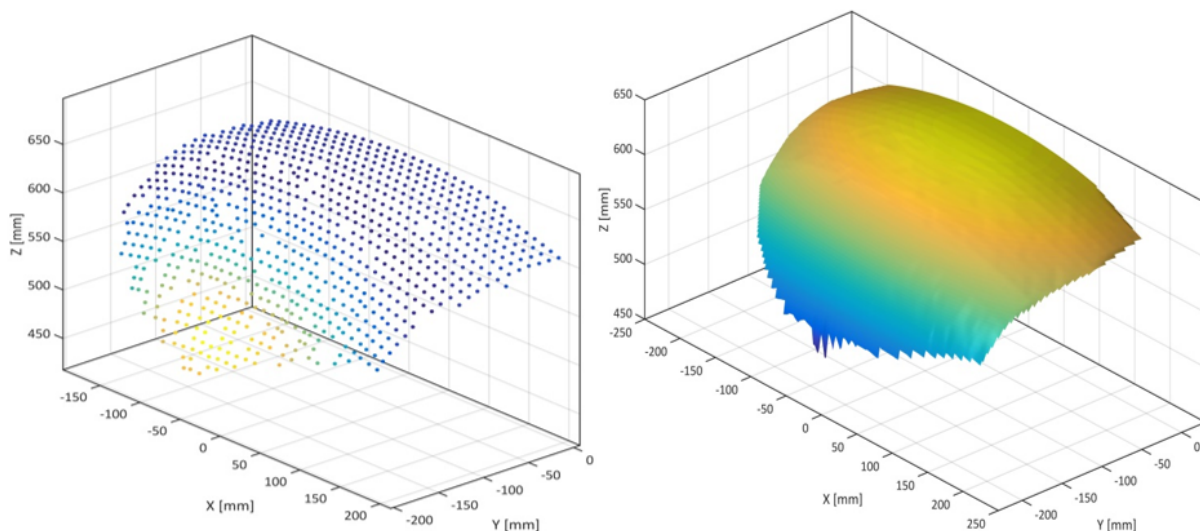


Figure 6-14 Carcass markers in global coordinate system

Measurements conducted to create the CAD model of the tyre determined that the tyre has an inner radius of 641.5mm. The inner tyre radius, as determined by the camera method, was determined to be 642.2mm. The figures also show that the tracked markers cover slightly more than half of the tyre width in the axial direction (Y direction). In the longitudinal direction, the

markers cover a length of about 350mm. The markers thus cover more than a quarter of the tyre diameter in the longitudinal direction (X direction) and a third of the tyre sidewall in the radial direction (Z direction).

The inner lining of the CAD model is superimposed onto the interpolated tyre carcass to illustrate the total area that is covered by the tracking markers. The results are shown in Figure 6-15. A relatively small area of the total tyre is observed during the test. This area is however of greatest interest and should show the largest deformation.

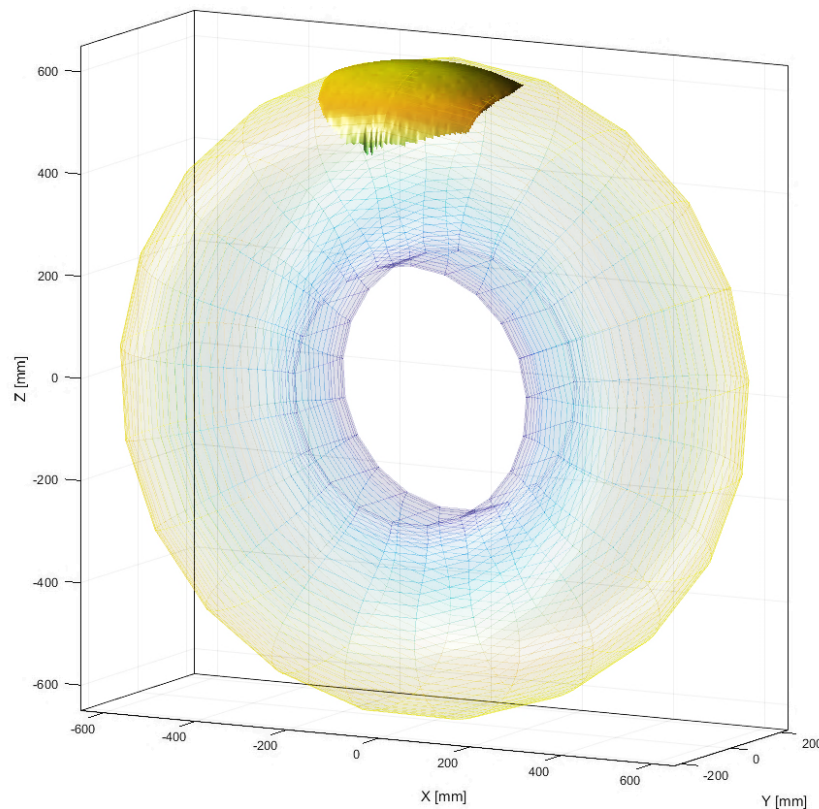


Figure 6-15 Observed tyre carcass area

Small indents can be seen in the inner tyre lining. These can be attributed to markers that are glued to rubber ridges that are located on the inner lining. The ridges can clearly be seen in Figure 6-14 and Figure 6-15.

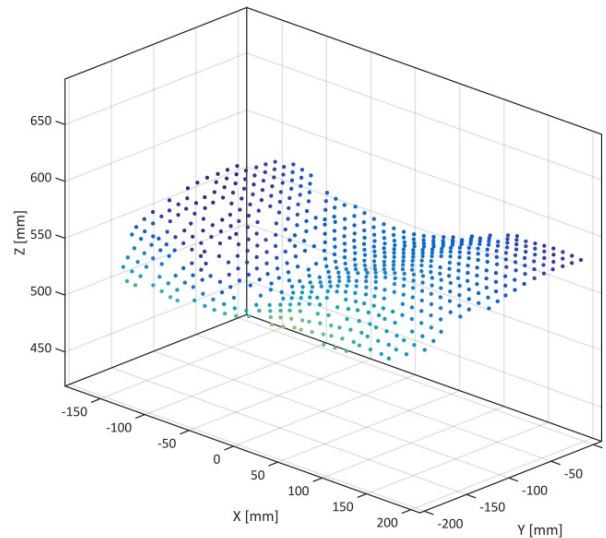


Figure 6-16 Lateral cleat test result, 50mm, 1bar

Figure 6-16 shows the marker locations during a 50mm lateral cleat test. The test was conducted with an inflation pressure of 1 Bar. The carcass deformation due to the cleat is clearly visible in the figure. The image also shows fewer tracking markers in the lateral direction. This is because the markers are not visible in one or both images. This is due to the large tyre deformation and the position of the cameras on the inside of the tyre. Figure 6-17 shows the un-deformed inner tyre carcass and the deformed carcass during the 50mm cleat test.

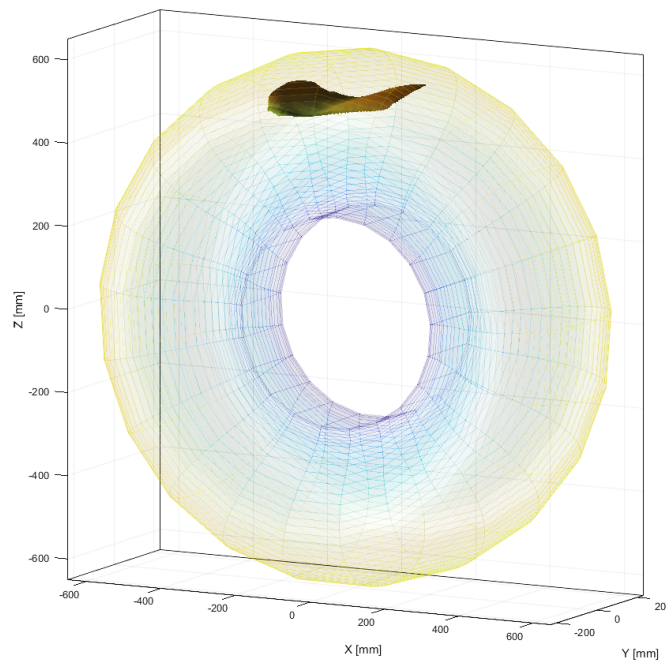


Figure 6-17 Local carcass deformation during lateral cleat test

The three-dimensional displacement of a single tracking marker is shown in Figure 6-18. The marker is located near the middle of the tyre contact patch. From the figure, the tyre was loaded to three different loads. The cleat was moved towards the tyre at a constant speed. When the desired deflection was reached, the loading process was paused for a few seconds. The cleat was then moved back to the starting position.

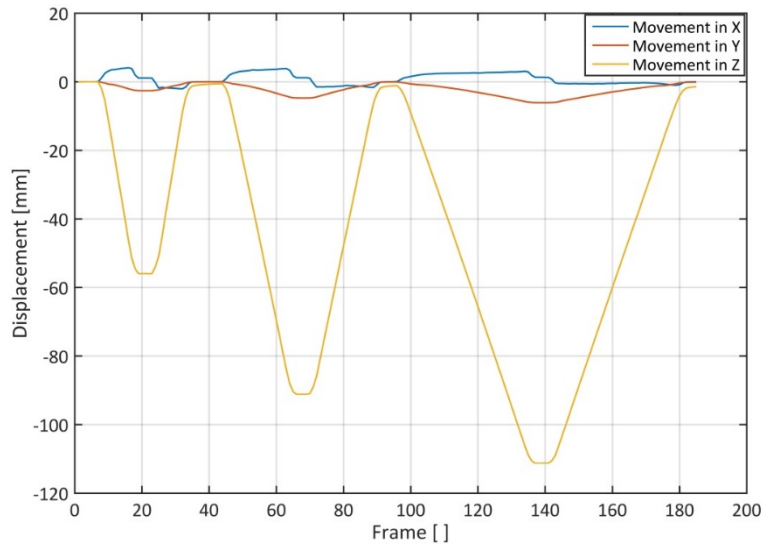


Figure 6-18 Marker movement during 50 mm cleat test

Figure 6-19 shows the precision of the camera setup. The figure shows the unfiltered radial displacement of the marker during the static part of the tyre tests. The radial position, as determined by the marker tracking algorithm, varies less than 0.1mm during this time.

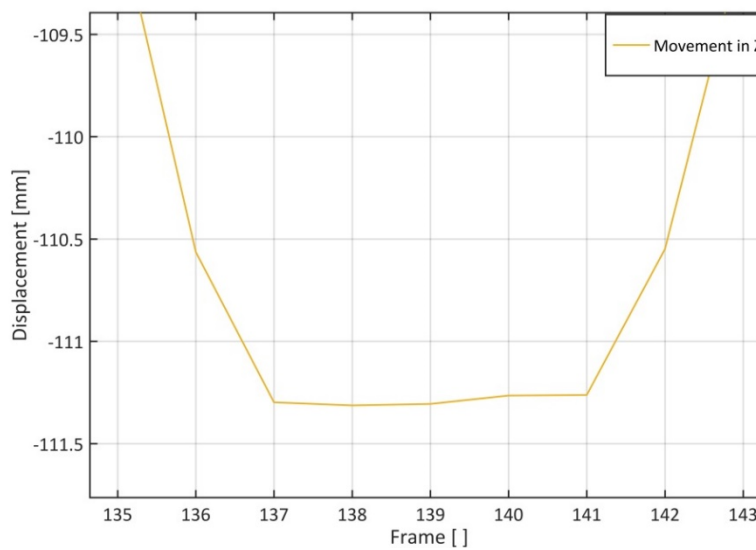


Figure 6-19 Precision of measurement

6.3. Tyre deformation for FEM validation

Tyre contact size and shape, as well as pressure distribution, are commonly used to validate finite element tyre models. These tests are however limited to smooth road surfaces and don't allow for uneven contact surfaces. Footprint tests are furthermore limited to static tyre tests.

It is thus proposed to use the carcass deformation to validate finite element tyre models. A numerical model is only capable to predict a comparable carcass deformation, for a set of applied boundary conditions, if the local tyre stiffness is modelled accurately. Good correlation between the measured and simulated local tyre stiffness would inherently result in an accurate global tyre behaviour. Using full field carcass deformation measurements, rather than global force displacement measurements, during the model validation process would result in higher confidence levels in the model.

6.3.1. FEM validation metric

To use the measured full-field carcass deformation test results for validation purposes a numerical analysis should be conducted that replicated that boundary conditions of the test in the finite element environment. The measured and simulated carcass shape, during a vertical stiffness test on a smooth surface, is shown in Figure 6-20. The unladed tyre carcass is shown on the left of Figure 6-20 while the laden case is depicted on the right. The figure shows the carcass shape of the test tyre with an inflation pressure of 1 Bar. To assist in the visual inspection of the results only the bottom half of the tyre is shown in the figure.

Figure 6-20 shows that the measured carcass shape, of an unloaded and laden tyre, can be accurately represented by the model. The carcass deformation results, obtained from experiments and numerical analyses, however contain enormous amounts of information that cannot be analysed by visual inspection only. Appropriate features of the experimental data and the model outputs must be carefully identified. An important feature that can be investigated is the relative deformation that occurs during the tests. This means that the measured displacement field, because of the loading condition, should be compared to the predicted displacement field.

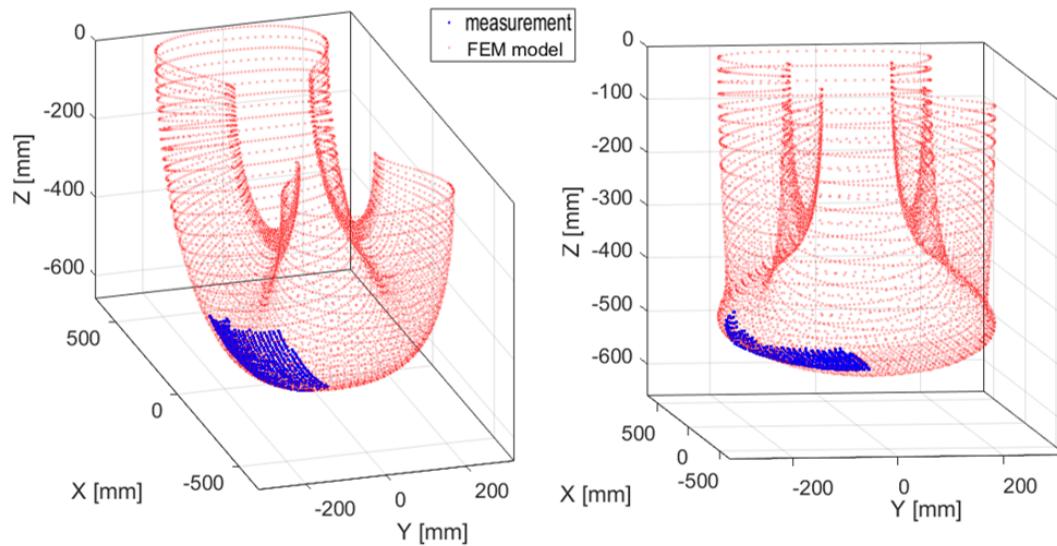


Figure 6-20 Tyre carcass deformation on a flat surface, 1Bar. Left: Unladen. Right: Laden

To investigate this, the error between the measured and predicted carcass shape needs to be determined. The error was determined by calculating the distance between the three dimensional location of a measurement marker and its projected location on the simulated carcass. A Delaunay triangulation method is used to fit a set of triangles onto the finite element node location. The projection is determined by calculating shortest line connecting the measurement marker and a triangulation in three-dimensional space. A graphical representation of this method is shown in Figure 6-21.

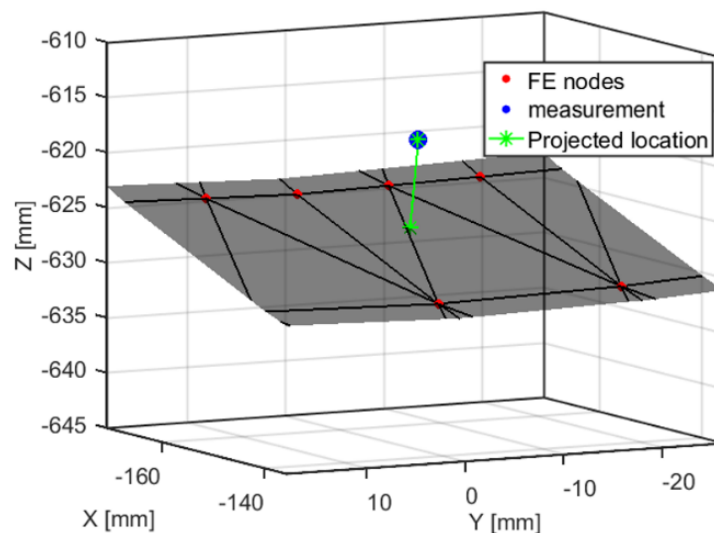


Figure 6-21 Projected node location

The error is defined as the length of the line connecting the measurement marker and its projection onto the triangulated surface. The error is thus given by:

$$Error_{i,undeformed} = \sqrt{(x_{i,p} - x_{i,m})^2 + (y_{i,p} - y_{i,m})^2 + (z_{i,p} - z_{i,m})^2} \quad (6.1)$$

Where $x_{i,m}$, $y_{i,m}$ and $z_{i,m}$ are the measured x, y, and z coordinates of the i th marker and $x_{i,p}$, $y_{i,p}$ and $z_{i,p}$ are the coordinates of the i th marker projection onto the triangulated surface. Furthermore, the normal vector of the triangulated surface is determined to assign a sign to the calculated error.

The position of the projected marker, relative to the three nodes of the triangulated surface, is determined. The same node connectivity is used to fit a triangulated surface through the nodes of the laden test case. A linear interpolation method is used to determine the three-dimensional location of the projected marker on the laden triangulated surface. The deformation error can be defined as the difference between the measured marker deformation and the deformation of the projected marker. The error is then given by:

$$Error_{i,deformed} = \sqrt{(\Delta x_{i,p} - \Delta x_{i,m})^2 + (\Delta y_{i,p} - \Delta y_{i,m})^2 + (\Delta z_{i,p} - \Delta z_{i,m})^2} \quad (6.2)$$

Where:

$$\Delta x_{i,m} = x'_{i,m} - x_{i,m} \text{ and } \Delta x_{i,p} = x'_{i,p} - x_{i,p} \quad (6.3)$$

$$\Delta y_{i,m} = y'_{i,m} - y_{i,m} \text{ and } \Delta y_{i,p} = y'_{i,p} - y_{i,p} \quad (6.4)$$

$$\Delta z_{i,m} = z'_{i,m} - z_{i,m} \text{ and } \Delta z_{i,p} = z'_{i,p} - z_{i,p} \quad (6.5)$$

Where x_i , y_i and z_i are the x, y, and z coordinates of the i th marker during the unladen test condition and x'_i , y'_i and z'_i are the coordinates of the i th marker during the laden tyre condition.

6.3.2. FE validation results

The results of the validation metric for a vertical stiffness test on a flat surface is shown in Figure 6-22. The figure on the left shows the deviation between the measured and simulated carcass shape after the tyre is inflated to 1Bar. Good correlation is found in the tread region of the tyre. The measured results deviate the most from the simulation results on the tyre sidewall. The deviation can be a result of an incorrect CAD model of the tyre or due to the specific testing conditions. The CAD model was created based on measurements on an uninflated tyre and from

sections that were cut from the test tyre. It is thus difficult to get an exact match on the sidewall shape. Secondly the tests were conducted on a tyre that was mounted horizontally. The observed area during the tests was located on the lower side of the tyre. The sidewall and carcass was thus pulled down due to gravity. This effect was not modelled in the finite element environment. This effect decreases at higher inflation pressures due to an increase in the tyre pre-stiffness.

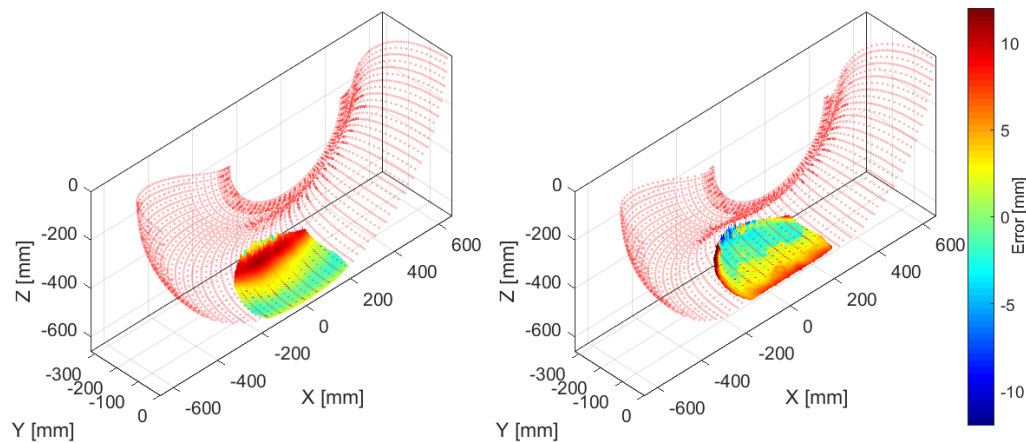


Figure 6-22 Tyre carcass deformation deviation, flat surface, 1Bar. Left: Unladen. Right: Laden

The figure on the right-hand side of Figure 6-22 shows the deviation in the carcass deformation due to the applied load. The figure shows that the finite element model is capable of accurately predicting the tyre deformation. The largest error, of about 7mm, was found in the centre of the tyre tread. Good correlation between the measurements and simulation results were found in the observed sidewall region. To validate the carcass behaviour of the finite element tyre model on an uneven road surface, the carcass deformation of a lateral cleat tests was compared. The tests were conducted at an inflation pressure of 3 Bar and a square cleat with a height and width of 50mm was used. The resulting carcass deformation is shown in Figure 6-23.

The simulated unladen carcass shape again correlates well with the measured results. The error in the tyre sidewall, at an inflation pressure of 3 Bar, is significantly decreased compared to the results of the 1Bar test.

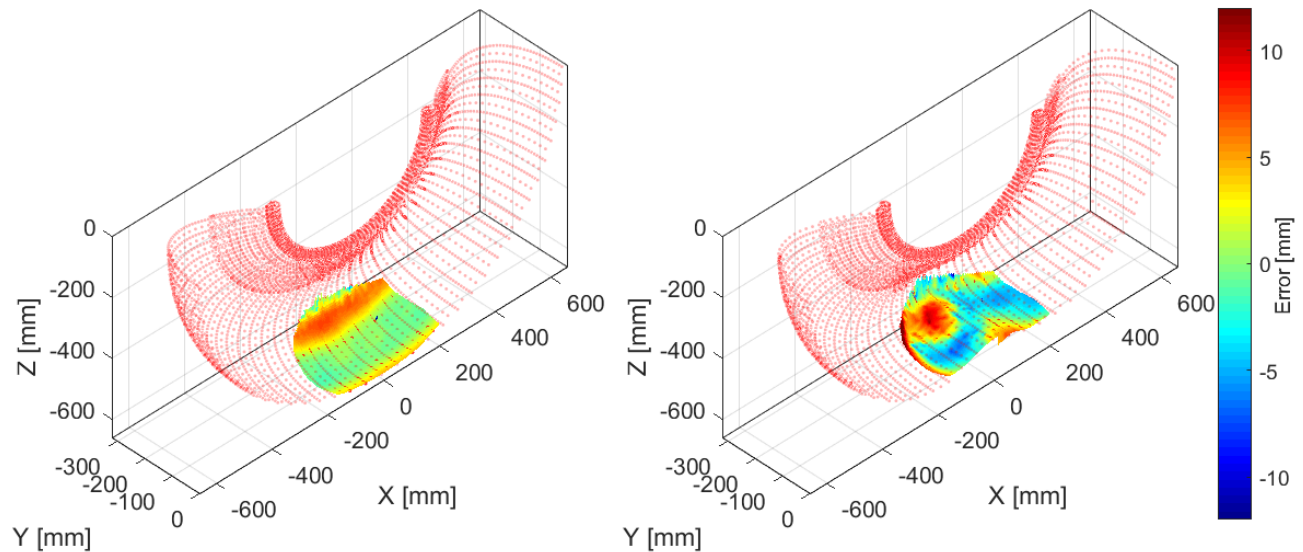


Figure 6-23 Tyre carcass deformation deviation, 50mm lateral cleat, 3Bar. Left: Unladen. Right: Laden

Good correlation is also found between the measured and simulated carcass deformation. The results are shown on the right-hand side of Figure 6-23. The variations in the deformation of the tyre carcass near the tread can be related to the aggressive tread pattern of the test tyre. The orientation of the tyre relative to the cleat influenced the results. The tyre tread orientations during the measurement and during the simulation are shown in Figure 6-24. The figure shows the slight offset that resulted in the different carcass deformation.

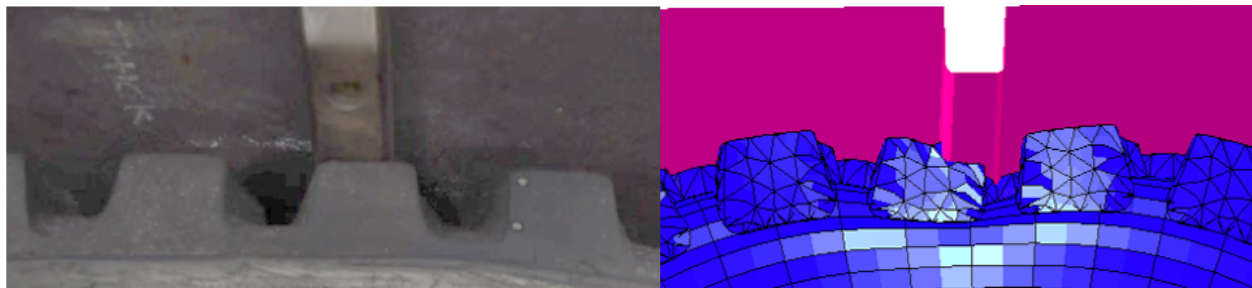


Figure 6-24 Tyre tread orientation. Left: Experiment. Right: Model

6.4. FTire parameterisation using carcass deformation data

Since the 2016-4 release of FTire, FTire/fit can extract model parameters from tyre carcass deformation results. A new data category, FE results, was created for this purpose. The aim of this new development is to identify a wide range of model parameters from a single test and to expand the list of tests that can be used to identify FTire parameters in an automated and

standardized method. This new feature is especially useful if traditional parameterisation data is difficult, or even impossible, to obtain.

The demo finite element results that are used to identify model parameters are vertical stiffness tyre tests on a flat surface. The inflation pressure, as well as vertical deflection, can be varied. Tests at various camber angles can also be used for parameter identification. The results that can be used are carcass node deformation relative to an undeformed, or unladen, tyre carcass. Experimentally obtained carcass deformation results can thus be used to supplement or replace results obtained from a finite element simulation. Currently only a small section of the tyre can be measured experimentally as discussed in section 6.2. It is however possible to capture a larger section of the tyre carcass with the correct cameras and camera lens selection. The data used in this section can thus easily be replaced with experimentally obtain results.

Finite element simulation results will be used in this section as the deformation of the entire tyre carcass can be observed. The simulation results show that the highest node displacements occur near the tyre contact patch. Carcass nodes on the top side of the tyre show little to no movement during the loading of the tyre. The figure furthermore shows that many nodes are used to model the tyre carcass. The model complexity can thus be reduced while still capturing the underlying tyre behaviour. The nodes of the reduced model are shown in Figure 6-25. The nodes that would be used for the parameter identification are shown in blue while and the finite element nodes are shown in red.

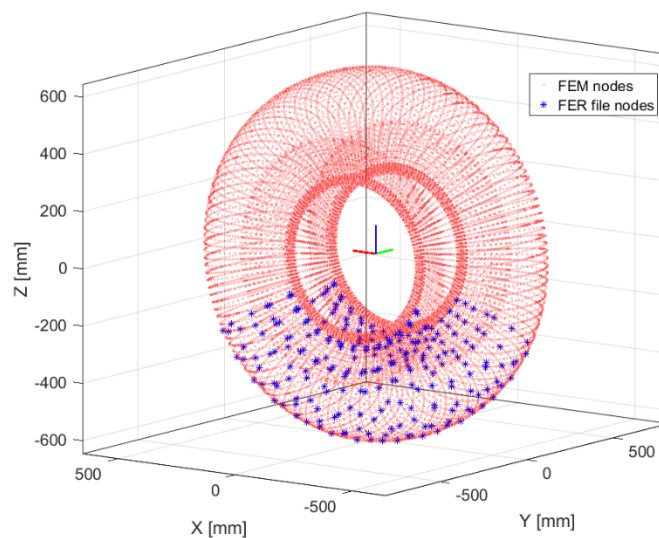


Figure 6-25 Nodes selected for FTire parameterisation file

To use the carcass deformation results a FER file is created. The FER file can be identified by the “.fer” file extension. The file contains the relevant load case information, including the rim position and orientation. The file furthermore specifies the resulting forces and moments that are generated due to the specified tyre deflection. The un-deformed, or unladen, node coordinates of all relevant nodes are also listed. In combination with the unladen node coordinates the node deformation, due to the rim deflection, is also listed in the FER file. The fer file format is shown in Figure 6-26.

```

$load_case
rim_center_position    0.000000    0.000000    288.261424    ! 3x[mm]
rim_orientation        6.000000    0.000000    0.000000    ! 3x[deg]
radial_deflection      29.634620    ! [mm]
inflation_pressure     2.400000    ! [bar]
tread_depth            8.000000    ! [mm]
sticky_surface         0           !

$results|
forces_moments
$    Fx          Fy          Fz          Mx          My          Mz
    0.000003    507.114513    4824.872366    5.273603    0.258465    -0.081389

nodes
$    x          y          z          dx          dy          dz
-164.623910    -75.749459    219.232334    0.000000    0.000000    0.000000
-215.262176    -81.400035    200.529383    0.367621    0.432943    0.857167
-252.628010    -90.827708    188.684723    2.496289    1.391591    4.754701
-294.749352    -67.068630    178.460572    -2.984691    1.908592    5.679510
-301.132167    -13.330234    182.137774    -4.983816    1.992326    5.343517
-301.574372    40.143871    187.850693    -5.426021    1.980817    5.434872
-296.075967    93.353686    195.599331    -4.311306    1.874065    5.953575
-252.739581    110.804683    210.260529    2.384717    -1.091122    4.877146
-215.102161    97.575449    219.461558    0.527636    -0.888013    0.839423
-164.623910    88.446106    236.489984    0.000000    0.000000    0.000000
-141.398406    -71.260472    176.522477    0.000000    0.000000    0.000000
-184.976005    -76.233075    144.746715    0.232265    -0.279920    1.017272
-217.464109    -85.085011    123.764377    1.666691    0.177525    6.023541
-253.986057    -58.765522    103.362978    -3.384197    2.255822

.
.
.

```

Figure 6-26 FTire FER-file format

Simulation results from various finite element simulations were post-processed and converted into FER files. To eliminate the effect that the tread pattern has on the carcass deformation, FE simulations where the tread depth was reduced to the tread base height, were used to create the FER files. The finite element result files were “checked-in” to create a new FTire/fit project. The tyre size and basic data was used to create a tyre model estimate. A detailed spline of the belt and carcass cross-section was used to define the actual shape of the belt and sidewall. The parameter identification tool was used to identify the tyre model parameters. The result, of two of the used tests, are shown in Figure 6-27 and Figure 6-28.

The FTire validation results of the tyre carcass for a vertical stiffness test, on a flat surface, is shown in Figure 6-27. The figure shows the deviation between the predicted FE and FTire model

carcass deformations. The best correlation was found in the tyre belt region. Large deviations can be seen on the tyre sidewall.

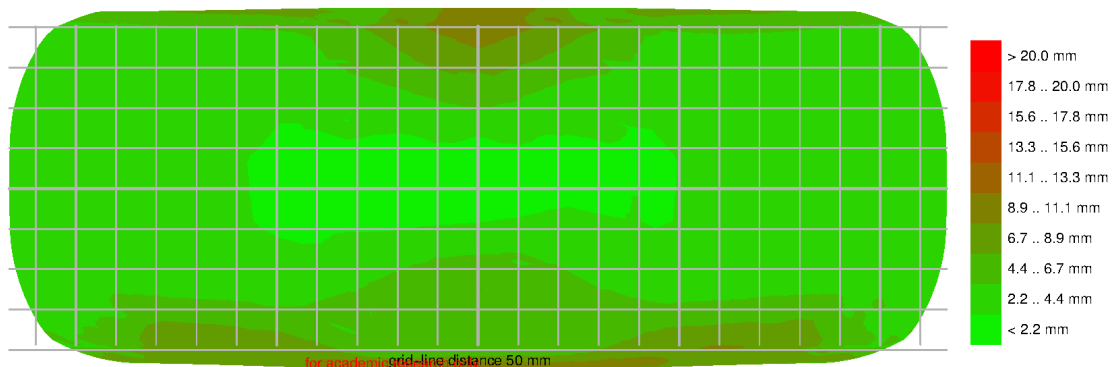


Figure 6-27 FTire FEM validation, flat surface, 3Bar, deflection 50mm

Figure 6-28 shows the deviation between the predicted FE and FTire model carcass deformations of a vertical stiffness test at negative four degrees camber. The correlation between the two models is slightly decreased when compared to the results at zero-degree camber. The largest deviation is again seen in the tyre sidewall.

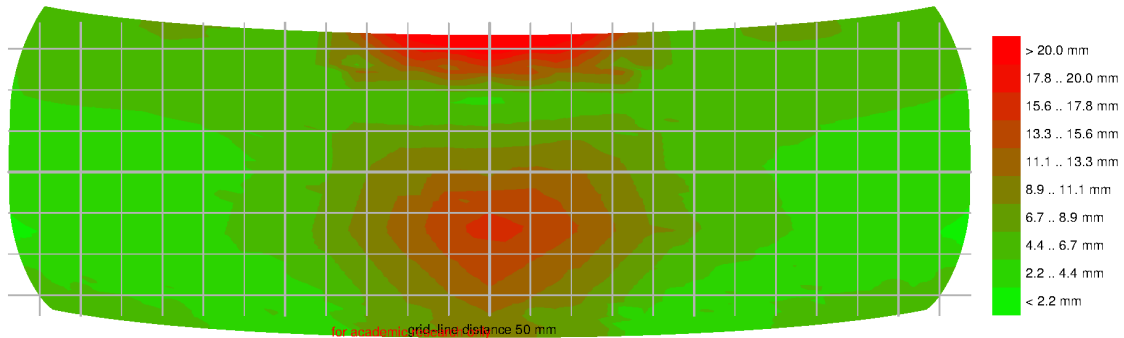


Figure 6-28 FTire FEM validation, flat surface, 1Bar, deflection 50mm camber -6deg

The interpretation the results, as presented in FTire/fit, were rather difficult due to the two-dimensional result presentation. It is furthermore unclear how the deviation, between the FE results and the FTire model prediction, is calculated. It was thus decided to re-run the FTire simulations to generate the output files that describe the distorted carcass and belt geometry of the FTire model. The results were post-processed with the FE validation metric as discussed in 6.3.1. The results of the vertical stiffness test, on a flat surface, is shown in Figure 6-29. The results are comparable to the FTire/fit results that were presented in Figure 6-27. The left-hand side of Figure 6-29 shows that the unladen tyre carcass shape is accurately represented by the

FTire model. This is expected as a detailed belt and carcass cross-section, that was obtained from the CAD model, was used to define the belt and carcass cross-section of the FTire model. The right-hand side of the figure shows the carcass deformation deviation between the two models. The deformation results from the FTire model were obtained from a tyre model where the tread pattern was deactivated. This was done to simplify interpretation of the results as it was difficult to exactly match the tyre orientation. The deviation of the carcass deformation, due to the tread pattern, is clearly visible at the centre of the tyre. Relatively large deviations in the predicted carcass deformation can be seen on the outer edges of the tyre contact patch. Large deviations are also seen in the sidewall deformations.

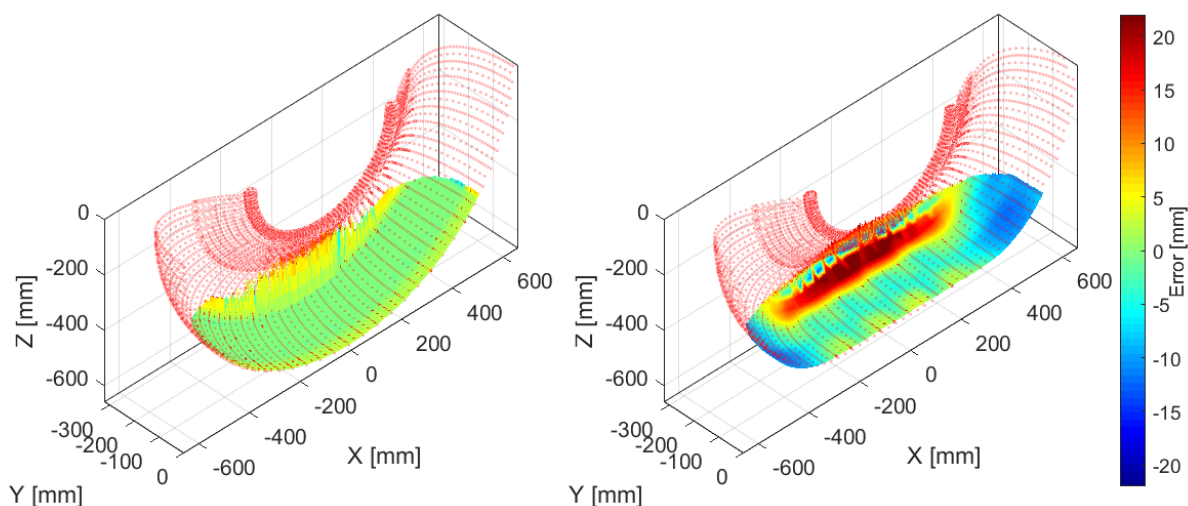


Figure 6-29 Tyre carcass deformation deviation, flat surface, 3Bar. Left: Unladen. Right: Laden

To investigate the reason for the large deviations, the cross section of the tyre carcass is extracted from the simulation results. The tyre carcass cross-sections are presented in Figure 6-30. It is again evident that the unladen tyre carcass shape is accurately matched by both models. Slight variations are seen near the tyre bead. The finite element cross section is obtained from the carcass layer nodes. In the FE model the carcass layer is wrapped around the bead, as shown in Figure 3-3 and Figure 5-14. The spline, defining the FTire carcass, is however defined to begin with the left bead centre.

The laden cross sections of the two tyre models show a different deformation behaviour of the tyre sidewall. The FTire model shows a uniform deformation of the tyre sidewall. The deformation of the finite element tyre model however shows a complex bending behaviour. The sidewall bending behaviour, near the bead, is influenced by the rim boundary conditions, and is thus not

free to bend as is the case in the FTire model. The sidewall thickness, and thus stiffness, is also varying from top to bottom. The sidewall is significantly stiffer on the top of the sidewall compared to the lower section. This behaviour is not modelled in FTire. The correlation of the tyre carcass in the belt region is significantly better. The variation is the largest on the outside of the tread. In this region, the tread is significantly thicker than the tread in the middle of the tyre. It must be investigated if this effect is accurately captured in FTire. It can further be seen that the tread stiffness in the finite element tyre model is slightly stiffer than the tread rubber in FTire. This results in a higher deformation, of the tyre carcass, in the finite element tyre model for the same rim displacement.

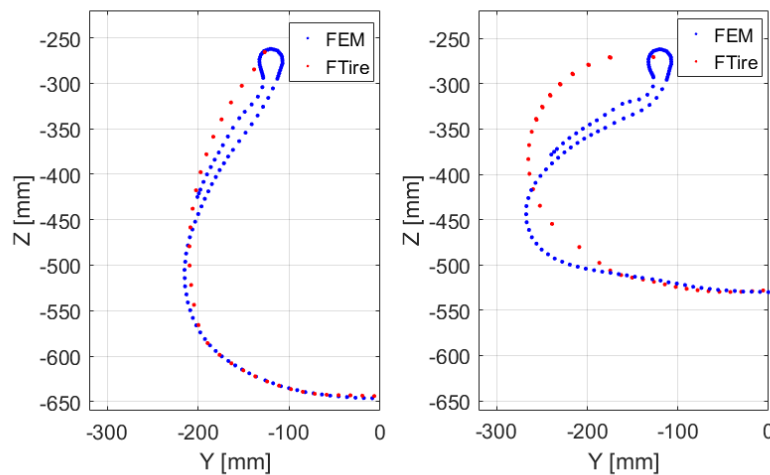


Figure 6-30 Cross-section of the carcass deformation. Left: Unladen. Right: Laden

Currently only FE results on a flat surface are presented, and can thus be used for the automated parameter identification process in FTire/fit. A static simulation can however be conducted to determine the FTire predicted carcass deformation. A 50mm square cleat test, at an inflation pressure of 3Bar, was conducted and the carcass deformation was compared to the simulation results of the finite element model. The results are shown in Figure 6-31. The figure shows that the carcass deformation is higher during the finite element analyses as compared to the FTire simulation.

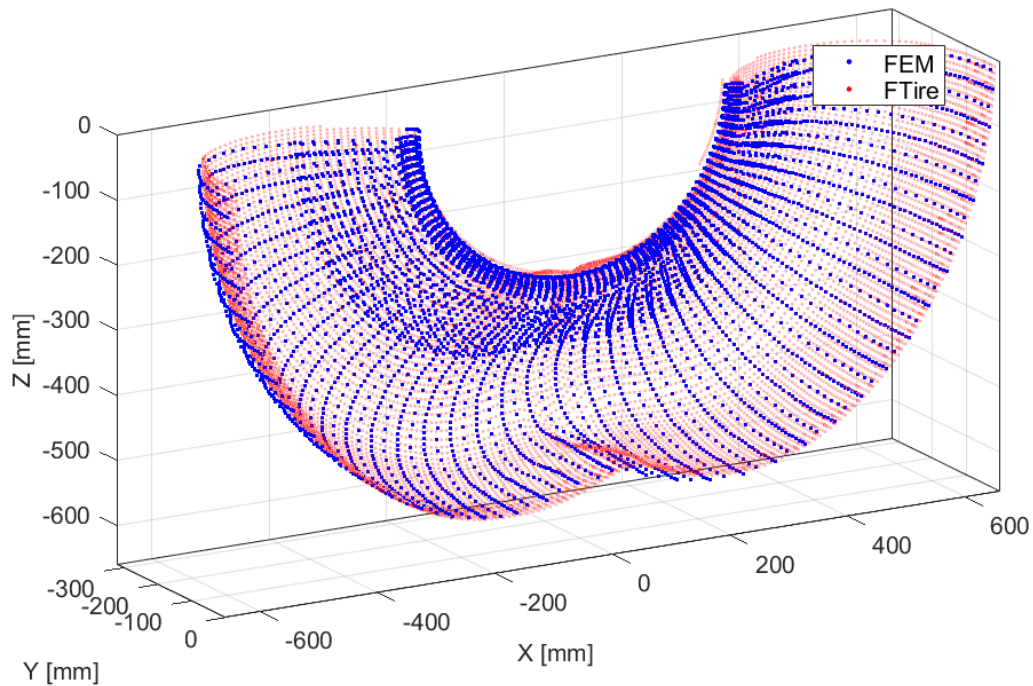


Figure 6-31 Simulated tyre carcass deformation, 50mm lateral cleat, 3Bar.

The results were again post-processed according to the FE validation metric. The post-processed results are presented in Figure 6-32. The results of the laden case again show that the Fire model has a lower degree of deformation, where the tyre contacts the cleat, compared to the finite element model. The sidewall deformation is also different between the two models. The biggest deviation, of the sidewall deformation, is seen in the middle of the tyre close to the tread.

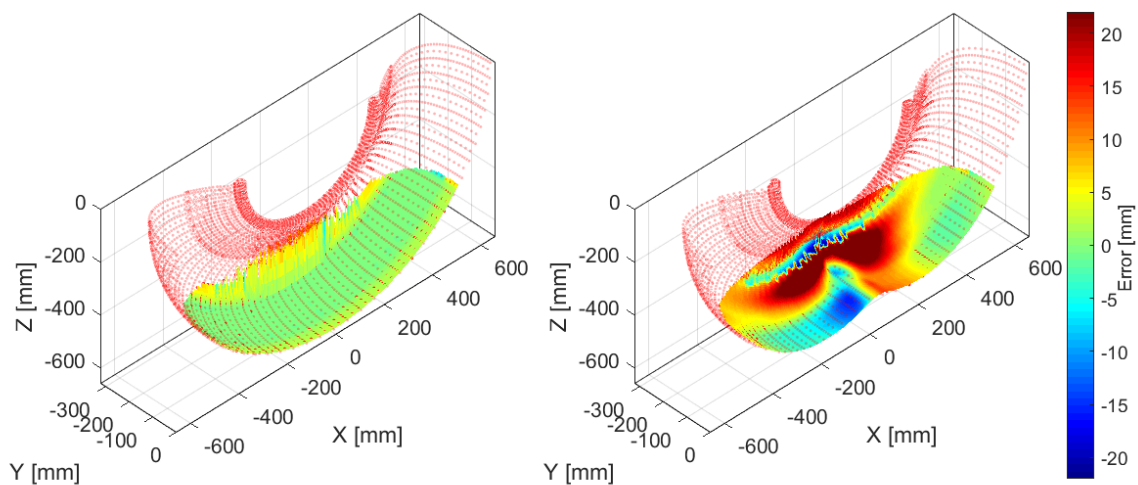


Figure 6-32 Tyre carcass deformation deviation, 50mm lateral cleat, 3Bar. Left: Unladen. Right: Laden

6.5. Chapter Summary

A method of measuring the three-dimensional shape of the tyre carcass was proposed in this chapter. The method is based on the principle of computer stereographic vision, or digital image correlation, technique. This technique extracts three-dimensional information from digital images. In this process, a set of cameras were used to capture images of the tyre from differing viewpoints. By comparing these images, the relative depth information was obtained.

Initial tests were conducted to determine the outer sidewall deformation during a set of vertical stiffness tests. A set of Point Grey, Grasshopper3 9.1 MP, cameras were used for this study. The study revealed that the sidewall deformation could be accurately measured with this technique. An algorithm was developed that could track the measurement markers during the entire test. The accuracy of the algorithm was further improved by incorporating a subpixel edge detection algorithm. The algorithm is based on the on the partial area effect and improved the accuracy at which the centre of the measurement markers could be determined.

A camera setup was constructed that could be mounted on the inside of the Michelin 16.00R20 XZL test tyre. To ensure that the accuracy of the camera setup and the tracking algorithm a validation marker block was created. The validation of the test setup showed that the markers could be tracked with an expected absolute error of less than 0.35mm.

To be able to measure the entire carcass deformation, and not only the sidewall deformation, the camera setup was mounted to the inside of the tyre. Markers were glued to the inside of the tyre and about 830 markers were tracked during the tests. Laboratory tyre tests were conducted at various inflation pressures, camber angles and loading conditions. Various cleat tests were also conducted to investigate the tyre deformation behaviour on uneven terrain. The test results were post-processed and presented in section 6.2. The test results showed that the markers could be tracked with a high precision and resolution.

A method of using the three-dimensional carcass deformation measurements to validate finite element tyre models was also presented. The advantages of using the deformation information, rather than global stiffness data, to validate finite element models was discussed.

A validation metric was proposed that could be used to validate finite element tyre models. The metric calculates the error, between the measured and simulated carcass shape, of the unladen tyre and then the deformation error for the laden case. This was done to distinguish between errors, caused by initial carcass shape variances, from carcass deformation differences due to an

incorrect tyre stiffness representation. Various validation test results were presented and discussed. It was found that the overall correlation between the measured and predicted carcass deformation was very good. Variations could be linked to the test conditions that were not replicated in the simulation environment, such as gravity affects. It was also found the orientation of the test tyre should be accurately matched to the tyre in the simulation environment to reduce the variations due to the local tread behaviour. This problem is only noticeable due to the aggressive tread pattern of the test tyre.

Initial tests where the tyre deformation information is used to parameterise an FTire model was presented. A new feature in FTire/fit can be used to extract tyre model parameters from carcass deformation information. Carcass deformation information, obtained from the finite element tyre model, was used to supplement the simulation results used to parameterise an FTire model. Measured deformation information can also be used with the new feature.

Initial results show that the FTire parameterisation data set can be supplemented with carcass deformation results to extract model parameters. The FTire model failed to replicate the sidewall deformation behaviour as well as the belt deformation on the edges of the tyre. The FTire model is not capable to accurately match the localised geometry and stiffness variations that cause these effects.

Chapter 7

Comparison of parameterisation methods

7. Comparison of parameterisation methods

This chapter will discuss the advantages and shortcomings of the three presented parameterisation techniques for large tyres. The cost of the various methods is discussed briefly as it plays a significant role in the selection of the parameterisation technique. This discussion is based on the experiences that were made with the available test equipment at the University of Pretoria and should be viewed in that context.

7.1. FTire parameterisation using experimentally obtained test data

The first parameterisation method discussed in this thesis was the conventional parameterisation process where an extensive set of experimental test data of a tyre is used to extract the relevant model parameters.

The primary advantages of this method are:

- i. This method is well defined and cosin Scientific Software supplies tools that can be used to identify tyre model parameters from a standard set of test data. These tools simplify the parameterisation process and reduce the parameterisation effort as some processes are automated. The automated processes include the processing of experimentally obtained parameterisation data to be compatible with the model internal data structures. Secondly the tests are assigned to model parameters that are most sensitive to the tests, as well as model specific optimisation algorithms that are used to extract model parameters from the data. These automated processes reduce the parameterisation time and ensures that repeatable results can be obtained.
- ii. cosin Scientific Software specifies a list of recommended tests that should be conducted to parameterise a FTire model. These lists can be used as a reference to determine what data is required to parameterise a model to meet the advertised accuracy standards. The list covers a wide spectrum of the tyre operating conditions that can be tested with commercially available test equipment (at least for passenger car tyres).
- iii. Many tyre testing laboratories have specialised in performing the required parameterisation tests of passenger car and light truck tires. This has led to an increasing number of service providers that are supplying the industry with tyre test data as well as parameterised tyre models. The laboratories are in many cases only limited by the load ratings and permitted tyre size of the available test equipment. Some laboratories, such

as the Vehicle Dynamics Group at the University of Pretoria [VDG Solutions, 2017] have recently developed test equipment to perform tyre model parameterisation tests of large tyres.

- iv. By using experimentally obtained test data to extract the model parameters, the model outputs are simultaneously validated as well. This improves the confidence levels of the model.
- v. Most of the required parameterisation tests can be conducted on a static tyre test rig. These tests are relatively easy to control, fast and inexpensive to conduct, compared to the dynamic tests. This research has shown that a good correlation between the measured and simulated tyre response, while driving over hard uneven terrain, can be obtained if the static parameterisation tests are available.

The primary disadvantages are:

- i. Highly accurate parameterisation data is required. Errors in the measurements are automatically transferred to the model. If inaccurate parameterisation data is used the model would inaccurately predict the tyre behaviour. One of the biggest challenges of using experimentally obtained data is the accurate representation of the test equipment's compliance. Errors could arise from elastic deformations of the test rig due to high test loads. These deformations could result in inaccurate representation of the loading conditions as well as an inaccurate tyre response measurement. There is thus a need to ensure that the test equipment is sufficiently stiff or that the compliance of the test rig is incorporated in the parameterisation process. This is especially a concern for large tyres that operate under high loading conditions.
- ii. A large dataset needs to be available for a successful parameterisation. Due to the complexity of the models many tests need to be conducted to identify all model parameters. It is however not always possible to conduct all the required tests due to limitations of the test equipment. For large off-road tyres these limitations are the operating loads, at which the tyre needs to be tested, and the geometric constraints of the test equipment. If no data can be obtained, the parameters need to be approximated. The complexity of the model however makes this task extremely difficult or even impossible as detailed and fundamental knowledge of the tyre behaviour and experience with the tyre model parameters is required.
- iii. Experimental dynamic parameterisation and validation of large off-road tyre models is challenging. Isolation of the tyre response from the system behaviour is in many cases

difficult or even impossible. During dynamic validation tests the tyre is not connected to an infinitely stiff system with a known dynamic response, but is rather part of a system. It is furthermore difficult to accurately and exactly replicate the measurement conditions in the simulation environment.

- iv. Standardization of the test equipment, for large OTR tyres, is difficult. Due to the wide range of operating conditions, as well as a wide range of tyre and rim sizes that are being used, it makes it difficult to standardize the test equipment. The test equipment is often modified to accommodate these changes.
- v. A standard technique for addressing OTR tyre specific testing and parameterisation issues, such as the influences of an aggressive tread pattern, are not available yet. During the parameterisation, there is currently no documented method to describe the exact tyre orientation to match the measurement condition. The footprint, static cleat and dynamic cleat tests are the most sensitive to this problem and could influence the outcome of the parameterisation significantly.

Cost consideration of the parameterisation method:

- i. The test equipment is often very expensive. Test equipment for large off-road tyres, that can be used to perform tyre model parameterisation tests, is not as readily available commercially as tyre test rigs for passenger car tyres. The test equipment is thus often designed and build to specifications for a specialized laboratory. This increases the cost, complexity and duration of the project.
- ii. Uniquely designed test equipment raises problems to get accurate and repeatable results resulting in tests being repeated until satisfactory results are obtained. Expert knowledge is required to understand the test equipment and test conditions to ensure accurate and repeatable test results are obtained. The operating conditions of OTR tyres however vary greatly and thus making it difficult to transfer knowledge from one test to the next.
- iii. The cost of parameterisation is further increased due to the cost and availability of specialised equipment and their operators, test tracks and the increased wear and tear of the test tracks and test equipment due to the higher tyre operating loads.
- iv. This method is labour intensive and require multiple test engineers at the same time with a wide range of skills. The testing is highly specialised and human resources are difficult to obtain and to replace.
- v. Long periods of preparation and testing, and thus a slow turnaround time further increase the cost.

- vi. Standardization of the test equipment is difficult, and thus increasing the cost. A wide range of tyre and rim sizes require modifications to the test equipment resulting in extra costs.

7.2. FTire parameterisation using FE tyre models

The second parameterisation approach that was investigated was to obtain the required parameterisation data from a finite element model. The primary advantages of this method are:

- i. There are virtually no test rig limitations. No load or geometric limitations apply to the virtual FE test environment.
- ii. Conducting tyre parameterisation simulations is relatively easy, fast and cost effective compared to physical testing. On a standard desktop computer, the simulations can be completed in one to two weeks. The only limitation is the performance of the computer that is used to perform these simulations.
- iii. Simulations can be conducted in parallel, reducing the turnaround time.
- iv. The boundary conditions of the tyre tests can be accurately controlled. The same boundary conditions can also be applied in both simulation environments, FE and FTire, eliminating the unknown effect the boundary conditions have on the tyre response.
- v. The tests can easily be scaled. Tests should be conducted to determine the material properties of the tyre as well as the tyre geometry. These tests are conducted in the same way, and accuracy, regardless of the tyre size and operating conditions.
- vi. Experimental tyre test data at very low inflation pressures, and therefore low reaction forces, can be used to validate the finite element model. If load limitations are present, for the available test equipment, tyre tests at extremely low inflation pressures can be conducted. These results can be used to validate the finite element tyre model. This improves the confidence in the finite element tyre model.
- vii. This investigation has shown that an accurate FTire model can be parameterised from a finite element tyre model that was based on input data that was obtained from a tyre.

The primary disadvantages are:

- i. Expert knowledge, and specialized skills, are required to create and perform the required non-linear FE tyre analysis. A detailed understanding of the capabilities and limitations of the FE tyre model are key to ensure accurate results are obtained.

- ii. A highly accurate finite element tyre model is required. The finite element tyre model must be created in such a way that the user confidence in the model is high. This is especially true if no, or very limited, data is available that can be used to validate the finite element tyre model.
- iii. Accurate damping and friction behaviour of the tyre is difficult to predict. Predicting the overall tyre damping and friction behaviour from material tests is challenging. Research is conducted in this field to improve the accuracy of the material models in this regard. It should further be noted that the friction coefficient is in many cases different to the conditions found during the parameterisation tests. A relationship between friction coefficient used during the finite element simulations and the real road needs to be determined to scale the parameters accordingly. Nonetheless – good results were achieved with first order estimates.
- iv. Accurate material and geometry data is required. Obtaining accurate material properties of all the materials used in the tyre construction can be cumbersome and requires the destruction of a tyre. The biggest challenge is to isolate the materials and to obtain enough high-quality samples for material testing. Obtaining the FE tyre model input data requires hard manual labour and can be very challenging to extract useable tyre samples.
- v. Tyre model validation is a challenge. As no, or only limited, test data is available at the normal operating conditions of the tyre the model validation might be difficult.

Cost consideration of the parameterisation method:

- i. Inexpensive test equipment is required. Material test equipment and geometric measurement devices are commercially available.
- ii. Highly accurate geometric and material properties can be obtained from external testing laboratories. Materials, like the materials used in the construction of tyres, are tested for a wide range of application and industries increasing availability of the testing laboratories and thus decreasing the cost.
- iii. Inexpensive to conduct material tests. A single test rig is required to conduct material property tests. Test engineers that can perform material tests are readily available.
- iv. Additional and expensive software licenses are required of a non-linear FE package.
- v. Requires highly skilled engineers to perform the non-linear FE analysis that is required, and to ensure that the results are meaningful.
- vi. Fast output, as finite element simulations can be executed in parallel on multiple machines. The process can also be automated to limit human intervention.

- vii. The cost of the tyre may significantly increase the cost of the parameterisation as a tyre needs to be destroyed to obtain the required FE input data.
- viii. Testing effort and cost is largely independent on the tyre, or rim, size and operating load conditions.

7.3. FTire parameterisation using carcass deformation information

A preliminary investigation was conducted to identify tyre model parameters for tyre carcass deformation results. Both physical tyre tests and finite element simulation results were used for this method.

The primary advantages of this method are:

- i. A large amount information is available in a single test. Fewer tests are thus be necessary to conduct, as more parameters can be identified from a single measurement.
- ii. Test method is largely independent on the tyre size. The cameras that are being used are relatively small and a wide range of camera lenses are available to cover a wide range, if not all, of the available OTR tyre sizes.
- iii. Highly accurate deformation results can be obtained ensuring that the parameterisation data is of a high quality.
- iv. The data is simultaneously used to validate the parameterised tyre model to improve the confidence in the model.
- v. In-situ testing is possible. Since the only modifications are made to the inside of the tyre, the rim can still be mounted to the test vehicle.
- vi. Carcass deformation method is suitable for experimentally obtained carcass deformation data as well as data obtained from an FE tyre model.

The primary disadvantages are:

- i. Difficult to modify the rim to accommodate the test equipment on the inside of the tyre.
- ii. The mounting and assembly is challenging to ensure that the delicate test equipment is not damaged or that the camera calibration is not lost.
- iii. Relatively new approach with only limited information available to compare and improve test methods.
- iv. Undocumented and limited test case support is currently available to use the data to parameterise FTire.

- v. The applied load, or tyre reaction forces and moments, still need to be measured. This limits the application of this method. The use of WFT or weight bridges, if tested on the vehicle, is required.
- vi. Only static tests can currently be conducted and used to extract model parameters, thus limiting the application range.
- vii. More research required to identify model parameters that influence the carcass deformation of the current test.

Cost consideration of the parameterisation method:

- i. Test equipment is inexpensive, to moderately expensive. The cost of the cameras is relatively low.
- ii. Expensive to conduct tests, limited but specialized test equipment required. The test equipment is thus often designed and build to specifications for a specialized laboratory. This increases the cost, complexity and duration of the project.
- iii. Test must be conducted on site and in-situ to avoid the need of the specialized tyre test equipment, such as a static or trailer tyre test rig. In-situ testing raises problems to get accurate and repeatable results, resulting in tests being repeated until satisfactory results are obtained. Expert knowledge is required to understand the test equipment and test conditions to ensure accurate and repeatable test results are obtained
- iv. On-site testing might be logistically difficult and dependent on the client, making it difficult to standardize the testing procedure.
- v. Limited but highly specialized test personnel is required. A wide range of skills are required to perform these tests.
- vi. Long period of testing and slow output as the test rim needs to be modified and on-site testing needs to be organized.

Chapter 8

Conclusions and Recommendations

8. Conclusions and Recommendations

This chapter presents the conclusions and recommendations that can be drawn from the work that was discussed in this thesis. The aim of this thesis was to investigate various methods that can be used to parameterise a FTire model of a large OTR tyre. The focus of this thesis was to investigate methods that can be used to parameterise a FTire model that can accurately predict the tyre forces and moments that are generated in the tyre contact patch during simulations on uneven terrain.

8.1. Conclusions

A literature review on tyre models and their applications in the vehicle research and development environment was presented in Chapter 2. The review discussed various tyre models that can be used to simulate the tyre behaviour while driving on uneven terrain. The parameterisation approaches of the respective tyre models were also discussed. It was found that the parameterisation methods are predominantly based on extracting model parameters from experimentally obtained test data that is representative of the operating conditions of the tyre. The chapter further highlights the importance of a physical modelling approach to ensure physical meaningful results are obtained, especially if insufficient tyre parameterisation data is available to extract all model parameters. This is often the case for large OTR tyres due to the limitations of available test equipment. The importance and challenges to obtain accurate validation test results were also discussed. Without accurate measurements, of which the test conditions are known, it is very difficult to validate the models. This affects the confidence in the model and thus also the application of the model.

In chapter 3 the established FTire parameterisation method was presented and discussed. The test setup and the experimentally obtained test results were presented. The parameterisation process, using the experimental data set, was discussed. The established process was modified to accommodate data from large OTR tyres. The obtained FTire model was validated against experimental results. The validation process showed that the parameterised model can be used to accurately predict the tyre forces and moments while driving over uneven terrain. This method can thus successfully be used if the tyre forces and moments, and the applied boundary, as well as environmental conditions, can accurately be measured. The limitations of this method however was that the high loads, at which these OTR tyres operate, and the size of the tyres make it difficult to obtain the required parameterisation and validation test data. Test rigs to conduct the required tests are not commercially available and probably will not be available soon. Specifically

designed, and constructed, tests rigs are currently the only alternative to obtain any parameterisation test data.

One alternative, to the use experimentally obtained data for the parameterisation process, is to use finite element models to obtain the relevant parameterisation data. Geometric and material properties tests were conducted and the results were presented. A nonlinear finite element model was created and validated against experimental results that were discussed in Chapter 4. The finite element tyre model could accurately represent the tyre behaviour for all static test conditions. This was achieved without the need to modify, or tune, the FE model or model properties. It is thus possible to create an accurate FE tyre model that is based entirely on geometric and material test results. This is especially useful if no, or only limited, test results are available of the test tyre. The finite element tyre model was used to replicate the parameterisation tests that were required to parameterise a FTire model. Only static tests were used, to parameterise the FTire model, due to the limitation of the chosen FE material models that were used to model the rubber and steel cords of the tyre. An engineering guess was used to define the damping parameters of the FTire model. The validation of the model however showed that although no dynamic test results were used to parameterise the FTire model, an accurate model was obtained that could predict the tyre forces while driving over uneven terrain. This FE method can thus be used to parameterise large OTR FTire models for simulations over uneven terrain if no, or limited test data can be obtained.

Another method that was investigated was the use of carcass deformation results to parameterise FTire models. The carcass deformation data can be obtained from experimental testing or from FE simulation results. To obtain the measured carcass deformation data, a set of cameras were mounted to the inside of the test tyre. The cameras, and their lenses, were calibrated and the relative position and orientation of the two cameras were obtained. The stereo vision principle was applied to obtain the three-dimensional position of features in the images. For this investigation 830 markers were glued to the inner liner of the test tyre. The carcass deformation was recorded for various static tyre tests. Tests were conducted on a flat surface and on various cleats, as well as at various camber angles. The obtained results were compared to the simulation results of the finite element model, to validate the FE tyre model. The results show that the carcass deformation measurements correlated well to the simulated results. These tests can thus also be used to validate FE tyre models if force-displacement measurements are non-existent. Initial results of using the carcass deformation data to parameterise a FTire model are also presented. Only static tests on smooth road surfaces, at various camber angles, is currently documented by the FTire/fit software. Comparable FTire results could be obtained with the use of this method.

The carcass deformation results from cleat tests were compared to FTire simulation results. Overall good correlation was found. The orientation of the tyre, due to the aggressive tread pattern, influenced the results and should be taken into consideration. Furthermore, the deformation of the sidewall, in the FTire model is not accurately captured. This is due to the modelling approach, of FTire, that disregards the varying sidewall stiffness as well as the modelling approach of the contact between the rim and the tyre. The belt, and tread, region is however accurately represented in the FTire model. This is the most important section of the tyre, as it defines how the forces and moments are generated in the tyre contact patch.

A discussion about the advantages and disadvantages, as well as some cost considerations, was also presented. All methods have some important advantages but also disadvantages that should be considered. The cost of parameterisation was also an important factor that needs to be considered. The parameterisation method that was based on using experimentally obtained test results delivers accurate and repeatable results. The parameterisation process was also supported by the FTire/fit software, which decreases the parameterisation effort. Obtaining the required parameterisation data is however often difficult as only limited test equipment is available. The large variety of OTR tyres, including operating load and tyre size, also makes it difficult to have standardized test equipment, which further increases the effort to conduct the relevant tests. These factors also increase the cost of parameterisation. The main advantage of this method is that the model is validated against measurements that represent the operating conditions of the tyre.. This research has show that this method is still the preferred method of parameterising a FTire model. Measurements that are obtained form well controlled, and well understood, testing conditions are used for both parameterisation and validation. This is the closest researchers can get to the actual tyre behaviour, as it includes material and manufacturing inconsistencies that could influence the tyre behaviour. This increases the level of confidence that the user has in the model to accurately predict the tire behaviour in the simulation environment.

The FE parameterisation approach is largely independent of the size and operating load conditions of the OTR tyres. Geometric properties and material properties can be determined relatively easily, and the method is not dependent on the size of the tyre. This study found that an accurate FE model, that can predict the tyre forces and moments on a non-rolling tyre, can be created without the need of any model tuning. These factors reduce the cost of parameterisation. The research conducted shows that an accurate FE tyre model can be used to parameterise FTire model of a large OTR tyres if no, or limited, parameterisation measurements are available. The presented results show that this method is an alternative option to parameterise FTire models of

large OTR tires that are operating at low to medium speeds. This method is especially interesting if validated FE tyre models, or results, are available or can easily be obtained. This approach is thus applicable for both research and industrial applications.

Using carcass deformation results, to parameterise FTire was also shown to be possible. The method needs to be expanded to include a larger variety of test conditions. The carcass deformation can be measured accurately and is largely independent on the tyre size and the operating loads of the tyre. This approach shows great potential to be used, or to supplement other measurements, to parameterise FTire. More research is however required to make this a viable parameterisation method for research and industrial applications.

8.2. Recommendations on future research

Future research should be conducted to expand and improve these alternative parameterisation methods.

For the measurement based parameterisation approach, more research should be conducted to:

- i. Extend the parameterisation tests on a non-rolling tyre. Investigate if other static tests can be developed and conducted to extract more tyre model parameters. This research has shown that if the static tests are exclusively used to parameterise an FTire model and engineering guesses are made for the friction and damping parameters a good first order model can be created that is useful in the development of large OTR vehicles.
- ii. Investigate methods to accurately measure the boundary conditions that are applied during the tests. If these conditions are known they can be used to replicate the conditions during the FTire parameterisation process. This would improve the accuracy of the model.
- iii. Investigate the use of in-situ tyre testing to reduce the limitation of existing dynamic test equipment. The availability of wheel force transducers to measure the tyre forces and moments, as well as sensors to determine the operating conditions during the tests, might be the breakthrough required to complete the FTire parameterisation.

For the finite element parameterisation approach the following should be considered:

- i. Including damping and hysteresis in material models.
- ii. Investigating the friction behaviour and how it can be incorporated into the FE model.

- iii. Investigate the localized material operating conditions of the tyre rubber and reinforcing cords. Investigate the possibility of using rubber hardness measurements, ShoreA, to parameterise the rubber material models.
- iv. Further investigate the possibility to conduct validation tests at lower inflation pressures. If validation test can be conducted at very low inflation pressures, up to the point where the tyre is not inflated, smaller and more sensitive test equipment can be used to obtain experimental results. If this would be possible it would increase the range of tyres that can be tested. This would make it possible to parameterise a wider range of OTR tyres as well as decreasing the cost.

For the carcass deformation approach, more research should be conducted to:

- i. Include carcass deformation measurements on the rolling tyre.
- ii. Investigate the use of better suited cameras and camera lenses to improve the measurement accuracy and to increase the measurement area.
- iii. Investigate the use of multiple cameras to capture the entire tyre carcass deformation during tyre tests.
- iv. Expand the list of tests that can be used to extract FTire model parameters
- v. Investigate model parameter sensitivities to certain deformation test cases. This would improve the model accuracy and decrease parameterisation time.

9. Bibliography

Antoine, R.C., Schmeitz, J.C., Jansen, S.T.H., Verhoeff, L. and Besselink, I.J.M., 2005, MF-Swift simulation study using benchmark data. *Vehicle System Dynamics*, 43:92–101.

Abbey, T., 2014, *Structural FEA in the Automotive Industry*.
<http://www.digitaleng.news/de/structural-fea-in-the-automotive-industry/> [Accessed 23 July 2016].

Ali, A., Fouladi, M.H. and Sahari, B., 2010. A review of constitutive models for rubber-like materials. *American Journal of Engineering and Applied Sciences*, 3(1), pp.232-239.

ASTM D2240-15e1, Standard Test Method for Rubber Property—Durometer Hardness, ASTM International, West Conshohocken, PA, 2015, www.astm.org

Babulal, Y., Stallmann, M.J. and Els, P.S., 2015. Parameterisation and modelling of large off-road tyres for on-road handling analyses. *Journal of Terramechanics*, 61, pp.77-85.

Balaramakrishna, N. and Kumar, R.K., 2009. A study on the estimation of SWIFT model parameters by finite element analysis. *Proceedings of the Institution of Mechanical Engineers, Part D: Journal of Automobile Engineering*, 223(10), pp.1283-1300.

Barbani, D., Pierini, M. and Baldanzini, N., 2012. FE modelling of a motorcycle tyre for full-scale crash simulations. *International Journal of Crashworthiness*, 17(3), pp.309-318.

Becker, C.M. and Els, P.S., 2014. Profiling of rough terrain. *International Journal of Vehicle Design*, 64(2-4), pp.240-261.

Becker, C.M., 2008, *Profiling of rough terrain*, Unpublished Master's Thesis, University of Pretoria, Pretoria, South Africa.

Behroozi, M., Olatunbosun, O.A. and Ding, W., 2012. Finite element analysis of aircraft tyre—Effect of model complexity on tyre performance characteristics. *Materials & Design*, 35, pp.810-819.

Benz, R., 2008. *Fahrzeugsimulation zur Zuverlässigkeitsabsicherung von karosseriefesten Kfz-Komponenten*. Univ.-Verlag Karlsruhe.

Benzley, S.E., Perry, E., Merkley, K., Clark, B. and Sjaardama, G., 1995, October. A comparison of all hexagonal and all tetrahedral finite element meshes for elastic and elastoplastic analysis. In *Proceedings, 4th International Meshing Roundtable* (Vol. 17, pp. 179-191). Sandia National Laboratories Albuquerque, NM.

Botha, T.R., 2015. *Digital image correlation: applications in vehicle dynamics* (Doctoral dissertation, University of Pretoria, Pretoria).

Botha, T.R., Els, P.S., Becker, C.M. 2012. Measuring Tyre Contact Patch Deformation Using Stereography. *12th European Regional Conference of the International Society for Terrain-Vehicle Systems – September 24-27, 2012, Pretoria, South Africa*

Bower, A.F., n.d., *Applied Mechanics of Solids*, from http://solidmechanics.org/text/Chapter3_5/Chapter3_5.htm [Accessed 13 August 2016].

Bussler, M.L. and Ramesh, A., 1993. The eight-node hexahedral element in FEA of part designs. *Foundry management & technology*, 121(11), pp.26-28.

Cao, D., Song, X. and Ahmadian, M., 2011. Editors' perspectives: road vehicle suspension design, dynamics, and control. *Vehicle system dynamics*, 49(1-2), pp.3-28.

CDTire. 2017. *CDTire – Scalable tire model for full vehicle simulations*. [online] Available at: <https://www.itwm.fraunhofer.de/en/departments/mdf/services-and-products/cdtire.html> [Accessed 31 Jan. 2017].

CDTire/3D. 2014a. 2014 ed. [pdf] *Fraunhofer Institute for Industrial Mathematics ITWM*. Available at: <https://www.itwm.fraunhofer.de/en/departments/mdf/services-and-products/cdtire/cdtire-pdf-download.html> [Accessed 31 Jan. 2017].

CDTire. 2014b. CDTire/PI [pdf] *Fraunhofer Institute for Industrial Mathematics ITWM*. Available at: <https://www.itwm.fraunhofer.de/en/departments/mdf/services-and-products/cdtire/cdtire-pdf-download.html> [Accessed 31 Jan. 2017].

Cifuentes, A.O., and Kalbag, A., 1992, A performance study of tetrahedral and hexahedral elements in 3-D finite element structural analysis. *Finite Elements in Analysis and Design*, 12 (1992) 313-318.

Conradie, J.M., Els, P.S. and Heyns, P.S., 2015. Finite element modelling of off-road tyres for radial tyre model parameterisation. *Proceedings of the Institution of Mechanical Engineers, Part D: Journal of Automobile Engineering*

cosin scientific software. 2017a, *FTire/calc, FE-Based FTire Parameter Calculation* [pdf]. 2017-1-r14630. [pdf]. Software documentation and user guide.

cosin scientific software. 2017b, *The FTire Tire Model Family*. 2017-1-r14630. [pdf]. Software documentation and user guide.

cosin scientific software, 2017c, *FTire Parameterisation*. 2017-1-r14630. [pdf]. Software documentation and user guide.

cosin scientific software, 2017d, *FTire/fit, Measurement-Based FTire parameterization*. 2017-1-r14630. [pdf]. Software documentation and user guide.

cosin scientific software, 2017e, *FTire, Modelization and Parameter Specification*. 2017-1-r14630. [pdf]. Software documentation and user guide.

Daimler, 2015. *Patent certificate, DRP 37435 from 1886*. [online] Available at: <http://media.daimler.com/marsMediaSite/en/instance/picture/Benz-Patent-Motorwagen-Modell-1-Patentschrift-Nr-37435.xhtml?oid=7547881> [Accessed 19/11/2016].

Eckermann, E., 2001. *World history of the automobile*. Training, 2011, pp.04-20.

Einsle, S., 2010. *Analyse und Modellierung des Reifenübertragungsverhaltens bei transienten und extremen Fahrmanövern*. http://www.qucosa.de/fileadmin/data/qucosa/documents/6515/Einsle2010_Dissertation_Reifen%C3%BCbertragungsverhalten_bei_transienten_und_extremen_Fahrman%C3%B6vern.pdf [Accessed 19/11/2016].

Els, P.S., Stallmann, M.J., Botha, T.R., Guthrie, A.G., Wright, K.R.S., Augsburg, K., Höpping, K., Bernius, V., Sandu, C. and Jimenez, E., 2016, August. Comparison of Tire Footprint Measurement Techniques. *ASME 2016 International Design Engineering Technical Conferences and Computers and Information in Engineering Conference* (pp. V003T01A027-V003T01A027). American Society of Mechanical Engineers.

Els, P.S., Theron, N.J., Uys, P.E. and Thoresson, M.J., 2007. The ride comfort vs. handling compromise for off-road vehicles. *Journal of Terramechanics*, 44(4), pp.303-317.

Fervers, C.W., 2004. Improved FEM simulation model for tire–soil interaction. *Journal of Terramechanics*, 41(2), pp.87-100.

Fiala. E., 1954. Seitenkraefte am Rollenden Luftreifen, VDI Zeitschrift, vol.96, 1954

fka. 2017. 'tyres in motion '. [online]. Available at: <http://www.fka.de/produktloesungen/tyres-in-motion.php> [Accessed 31 January. 2017].

Ghosh, P., Saha, A., and Mukhopadhyay, R., 2003. Prediction of tyre Rolling Resistance Using FEA. *Constitutive Models for Rubber III*, Busfield, J. (Ed.). AA Balkema Publishers, UK.,

Gerotek Test Facilities. 2017. *Gerotek Test Facilities* Available at: <https://www.gerotek.co.za> [Accessed 31 January. 2017].

Gipser, M., 1999, FTire a New Fast Tyre Model for Ride Comfort Simulations, *1999 International and 14th European ADAS User Conference*.

Gipser, M., 2002, ADAMS/FTire – A Tyre Model for Ride & Durability Simulations, *Proc. ADAMS User's Conf., Tokyo*.

Gipser, M., 2016. FTire and puzzling tyre physics: teacher, not student. *Vehicle System Dynamics* 54.4 (2016): 448-462.

Grimson, W.E.L., 1981. A computer implementation of a theory of human stereo vision. *Philosophical Transactions of the Royal Society of London B: Biological Sciences*, 292(1058), pp.217-253.

Grob, M., Blanco-Hague, O. and Spetler, F., 2015, April. Tametire's testing procedure outside Michelin. *International Tyre Colloquium*, 4th, 2015, Guildford, United Kingdom.

Guo, H. (2014) An investigation into the finite element modelling of an aircraft tyre and wheel assembly. Unpublished PhD Thesis. Coventry: Coventry University.

Guthrie, A.G., Botha, T.R. and Els, P.S., 2017. 3D contact patch measurement inside rolling tyres. *Journal of Terramechanics*, 69, pp.13-21.

Hennessy, J.L., and Patterson, D.A., 2011. Computer architecture: a quantitative approach. Elsevier.

Hoever, C., 2014, *The simulation of car and truck tyre vibrations, rolling resistance and rolling noise*. PhD thesis, Chalmers University of Technology, Göteborg, Sweden

Hohenheimer Reifenmodell, 2017. *Test stands*. [online] Reifenmodell.uni-hohenheim.de. Available at: <https://reifenmodell.uni-hohenheim.de/en/test-stands> [Accessed 31 Jan. 2017].

Hölscher, H., Tewes, M., Botkin, N., Löhndorf, M., Hoffmann, K. and Quandt, E., 2004. Modeling of pneumatic tires by a finite element model for the development a tire friction remote sensor [J]. *Computer and Structures*, 28, pp.1-17.

IPG-Automotive. 2017. TameTire 3.0 powered by Michelin. 1st ed. [ebook] Karlsruhe:. Available at: <https://ipg-automotive.com/pressmedia/media-library/media-download/23/> [Accessed 31 Jan. 2017].

International Organisation for Standardisation ,1995, ISO 8608: Mechanical Vibration – Road Surface Profiles – Reporting of Measured Data, *International Standard*.

Jeong, K.M., 2016. Prediction of Burst Pressure of a Radial Truck Tire Using Finite Element Analysis. *World Journal of Engineering and Technology*, 4(02), p.228.

Jeong, K.M., Kim, K.W., Beom, H.G. and Park, J.U., 2007. Finite Element Analysis of Nonuniformity of Tires with Imperfections 5. *Tire Science and Technology*, 35(3), pp.226-238.

Kabe, K. and Koishi, M., 2000. Tire cornering simulation using finite element analysis. *Journal of Applied Polymer Science*, 78(8), pp.1566-1572.

Koishi, M., Kabe, K. and Shiratori, M., 1998. Tire cornering simulation using an explicit finite element analysis code. *Tire Science and Technology*, 26(2), pp.109-119.

Korunović, N., Trajanović, M., Stojković, M., Mišić, D. and Milovanović, J., 2011. Finite element analysis of a tyre steady rolling on the drum and comparison with experiment. *Strojniški vestnik- Journal of Mechanical Engineering*, 57(12), pp.888-897.

Lugner, P., Pacejka, H. and Plöchl, M., 2005. Recent advances in tyre models and testing procedures. *Vehicle System Dynamics*, 43(6-7), pp.413-426.

Magori, V., Magori, V.R. and Seitz, N., 1998. On-line determination of tyre deformation, a novel sensor principle. In *Ultrasonics Symposium, 1998. Proceedings., 1998 IEEE* (Vol. 1, pp. 485-488). IEEE.

Michelin engineering and services. (2017). *Tire Test and Measurement*. [online] Available at: <http://www.michelin-engineering-and-services.com/eng/Test-and-Measurement/Tire> [Accessed 31 Jan. 2017].

Michelin, n.d., Michelin Americas Truck Tires XZL, from <http://www.michelintruck.com/michelintruck/tires-retreads/tireInfo.do?tread=XZL> [Accessed 13 August 2013].

Miller, K., 2000. Testing elastomers for hyperplastic material models in finite element analysis. *Axel Products Testing and Analysis Report*.

Mohsenimanesh, A., Ward, S.M. and Gilchrist, M.D., 2009. Stress analysis of a multi-laminated tractor tyre using non-linear 3D finite element analysis. *Materials & Design*, 30(4), pp.1124-1132.

Moser, R.A., Sube, H.J., Turner, J.L. and Zakelj, P., 2010. 3D Digital Imaging Correlation: Applications to Tire Testing. *Tire Science and Technology*, 38(2), pp.100-118.

MSC Software Corporation, 2016, Nonlinear finite element analysis of elastomers, viewed 23 May 2016, http://www.mscsoftware.com/assets/103_elast_paper.pdf

MSC Software, 2015, *DOC 10023- Help Document for Adams/Tire*, from <http://simcompanion.mscsoftware.com/infocenter> [Accessed 2 July 2015].

Mullineux, N., 2011, History of the Tire-World Tire Industry Report, viewed 10 August 2013, from <http://www.worldtirereport.com/Contents/SectionOneIntroduction/TireHistory>

Nakajima, Y. 2011, *Application of Computational Mechanics to Tyre Design -Yesterday, Today, and Tomorrow*, *Tire Science and Technology*, TSTCA, Vol. 39, No. 4.

Oertel, C. and Fandre, A., 1999. Ride comfort simulations and steps towards life time calculations: RMOD-K tyre model and ADAMS. <https://opus4.kobv.de/opus4-fhbrb/frontdoor/index/index/docId/606> [Accessed 31 Jan. 2017].

Olatunbosun, O.A. and Bolarinwa, O., 2004. *FE simulation of the effect of tire design parameters on lateral forces and moments*. *Tire Science and Technology*, 32(3), pp.146-163.

OpenCRG, 2011., User Manual, Available at: <http://www.vires.com/opencrg/docs/OpenCRGUserManual.pdf> [Accessed 31 Jan. 2016]

Pacejka, H., 2005. *Tire and vehicle dynamics*. Elsevier.

Pacejka, H.B., Bakker, E., and Lidner, L., 1987, *Tyre modelling for use in vehicle dynamics studies*, SAE paper 870421.

Pacejka, H.B., and Sharp, R.S., 1991, *Shear force development by pneumatic tyres in steady state conditions: A review of modelling aspects.*, *Vehicle System Dynamics* 20. pp121-176.

Pearson, M., Blanco-Hague, O. and Pawlowski, R., 2016. TameTire: Introduction to the Model. *Tire Science And Technology*, 44(2), pp.102-119.

Point Grey, 2016a, Point Grey Grasshopper 3 9.1MP. Available at: <http://www.ptgrey.com/grasshopper3-91-mp-color-usb3-vision-sony-icx814-camera> [Accessed 10 Sep. 2016]

Point Grey, 2016b, Point Grey Flea 3 1.3MP. Available at: <https://www.ptgrey.com/flea3-13-mp-mono-usb3-vision-e2v-ev76c560-camera> [Accessed 10 Sep. 2016]

Qi, H.J., Joyce, K. and Boyce, M.C., 2003. Durometer hardness and the stress-strain behavior of elastomeric materials. *Rubber chemistry and technology*, 76(2), pp.419-435.

Qian, N., 1997. Binocular disparity and the perception of depth. *Neuron*, 18(3), pp.359-368.

Rill, G., 2006, *Vehicle Dynamics*, Lecture notes, Fachhochschule Regensburg, viewed 10 August 2013, from <https://hps.hs-regensburg.de/~rig39165/>.

Rill, G., 2013, TMeasy—A Handling Tire Model based on a three-dimensional slip approach. *Proceedings of the XXIII International Symposium on Dynamic of Vehicles on Roads and on Tracks (IAVSD 2013)*. Qingdao, China.

Rill, G., 2015, April. *An engineer's guess on tyre model parameter made possible with TMeasy*. In *International Tyre Colloquium*, 4th, 2015, Guildford, United Kingdom.

RMOD-K, 2017a. Flexible Belt (FB). [online] RMOD-K. Available at: <http://www.rmodk.com/flexible-belt-fb> [Accessed 31 Jan. 2017].

RMOD-K, 2017b. Measurement and Parameter determination of the Modeling System. (2016). Version 2-1. [pdf] Available at: http://www.rmodk.com/images/stories/media/downloads/measurements/RMOD-K_Measurements_Parameterdetermination_en_V2p1_2016_10_04.pdf [Accessed 31 Jan. 2017].

Schiehlen, W. , 2013. *Advanced multibody system dynamics: Simulation and Software tools* (Vol. 20). Springer Science & Business Media.

Schlippe, B. von; Dietrich, R, 1942. *Zur Mechanik des Luftreifens*, Zentrale für wissenschaftliches Berichtwesen der Luftfahrtforschung des Generalluftfahrzeugmeisters (ZBW), Berlin Adlershof, 1942.

Schmeitz, A.J.C. and Verstedden, W.D., 2009. Structure and Parameterisation of MF-Swift, a Magic Formula-based Rigid Ring Tire Model 3. *Tire Science and Technology*, 37(3), pp.142-164.

- Schmeitz, A.J.C., 2004. A Semi-Empirical Three-Dimensional Model of the Pneumatic Tyre Rolling over Arbitrarily Uneven Road Surfaces, PhD Thesis, Delft University of Technology, Delft, The Netherlands.
- Schmid, A. and Förschl, S., 2009. From Real to Virtual Tyre Tyre Model Parameterisation. *ATZ worldwide*, 111(3), pp.22-27.
- Schmid, M., 2011. *Tire Modeling for Multibody Dynamics Applications*. University of Wisconsin-Madison.
- Seibert, H., Scheffer, T., and Diebels, S., 2014. Biaxial testing of elastomers-Experimental setup, measurement and experimental optimisation of specimen's shape. *Technische Mechanik*, 34(2), 72-89.
- Shoop, S.A., 2001. Finite Element Modeling of Tyre-Terrain Interaction, *U.S. Army Engineer Research and Development Center Cold Regions Research and Engineering Laboratory*. USA.
- Song, G., Conard, B. and Iyengar, S.K.R., 2008. Damping Characterization Using Hysteresis on Static Nonrolling and Dynamic Rolling Behavior of Farm Tires 4. *Tire Science and Technology*, 36(2), pp.108-128.
- Sovamotion, 2017. Tire Modeling. [online]. Available at: <http://www.sovamotion.com/tire-modeling.html> [Accessed 31 January. 2017].
- Stackpole Engineering Services. 2017. Tire Testing and Analysis Services. [online]. Available at: http://www.stackpoleengineering.com/index_tire_testing.php [Accessed 31 January. 2017].
- Stallmann M.J., and Els, P.S., 2014. Parameterisation and modelling of large off-road tyres for ride analyses: Part 2 – Parameterisation and validation of tyre models. *Journal of Terramechanics*, October 2014, Volume 55, pp. 85-94
- Stallmann M.J., Els, P.S., and Becker, C.M., 2014. Parameterisation and modelling of large off-road tyres for ride analyses: Part 1 – Obtaining parameterisation data. *Journal of Terramechanics*, October 2014, Volume 55, pp. 73-84
- Taheri, S., Sandu, C., Taheri, S., Pinto, E. and Gorsich, D., 2015. A technical survey on Terramechanics models for tire-terrain interaction used in modeling and simulation of wheeled vehicles. *Journal of Terramechanics*, 57, pp.1-22.
- Thacker, B.H., Doebeling, S.W., Hemez, F.M., Anderson, M.C., Pepin, J.E. and Rodriguez, E.A., 2004. *Concepts of model verification and validation* (No. LA-14167). Los Alamos National Lab., Los Alamos, NM (US).
- TMeasy. 2017. *TMeasy Tire Model easy to use*. [online] Available at: <http://tmeasy.de> [Accessed 31 Jan. 2017].
- TNO, 2013, MF-TOOL 6.1 Users Manual, www.delft-tyre.nl [Accessed 2 July 2013].
- Tuononen, A., 2009. On-board estimation of dynamic tyre forces from optically measured tyre carcass deflections. *International journal of heavy vehicle systems*, 16(3), pp.362-378.

Tönük, E. and Ünlüsoy, Y.S., 2001. *Prediction of automobile tire cornering force characteristics by finite element modeling and analysis*. *Computers & Structures*, 79(13), pp.1219-1232.

Trujillo-Pino, A., Krissian, K., Alemán-Flores, M., and Santana-Cedrés, D. 2013. Accurate subpixel edge location based on partial area effect. *Image and Vision Computing*, Volume 31, Issue 1, January 2013, Pages 72–90

Universität Hohenheim. 2017. Weiterentwicklung des Reifenmodells: Hohenheimer Reifenmodell. [online] Reifenmodell.uni-hohenheim.de. Available at: <https://reifenmodell.uni-hohenheim.de/93444> [Accessed 31 Jan. 2017].

Universität Hohenheim, 2017b. *Test stands*. [online] Reifenmodell.uni-hohenheim.de. Available at: <https://reifenmodell.uni-hohenheim.de/en/test-stands> [Accessed 31 Jan. 2017].

Unrau, H.J., Zamow, J. 1997. TYDEX-Format - Description and Reference Manual, Release 1.3, Available at: https://www.fast.kit.edu/download/DownloadsFahrzeugtechnik/TY100531_TYDEX_V1_3.pdf [Accessed 10 Sep. 2016]

VDG Solutions. 2017. Vehicle Dynamics Group. [online]. Available at: <http://www.enterprises.up.ac.za/research-solutions/business-units/vehicle-dynamics-solutions> [Accessed 31 Jan. 2017].

Wang, H., Al-Qadi, I. L., and Stanciulescu, I. (2012). Simulation of tyre–pavement interaction for predicting contact stresses at static and various rolling conditions. *International Journal of Pavement Engineering*, 13(4), 310-321.

Wei, C., 2015, *A finite element based approach to characterising flexible ring tyre (FTyre) model for extended range of operating conditions*. Ph.D. Thesis, University of Birmingham

Wei, C., Olatunbosun, O.A., and Behroozi, M., 2016. Simulation of tyre rolling resistance generated on uneven road, *Int. J. Vehicle Design*, Vol. 70, No. 2

Witzel, P., 2016. Ein validiertes Reifenmodell zur Simulation des fahrdynamischen und fahrkomfortrelevanten Verhaltens von Ackerschleppern bei Hindernisüberfahrt. Available at: <http://opus.uni-hohenheim.de/volltexte/2016/1207/> [Accessed 31 Jan. 2017]

Xiong, Y. and Tuononen, A., 2015. Rolling deformation of truck tires: measurement and analysis using a tire sensing approach. *Journal of Terramechanics*, 61, pp.33-42.

Yang, X., Olatunbosun, O. and Bolarinwa, E., 2010. Materials testing for finite element tire model. *SAE International Journal of Materials and Manufacturing*, 3(2010-01-0418), pp.211-220.

Zegelaar, P.W.A., 1998, *The dynamic response of tyres to brake torque variations and road unevenness*, PhD Thesis, Delft University of Technology, Delft, The Netherlands.

Zhang, X., 2001, *Nonlinear Finite Element Modeling and Incremental Analysis of A Composite Truck Tyre Structure*. PhD thesis, Concordia University, <http://spectrum.library.concordia.ca/1424/> [Accessed 23 May 2016]

Zheng, D., 2006. Challenges in Tyre FEM Simulation, Continental. Available at:
<https://www.wias-berlin.de/events/insk/herbst05/zheng.pdf> [Accessed 23 July. 2016]

10. Appendix A

A. Modelling and parameterisation approaches of commercially available tyre models

A short review of some of the commonly used tyre models, parameterisation procedures and corresponding test data, is discussed in the following section. Some of this material has already been discussed in Chapter 2 but is included here again for completeness. A short discussion of the Hohenheimer tyre model will also be included in this section as the tyre model was developed for large agricultural tyres and thus fall within the scope of this research. The descriptions presented here are based entirely on the documentation as published by the respective tyre model developer.

MF-Swift – Magic Formula - Short Wavelength Intermediate Frequency Tyre Model

Delft tyre consists of two semi empirical tyre models [TNO, 2013]. The first model, MF-Tyre, is a standard implementation of the renowned Pacejka magic formula. The model consists of a set of formulae that are partly based on empirical data and partly based on the physical behaviour of the tyre. The model includes the latest developments of the Magic formula as presented in Pacejka [2005]. The model can predict the lateral and longitudinal tyre behaviour for steady state and transient tyre simulations. The model has been validated for handling simulations up to 8Hz and can accurately describe pure cornering and braking as well as combined simulation conditions [TNO, 2013]. A single point contact model is used to model the tyre contact with the road.

For simulations on shorter wavelength road irregularities the second model, MF-Swift, was developed. This tyre model is based on a rigid ring tyre modelling approach. With this approach, the in-plane and out-of-plane tyre behaviour is represented up to frequencies of 60-100Hz [TNO, 2013]. MF-Swift is thus a high frequency extension of MF-Tyre.

Five key elements are used to compose the MF-Swift tyre model [TNO, 2013]. The first element is a rigid ring that is elastically suspended from the rim. The rigid ring has 6 degrees of freedom and represents the tyre belt and carcass with its mass and inertia properties. The rigid ring thus represents the primary vibration modes of the tyre. The second element is the residual stiffness and damping model between the rigid ring and the contact patch. The stiffness and damping model was introduced to accurately model the quasi-static tyre stiffness in the vertical, longitudinal, lateral and yaw direction. A contact patch model, or slip model, is also introduced in the model. The brush model represents the contact patch featuring horizontal tread element compliance as well as the partial sliding effect. The model thus includes the effects of the finite length and width of the tyre contact patch. The fourth element is the Magic Formula steady state slip model. The model uses the MF-Tyre representation to describe the nonlinear force and

moment handling characteristics. The fifth element is the three-dimensional enveloping contact model. The model comprises of several cams that are positioned in such a way that they correspond to the outside of the contact patch. The positions and orientations of all cams are calculated during the simulation to determine the effective road height, slope, and curvature as well as the effective road camber angle. These effective road parameters are used in the rigid ring model to determine the forces that are generated in the tyre contact patch.

The MF-Swift tyre testing and parameter identification process is presented in Schmeitz and Verstedden [2009] and forms the basis of this section. Due to the semi-empirical structure of the MF-Swift tyre model the parameter identification process can be divided into several dependent identification steps. In each step, a set of unique parameters are determined and fixed during the following parameter identification steps. Schmeitz and Verstedden [2009] noticed that the experiments used during a specific identification step must be chosen such that the model results only depend on the parameters that are identified in the preceding and current identification step.

The first step of the MF-Swift parameter identification process is to determine the parameters of the Magic Formula (MF). Experimental tests that are required for this step include pure and combined steady state slip characteristic tests. The slip characteristic tests should be conducted at various vertical loads, inflation pressures and at various camber angles.

The second step extracts the model parameters that describe the basic tyre properties such as the tyre stiffness, rolling radius, contact patch dimensions, and rolling resistance. Tests need to be conducted to describe the loaded tyre radius as a function of vertical load, forward velocity, inflation pressure, and longitudinal, and lateral forces acting at the contact patch. The effective rolling radius needs to be tested as a function of radial tyre load. Tyre footprints tests need to be conducted to determine the contact patch length and width as a function of tyre deflection. Tests should also be conducted to determine the tyre longitudinal and lateral stiffness as well as rolling resistance of the tyre.

The final step of the parameter identification process is to determine the enveloping and in- and out-of-plane tyre dynamics. These parameters are determined from cleat tests. Cleat test at low speeds are used for the enveloping identification step while high speed cleat tests are used to parameterise the rigid ring model parameters.

To aid the user in the parameter identification process a commercial software tool, called MF-Tool, was developed [TNO, 2013]. For each parameter identification step MF-tool uses a

numerical optimisation procedure to determine the model parameters that result in the closest match with the tyre measurements. MF-Tool also offers a tool to automatically scale tyre model properties to investigate the effects on the tyre due to a change in tyre inflation pressure, friction level, or cornering stiffness.

TameTire - Thermo-mechanical Tire Model

Tame Tire is a coupled thermo-mechanical tyre model that was developed by Michelin. The model was developed to improve the handling simulations of passenger car tyres. TameTire can be used to determine the tyre forces and moments for a wide range of conditions including thermal effects, speed effects, tyre inflation pressure and transient effects [IPG-Automotive, 2017; Pearson et al., 2016]. The model consists of three parts namely the mechanical model, the rubber model, and the thermal model. The mechanical part of the model is based on a one-dimensional brush model. The forces and moments that are developed in the tyre contact patch are determined for both the adherent and sliding conditions. The contact patch model uses the rubber shear modulus to determine the tread stiffness in the adherent region. The shear modulus of the rubber is modelled to be dependent on the internal temperature of the tyre. The forces and moments of the sliding part of the tyre model are governed by friction laws which are coupled to the contact temperature. The thermal model uses a physical approach to determine the inner liner and outer surface temperatures during one wheel revolution. The thermal model does not consider any discretization of the tyre body. The conduction of heat, in the contact patch area, is governed by the heating due to friction, viscous heat generation in the tread, and the temperature difference between the tyre and the road.

Michelin has developed a standardized testing procedure to obtain the required parameterisation data. A flat track tyre test machine is used to simulate track conditions of a standard reference test track. In addition to these tests additional tests are conducted at various loads, velocities, and inflation pressures. During the measurements, the thermal state of the tyre is recorded. The rolling resistance of the tyre is also tested using the ISO 28580 standard [Pearson et al., 2016].

The test data is post processed and the Tame Tire model parameters are automatically determined. A reliability index is used to validate the quality of all obtained model parameters [Michelin engineering and services, 2017].

A database of available tyre models is also available with TameTire [IPG-Automotive. 2017]. The database includes several tyre models in different tyre classes and tyre brands. The database is regularly updated by adding new tyre models to the database.

TMeasy - Tire Model easy to use

TMeasy is a handling tyre model that is based on a semi-physical modelling approach. The semi-physical model is based on a three-dimensional slip approach [TMeasy, 2017, Rill, 2013]. The longitudinal and lateral forces are described as functions of the longitudinal and lateral slip. Five parameters define the handling characteristics: initial inclination and the location and magnitudes of the maximum lateral and longitudinal force as well as the sliding limits and corresponding forces. A friction circle approach is used for combined slip conditions.

The TMeasy tyre model provides a smooth transition from stand still to normal driving conditions and includes an effective dynamic parking torque model. For simulations on an uneven terrain the contact area within TMeasy is approximated by a local road plane that is determined from adjacent points on the track surface. The vertical tyre force is separated into a static and a dynamic part which are dependent on the tyre deflection and its time derivative. The static tyre stiffness is described by a nonlinear function while the dynamic part is roughly approximated by a linear damper element. The model also includes camber effects.

The modelling approach of TMeasy allows a skilled engineer to estimate appropriate model parameters by estimating, or knowing, the tyre size, the payload of the tyre, as well as the tyre-road friction properties [Rill, 2015]. TMeasy tyre model parameters can also be adjusted to fit dynamic tyre measurements.

According to TMeasy [2017] the tyre characteristics of TMeasy are determined and specified with respect to two loading conditions, the payload of the tyre and twice the payload. A maximum payload is also specified to ensure that the extrapolation formulas used in TMeasy produce realistic results. Tests can be conducted to determine the vertical, lateral, longitudinal, and torsional stiffness and damping parameters of the tyre. Alternatively, an engineer's guess can estimate these values [TMeasy, 2017]. Tests to determine the rolling resistance coefficient and the dynamic rolling radius need to be conducted. The lateral and longitudinal force characteristics are defined by an initial slope, maximum force, slip where the maximum force occurs, sliding force, and the slip where sliding occurs. A set of aligning parameters are used to determine the self-aligning torque. Tests need to be conducted to determine the normalized pneumatic trail, lateral slip where the pneumatic trail changes sign, and the slip where the trail tends to be zero. Additional factors that determine the camber influence, bore radius, and longitudinal force characteristic can be specified to improve the accuracy of the model.

Hohenheimer Reifenmodell - Hohenheimer tyre model

To simulate the ride vibration of agricultural vehicles the Hohenheimer Reifenmodell was developed [Hohenheimer Reifenmodell, 2017]. The real-time tyre model was developed with the aim to only use physical parameters, to ensure that the model is valid for a wide range of operating conditions, and with only a small number of model parameters, to simplify the parameter identification process. The availability and accessibility of test data from large tyres was the driving factor in the development of this model. The basis of the model is constructed on a spoke model. Good correlation between simulation results and measurements were found for manoeuvres over discrete obstacles [Witzel, 2016].

The seventeen model parameters can be extracted from test data from a flat track and single wheel tyre tester found at the University of Hohenheim [Hohenheimer Reifenmodell, 2017]. Data that is required to parameterise the tyre model includes the tyre radius, roll radius, radial runout and tests that can be used to extract the radial, tangential, axial-spring and damper coefficients as well as the inter-radial spring coefficients.

RMOD-K - Reifenmodell für Komfortuntersuchungen (tyre model for comfort analyses)

RMOD-K consists of a collection of tyre models that were developed for vehicle comfort studies. For cornering analyses, a rigid belt model, RMOD-K 7 RB, was developed. The model simplifies the tyre belt to a rigid belt body, based on a priori discretization, and Lagrange formulation is used [Oertel and Fandre, 1999]. The contact area, between the tyre and the road, is determined by cutting a parameterisable geometry with the road surface. The model is valid for low to medium frequency cornering excitations and road disturbance wavelengths of about 100 millimetres. The rigid belt model covers the rigid belt modes of the tyre up to a frequency of 100Hz.

A flexible belt model, RMOD-K 7 FB, was introduced to accurately represent the tyre during simulations on roads with short wavelength obstacles. The flexible belt model represents the tyre structure as discrete finite elements.

Two different rebar elements are used to model the belt and sidewall of the tyre. The main stiffness of the belt structure is due to the planar rebar elements. A variable number of rebar's are used within the planar rebar element. The tyre structure is loaded with the forces resulting from the internal inflation pressure as well as the forces resulting from the tyre contact with the road. The tyre contact is determined with gap sensors, that are located on the outer tyre surfaces, and a contact algorithm that is based on the penalty method.

The flexible belt model also includes a misuse model extension. The model extension allows the solver to handle large sidewall deformations. During misuse conditions, the inner surface of the tyre contacts the rim and thus increases the tyre stiffness.

To parameterise a RMOD-K tyre model a set of experimentally obtained measurements are required [RMOD-K, 2017b]. The tests are divided into six measurement groups, namely:

- i. General Data;
- ii. Topology Data;
- iii. Forces and Moments;
- iv. Cleat Tests;
- v. Modal Data;
- vi. Additional Data (Stiffness).

The general data group comprises of the tyre and rim dimensions, load index, reference inflation pressure, and tyre mass. The topology data describes the contour and the cross section of the tyre. The contour is defined by an outer and inner tyre contour while the tyre is mounted on the rim and inflated to the nominal inflation pressure. A scaled image of the cross section, indicating the belt layers and the width and height of the tread, is also required. The belt angle, Young's modulus of the tread rubber as well as the lateral and longitudinal tread stiffness ratios should also be determined. Tests should be conducted to determine the lateral and longitudinal force handling characteristics. The tests should be conducted at various loads and at a speed of 80-100km/h. Alternatively a Magic Formula 5.2 tyre file can be used to parameterise the handling characteristics of the RMOD-K tyre model. Cleat tests should be conducted on a drum with an orientation of 0 and 45 degrees. The tests should be conducted with a fixed hub for a set of longitudinal velocities. The cleat height and width, inflation pressure, and vertical load should also be varied during the tests. A modal analysis should be conducted to determine the modes and mode shapes of an unloaded tyre under nominal inflation pressure. Modes up to 300Hz should be identified. In addition to these tests the quasi-static vertical, lateral, longitudinal, and torsional tyre stiffness of the tyre should be determined. The dynamic vertical stiffness of the tyre is also of interest and should be investigated. The contact area pressure distribution at different loads and inflation pressures should also be determined. Finally, the rolling resistance as a function of rolling velocity at the reference load should be determined.

A software system has been developed to process the obtained test results and contains optimisation algorithms to obtain the necessary RMOD-K 7 model parameters [RMOD-K, 2017b].

Finally, the model and test data is validated to ensure that the model can accurately represent the tyre behaviour.

CDTire – Comfort and Durability Tyre Model

The Comfort and Durability Tyre Model, CDTire, is a 'family' of models that were developed to model radial tires in the context of multi body simulation for ride comfort, durability and vehicle handling assessment of passenger cars and commercial vehicles [CDTire, 2017]. CDTire is a physical tyre model family consisting of CDTire/3D, CDTire/Realtime, CDTire/Thermal and CDTire/MF++. CDTire was developed to accurately describe the tyre belt dynamics and the tyre interaction with a three-dimensional road surface.

CDTire/MF++ is a magic formula based tyre model. The model is based on the MF 6.1 formulation and includes the relaxation length concept. To include temperature effects the model was enhanced to couple the CDTire/Thermal model to the Magic Formula model. An empirical tread model determines the contact patch size and shape.

CDTire/Thermal is a thermodynamic tyre model that predicts the temperature, heat generation and heat propagation of a tyre. The model is based on a three-dimensional finite volume description. The thermodynamic model can be coupled to CDTire/MF++, CDTire/Realtime and CDTire/3D.

CDTire/realtime is a hard real-time capable tyre model. The belt is modelled as a flexible beam with global bending and strain properties. An analytical membrane is used to model the sidewall of the tyre. The assumption of symmetry is made for the left and right sidewalls. The tyre road contact model is modelled with a brush formulation and allows local stick-slip behaviour in different parts of the contact patch area.

CDTire/3D is a three-dimensional tyre model that was developed to accurately describe the local deformation behaviour of the tyre. The tyre model is based on a detailed materialized shell representation of the belt and sidewall.

An anisotropic elastic membrane and an adaptation of the Kirchhoff-Love hypothesis for bending is used to model the elastic properties of the shell. The elastic membrane is build up from separate component layers. These layers may include inner liner, carcass, steel belt layers, synthetic cord layers, cap plies, tread etc. The model can be constructed with an arbitrary number of belts layers with varying belt angles and specific local stiffness properties. In addition to the stiffness and

damping parameters of the reinforcing layers a local pre-stress can be defined. A brush type contact model is used for the contact formulation. The number of bristles and their lengths can be specified individually for every cell in the cross section.

The model parameters of the CDTire tyre model family can be extracted from standard tyre measurements. The following standard measurements are used by CDTire/PI [CDTire, 2014a] during the parameter identification process:

- i. Geometry of the tyre:
 - a. cross section;
 - b. foot prints;
- ii. Modal analysis results;
- iii. Quasi-statics test results (stiffness's, on cleat):
 - a. Vertical stiffness;
 - b. Lateral stiffness;
 - c. Longitudinal stiffness;
 - d. Torsional stiffness;
- iv. Steady-state test results:
 - a. Pure lateral slip;
 - b. Pure longitudinal slip;
- v. Transient test results:
 - a. 90° cleat;
 - b. 45° cleat;
- vi. Rolling resistance test results.

During the parameter identification process, parameters from an existing tyre model are adapted to better describe the current tyre behaviour. The parameter adaption can be done automatically, or semi-automatically, using suitable measures and mathematical optimization procedures. The obtained test data is compiled into a measurement database within CDTire/PI. Virtual tyre measurements are then performed by imitating the experimental test conditions in a multi-body-dynamics environment. A dedicated post processing feature is used to align the measurement and simulation results. Different local and fuzzy control based optimizers are used to determine the optimal model parameters [CDTire, 2014a]. The model parameters can also be obtained manually by visual inspection or based on expert experience.

To supplement the standard measurement results, which almost exclusively comprise of spindle forces, local tyre deformation information can also be used to identify model parameters. The local tyre deformation information that is currently supported in CDTire/PI are local tyre shape measurements of the belt and sidewall. The data can be obtained through experimental testing or extracted from detailed FE tyre models.

FTire - Flexible Structure Tire Model

FTire is a full 3D nonlinear in-plane and out-of-plane tyre model. The Model was developed by Gipser [1999; 2002] over the past 20 years. FTire was developed for vehicle comfort simulations and the prediction of road loads with extremely short wave-lengths obstacles but can also be used for handling simulations.

FTire is based on a structural dynamics approach. The tyre model describes the tyre belt as a flexible ring that can flex and extend in the radial, tangential, and lateral directions. The belt is approximated by a finite number of rigid belt elements that are connected to each other in such a way that in-plane as well as out-of-plane movement of the elements is possible. In general, 100 to 200 of these belt elements are used to represent the tyre.

Every belt element is again associated with a finite number, between 10 and 100, of mass less “tread blocks”. Tread blocks are connected to their neighbours with nonlinear stiffness and damping properties in the radial, tangential, and lateral directions. These tread blocks are located along parallel lines. The user can prescribe the tread pattern geometry. The tread blocks height will then be defined according to the tread pattern. All 6 tyre forces and torque components, acting on the rim, are calculated by integrating the forces in the elastic foundation of the belt.

Due to the structural dynamics approach, there are very few restrictions to the simulated operating conditions of the model. FTire can deal with large or short-wave obstacles. It works out of, and up to, complete stand still. FTire is also capable of running in strict real-time without any model switch or reduction of model accuracy.

An optional tyre thermal model is also provided with FTire. The model can be used to compute the actual inflation pressure as a function of the filling gas mass, cold tyre inflation pressure, tyre temperature, and actual interior volume. A heat generation and transfer model is introduced to determine the temperature of the tyre structure, the filling gas, and the temperature of each individual tread contact element. The rubber temperature of the tread, in addition to the ground

pressure and sliding velocity, is used to determine the friction coefficient between the tread blocks and the road.

In addition to the temperature model, a tread wear model, air vibration model, and flexible rim model is available with FTire. The tread wear model affects the tyre cross-section geometry, contact pressure distribution, radial tread stiffness, tread shear stiffness, tyre mass, and the tread's heat capacity. The air vibration model can be used to determine the fluctuations of air density, air pressure, and air flow velocity inside the tyre. The unbalanced tyre pressure results in an uneven reaction force on the tyre structure and rim and thus influences the tyre forces in higher-frequency ranges. The flexible and viscoplastic rim model determines the flexible and/or viscoplastic rim flange displacements and deformations from the spatial forces, exerted by the tyre on the left and right rim flanges. The rim can further undergo permanent plastic deformation.

Parameterisation of the tyre model is generally done with the FTire/fit code code [cosin scientific software, 2017d]. The code provides several optimization routines to minimize the error between measured results and the corresponding simulation with a FTire model. FTire/fit begins with an initial tyre estimate. The user can subsequently improve the tyre behaviour by supplying the parameterisation program with general tyre data and experimental test data.

FTire/fit identifies tyre model parameters from the following kinds of experimental data:

- i. static tyre properties (radial, longitudinal, lateral, and torsional stiffness on different surface geometries);
- ii. footprint shapes;
- iii. steady-state rolling tyre tests;
- iv. time- and/or frequency-domain measurements of cleat tests (large-amplitude tyre vibrations).

The first stage in the parameterisation process is the tyre model preparation stage. In the preparation stage, a new tyre model is created from general tyre data. The general tyre data comprises of the tyre dimensions, operational pressure, mass, and other physical properties. The user can then “check in” various test results to optimize the model to better represent the physical model. Additional data that can be used to improve the accuracy of the tyre model, include tyre footprint images, static tyre stiffness, static cleat tests, side force slip angle measurements, dynamic cleat tests and various other test results. During the “check-in” process FTire/fit automatically determines the kind of measurement, depending on the operating conditions,

inflation pressure, etc., and saves information on how the validation and/or identification is to be performed. The model parameterisation is done by minimizing the mean square deviation between the measurements and simulation results. Occasionally model parameters, such as radial, longitudinal, lateral, and torsional tyre stiffness, are directly extracted from the test data. If no test data, or only limited test data is available, the program will use the same parameter set that was loaded as the initial estimate. FTire/fit automatically generates diagrams during the parameter identification process showing the comparison between the simulation and measurement. The diagrams can be automatically compiled into a comprehensive parameterisation report.